



JACOBS  
UNIVERSITY

# Peak-to-Average Ratio Reduction for MIMO and Multi-user OFDM Systems

by

**Abdul Wakeel**

A thesis submitted in partial fulfillment  
of the requirements for the degree of

**Doctor of Philosophy  
in Electrical Engineering**

Approved, Dissertation Committee:

---

**Prof. Dr.-Ing. Werner Henkel**  
Jacobs University Bremen

---

**Prof. Dr. Hideki Ochiai**  
Yokohama National University

---

**Dr. rer. nat. habil. Mathias Bode**  
Jacobs University Bremen

Date of Defense: January 8<sup>th</sup>, 2016

---

Jacobs University Bremen



## Dedication

*To my whole family, especially to my father late Sarzamin Khan and my elder brother  
Prof. Dr. Manzoor Ahmad*



# Acknowledgements

This work is the result of my research in the School of Engineering and Sciences at Jacobs University Bremen, Germany.

First of all, I would like to thank Prof. Dr.-Ing. Werner Henkel for his guidance, motivation, support, and kind supervision of my PhD studies. This thesis would not have been completed without his academic supervision, valuable discussions, and kind support. I am really thankful for the friendly and convenient academic environment he provided throughout my stay at Jacobs. Furthermore, I am also grateful to Dr. habil Mathias Bode and Prof. Dr. Hideki Ochiai for accepting to join the dissertation committee.

I would also like to thank my current and previous colleagues Dawit Nigatu, Nazia Islam, Khodr Saaifan, Oana Graur, Vladimir Burstein, Hashem Moradmand Ziyabar, Khaled Hassan, Fangning Hu, Humberto Beltrao, Jalal Etesami, Neele von Deetzen, Apirath Limmanee, Attiya Mehmood, and Alexandra Filip for their valuable discussions, friendship, and support. You guys really made my stay at Jacobs memorable.

I am really in debt to my Pakistani friends at Jacobs University, Muhammad Aasim, Noorshad, Abdul Sadiq, Nawab Ali, Guftar Ahmad, Abu Nasar, Muhammad Farhan, Farhan Younus, Noor Muhammad, Tahir Zeb, Inamullah khan, Ishtiaq Hussian, Ali Haidar, Umair Seemab, Muhammad Jawad, Rashid Mehmood, and Laiq Shahid for their company, support, and friendship. I will never forget the love and respect I received from them. They were more like family than friends.

How could it be possible to forget mentioning the closest and the dearest friends from Pakistan. I would like to extend my deepest and sincere gratitude to Abdul Rahman, Omar Ali, Fayaz Ahmad, Nadar Khan, Siraj Ali, Muhamamd Suleman, Shah-i-Room Bacha and Rahiq-ur-Rahman for their love, their support in time and all the joys and fun of life we made together. They made my life full of happiness, pleasures, and rejoices.

I have no words to express my love and my profound gratitude to my family, to whom I am dedicating this work. I am really missing my father, late Sarzamin Khan, a man who sacrificed his present for our future, who sacrificed his dreams for ours to come true. The words fell short when it comes to my elder brother, Prof. Dr. Manzoor Ahmad, whose sincere love, moral and spiritual support, confidence, and continuous encouragement made me reach my goals. He is more like father to us than a brother. The whole credit of this work goes to him. I cannot express my gratitude for my mom Sahira, whose unconditional love and sincere prayers are always there for me at the odd of my times. I also owe to my younger brothers Abdul Aziz, Abdul Basit, and Abdul Wasaay and my sisters Islam Bibi, Watan Bibi, Farzana, Taj Bibi, Aneesa, Sidra and Sadaf for their love, their prayers and their kindness. The outcome of this work is all because of their constant prayers. Of course, I have to mention the love I got from my nieces Salwa, Mah-Para, Mah-Rukh, and Gul-Rukh.

Last but not the least, I would like to express my sincere love, deepest appreciation and special thanks to my wife, Shahnaz, for her love, consistent prayers, and moral encouragement which help me complete this thesis. And, how can i forget my little cute angels Khkwala and Zalaa. Though you were far but you were always in my heart. I am really sorry for not being there with you in the time you needed me.

Finally, I would like to thank the Higher Education Commission of Pakistan (HEC) and Jacobs University Bremen for their financial support.

# Declaration

I, hereby declare that I have written this PhD thesis independently, unless where clearly stated otherwise. I have used only the sources, the data, and the support that I have clearly mentioned. This PhD thesis has not been submitted for conferral of degree elsewhere.

I confirm that no rights of third parties will be infringed by the publication of this thesis.

*Abdul Wakeel*  
Bremen,

---

## Abstract

MIMO-OFDM is known to be a promising technique for modern high speed communication networks used for reliable data transmission at a higher rate. However, a major drawback of OFDM systems is its high Peak-to-Average Ratio (PAR). The signal is clipped when the peak values are higher than the linear operation range of non-linear devices. Clipping the signal results in in-band distortion (increases BER) and out-of-band radiation (spectral spreading), leading to a performance degradation. In order to avoid signal clipping, the non-linear devices are usually operated at higher power back-ups. This results in inefficient power usage and leads to high power dissipation. The problem of high PAR becomes even more complex when considering OFDM-based MIMO systems. Therefore, measure must be taken to limit all peaks crossing a certain threshold value. In this thesis, we therefore investigate and address the PAR problem of different MIMO-OFDM scenarios and provide countermeasures to limit the peak excursions in MIMO-OFDM systems.

First, we extend the Tone-Reservation algorithm to limit the peak excursions in point-to-point and multi-user MIMO-OFDM systems. For point-to-point MIMO-OFDM, one or more singular values are usually very weak such that the associated eigenchannels are hardly suited for data transmission. We thus reserve these eigenchannels to offer redundancy for PAR reduction. A spiky function is generated using these eigenchannels which is then iteratively added to the transmit signal for PAR reduction. Next, we consider a multi-user broadcast scenario. For broadcast scenarios, the spiky function is generated on a small number of tones reserved on all spatial dimensions in the conventional Tone-Reservation fashion. This spiky function is then iteratively used for PAR reduction of the multi-user MIMO-OFDM system. Simulation results are provided to show the effectiveness of the proposed algorithm.

Second, we introduce a novel Least-Squares iterative PAR reduction algorithm for MIMO-OFDM scenarios. In the case of a point-t-point MIMO-OFDM scenario, we again reserve the weakest eigenchannels to offer redundancy for PAR reduction. However, this time the reserved eigenchannels are used to approximate the peak excursions on the remaining spatial dimensions in a least-squares fashion. This model function is then added to the transmit signal for PAR reduction. However, there is a possibility that all peaks may not be well approximated, the algorithm is thus iterated to model the remaining peaks in the following iterations. By reserving the weakest eigenchannels, there is a loss in channel capacity. The capacity associated with the weakest eigenchannels is thus analyzed using random matrix theory. Moreover, addition of the modeled function to the transmit signal will result in an increase in the mean power of the transmit signal, thus, the algorithm is investigated with a constraint in the mean transmit power. Furthermore, we extend the LS-approach to PAR reduction in a multi-user broadcast scenario. For a broadcast system, we consider that one user is inactive and the channel associated to it is not used. This inactive channel is then used to approximate and model the peak excursion in the similar fashion. In both cases, the performance is analyzed using simulation results.

In a further part of this thesis, we consider PAR reduction using Trellis Shaping for single antenna systems. We concatenate an optimized irregular LDPC code with Trellis Shaping for PAR reduction. For the irregular LDPC code, we present the optimization of

the variable node degree distribution based on the irregularities in the bit error probabilities of the individual bits inside an  $\mathcal{M}$ -QAM symbol. Moreover, for the MSBs, the bit error probability is calculated exploiting the transfer function of the shaping code. A soft decision decoding on the shaping code sequence is considered to decode the useful information, using BCJR algorithm.

# Contents

<b>1</b>	<b>Introduction</b>	<b>1</b>
<b>2</b>	<b>Orthogonal Frequency Division Multiplexing</b>	<b>4</b>
2.1	Orthogonal frequency division multiplexing . . . . .	4
2.1.1	A brief history of OFDM . . . . .	5
2.1.2	Basic principle of OFDM modulation . . . . .	5
2.1.3	Discrete-time OFDM system model . . . . .	7
2.1.4	Channel model . . . . .	9
2.1.5	OFDM matrix representation . . . . .	10
2.2	Multi-antenna systems . . . . .	12
2.2.1	Point-to-point scenario . . . . .	13
2.2.2	Multi-user uplink and downlink scenarios . . . . .	14
2.3	OFDM-based MIMO systems . . . . .	17
2.4	Peak-to-average ratio of an OFDM signal . . . . .	19
2.4.1	Mathematical formulation . . . . .	20
2.4.2	Statistical analysis . . . . .	22
2.5	Consequences of high PAR . . . . .	23
2.5.1	Theoretical models of high power amplifiers . . . . .	24
2.6	Peak-to-average reduction techniques . . . . .	26
2.6.1	Peak-to-average reduction techniques in SISO systems . . . . .	27
2.6.2	Peak-to-average reduction techniques in MIMO systems . . . . .	32
<b>3</b>	<b>PAR Reduction with Tone Reservation in MIMO and Multi-user OFDM</b>	<b>34</b>
3.1	PAR reduction with TR in point-to-point MIMO-OFDM systems . . . . .	35
3.1.1	Key idea . . . . .	35
3.1.2	System model and pre-coding . . . . .	36
3.1.3	Designing an optimum spiky function . . . . .	38
3.1.4	Tone Reservation algorithm . . . . .	42
3.1.5	Results and discussion . . . . .	42
3.2	PAR reduction in multi-user MIMO-OFDM systems . . . . .	46
3.2.1	System model and TH precoding for multi-user broadcast . . . . .	47
3.2.2	Results and discussion for the multi-user BC . . . . .	49
<b>4</b>	<b>Least-Squares Iterative PAR Reduction for MIMO and Multi-user OFDM Systems</b>	<b>54</b>
4.1	Least-Squares iterative PAR reduction for P2P MIMO-OFDM systems . . . . .	55

4.1.1	Key idea . . . . .	55
4.1.2	System model and pre coding . . . . .	55
4.1.3	Exceedence spike representation . . . . .	57
4.1.4	Results and discussion . . . . .	60
4.2	Extension of the LS-algorithm to multi-user broadcast (BC) scenarios . . .	81
4.2.1	System model and precoding . . . . .	82
4.2.2	Results and discussion . . . . .	83
<b>5</b>	<b>Optimized LDPC Code Concatenated with Trellis Shaping for PAR Reduction</b>	<b>86</b>
5.1	Equivalent binary channels of an $\mathcal{M}$ -ary QAM modulation . . . . .	87
5.2	Trellis Shaping . . . . .	88
5.2.1	Sign-bit shaping with binary convolutional codes . . . . .	90
5.2.2	Metric selection for sign-bit shaping . . . . .	91
5.2.3	Soft-input soft-output decoding for the shaping bits, using the BCJR algorithm . . . . .	93
5.3	Irregular LDPC codes . . . . .	95
5.3.1	Notations . . . . .	97
5.3.2	Optimization of the variable-node degree distribution . . . . .	98
5.3.3	Optimization algorithm . . . . .	100
5.3.4	Code construction . . . . .	100
5.4	System model, results, and discussion . . . . .	101
5.4.1	Bit error probability for the MSBs . . . . .	102
<b>6</b>	<b>Summary</b>	<b>109</b>
<b>A</b>	<b>Convergence of the Least-Squares algorithm</b>	<b>111</b>
<b>B</b>	<b>Bit error probabilities of a 256-QAM symbol</b>	<b>114</b>
<b>C</b>	<b>Own Publications</b>	<b>116</b>

# Chapter 1

## Introduction

We are living in an era where life without data communication seems impossible. Audio/video calling, video downloading, texting, Internet surfing, and Facebook/Twitter are nowadays counted as basic needs of daily life. There is a growing demand for high data rate multimedia services, resulting in an increasing interest in high speed communication technologies. To cope with the public demands, the available resources have to be utilized more efficiently. For wireline applications, the channel is somehow stable and the effect of impairments on data is less, however, for wireless communication, efficient transmission is challenging. The challenges faced in wireless transmission are inter-symbol interference (ISI), channel noise, and frequency selective fading. One of the physical layer techniques which has gained a lot of popularity due to its flexibility and ease of implementation is multicarrier modulation (Orthogonal Frequency Division Multiplexing (OFDM)). OFDM optimally utilizes the available bandwidth with orthogonal subcarriers. Moreover, the system performance can be improved further by deploying multiple antennas at the transmitter and/or at the receiver, known as Multiple-Input Multiple-Output (MIMO). MIMO systems offer spatial diversity, which helps to cope with signal fading due to multipath propagation, and / or spatial multiplexing, which increases the channel capacity. OFDM-based MIMO is thus a choice of recent communication technologies which efficiently utilizes the available resources and offers high data rates with flexible data transmission.

Unfortunately, the main disadvantage of multicarrier signals is its large envelope fluctuation, compared to the average power, the peak power of the transmit signal is very high, i.e., high Peak-to-Average Ratio (PAR). The Quadrature Amplitude Modulated (QAM) symbol are independent and identically distributed (i.i.d.), which according to the central limit theorem results in Gaussian like distribution in the Time-domain. Thus, some of the tones may add-up constructively resulting in high amplitude peaks in the time-domain transmit signal. Since most of the practical transmission systems are peak-power limited, the signal is thus clipped when its value is higher than the linear operating range of the non-linear devices. However, clipping of the signal results in in-band distortion (noise which increases the BER) and out-of-band radiation (spectral widening of the signal). Therefore, measures must be taken before passing high peak signal through non-linear devices. In literature, a number of algorithms have been proposed to limit the peak excursions of an OFDM signal. These techniques, first presented for single-input single-output (SISO) OFDM systems, have recently been extended to multiple-input multiple-output (MIMO) systems. An overview of different PAR reduction tech-

niques can be found in [44–46] and the references therein. The most popular techniques amongst them are Clipping (clipping and filtering) [47–54], multiple signal representation (Selected Mapping (SLM), Partial Transmit Sequences (PTS)) [57–59,62,65], Trellis Shaping [64,67–70,99,100], and Tone Reservation (TR) [31,60]. Recently, some of these well optimized methods have been extended to MIMO-OFDM. In [74–84], the authors have presented different variants of SLM and PTS for the PAR reduction of MIMO-OFDM systems, with a thorough study by Siegel in [33]. Moreover, a similar approach has been made in [87], where the authors have extended Tone Reservation to MIMO systems.

It is well known from the literature that Tone Reservation is the least complex algorithm which works in time-domain with promising gains. Herein, we will first extend the TR algorithm for the PAR reduction of point-to-point and multi-user MIMO-OFDM scenarios followed by introducing a novel Least-Squares iterative PAR reduction approach to limit the peak excursions in different MIMO-OFDM scenarios. Last but not the least, we consider a Low-Density Parity-Check code concatenated with Trellis Shaping for PAR reduction of a single antenna systems. For the LDPC code, we optimize its variable-node degree distribution for constructing the  $\mathbf{H}$  matrix. Moreover, for Trellis Shaping, soft-decision decoding with the BCJR algorithm is used to decode the useful information. The rest of this dissertation is structured as follows.

Chapter 2 provides an overview of OFDM systems, MIMO systems and the problem statement. We first start with a brief history of the development of OFDM systems followed by a description of the discrete time OFDM system model and its matrix representation for a single antenna system. Next, we briefly introduce multiple antenna systems along with channel diagonalization for different MIMO scenarios. After introducing the MIMO systems, we next provide a mathematical representation of the OFDM-based multi antenna system (MIMO-OFDM). A major drawback of multicarrier modulation (OFDM) is its high PAR, thus, a mathematical as well as analytical analysis of the problem statement is provided. We define different high power amplifier models and will give a brief description of the characteristic curves of these power amplifiers. Subsequently, out-of-band radiation caused by high PAR of an OFDM signal is assessed. A brief overview to some existing PAR reduction algorithms popular in literature is presented at the end of the chapter.

Chapter 3 gives an extension to the Tone Reservation algorithm for PAR reduction in MIMO-OFDM. First, we consider a point-to-point MIMO OFDM system, where a joint signal processing is possible both at the transmitter as well as at the receiver ends. For a P2P MIMO-OFDM system, the weakest eigenchannel is reserved to offer redundancy for PAR reduction. This eigenchannel is then used to generate a spiky function, which, like in the TR algorithm for SISO systems, is iteratively added to the transmit signal for PAR reduction. However, in doing so, the mean power of the transmit signal increases, therefore, an analysis of the proposed algorithm under a mean power constraint is also provided. Next, a multi-user broadcast scenario is considered, where joint signal processing is possible only at the central base station. However, for a broadcast scenario, the spiky function is generated in the conventional TR fashion on a small number of reserved tones on all spatial dimensions. The spiky function is then iteratively used to reduce the peaks which cross a given threshold. Simulation results are provided to show the performance of the proposed algorithm in both scenarios.

Chapter 4 presents a novel Least-Squares iterative PAR reduction algorithm for P2P and multi-user scenarios. For the P2P scenario, we again reserve the weakest eigenchannel and use it for PAR reduction of the remaining spatial dimensions. However, for the Least-

Squares approach, this eigenchannel is used to approximate and model the peak excursion on the remaining dimensions in a least-squares sense. This model function is then added to the transmit signal for PAR reduction. First, the system model of the proposed algorithm is presented followed by a mathematical modeling. Simulation results are provided for a performance analysis. The algorithm is thoroughly analyzed under mean power constraints. The capacity loss associated with the reserved channel is studied using random matrix theory. An analysis on the convergence behavior of the algorithm is provided as well. A comparison to Tone Reservation and Selected Mapping algorithms is presented, considering the same computational complexity. The idea is then extended to a multi-user broadcast scenario with an inactive user. The channel associated with the inactive user is used to approximate the peak excursions on the remaining spatial dimensions in a similar fashion. Simulation results are provided for the multi-user broadcast scenarios.

Trellis Shaping we concluded to be another promising PAR approach, which, however, still has some open problems in the optimum link to error correcting codes. Chapter 5 thus deals with optimization of an irregular LDPC code concatenated with Trellis Shaping for PAR reduction of single antenna OFDM. We first start with Trellis Shaping, especially Sign-Bit Shaping. A suitable metric in the Viterbi algorithm for the sign bit shaping is then presented. In order to decode the useful information of the shaping code sequence using soft-input soft-output decoding, we will discuss the use of a BCJR algorithm for the shaping bit sequence. We will next provide an optimization of the variable-node degree distribution for an irregular LDPC code exploiting the irregularities in the bit error probabilities of the individual bits inside an  $\mathcal{M}$ -QAM symbol. Based on the transfer function of the inverse syndrome former  $(\mathbf{H}^{-1})^T$ , we will also derive the bit error probability for the input bit sequence. At the end of the chapter, simulation results for regular and irregular LDPC codes concatenated with Trellis Shaping are provided.

Chapter 6 summarizes this thesis.

# Chapter 2

## Orthogonal Frequency Division Multiplexing

In 1948, Claude Shannon presented in his landmark paper [1] that error-free transmission over a communication channel is possible when  $R \leq C$ , where  $R$  is the transmission rate,  $C$  is the capacity of the channel, and the codeword length goes to infinity. Thus, achieving data rates that approach capacity over noisy channels require sophisticated transmission schemes. In order to provide high data rates reliably and flexibly, multicarrier modulation is nowadays making its way to modern-day communication systems. One such multicarrier transmission technique is Orthogonal Frequency Division Multiplexing (OFDM). The performance of an OFDM system can even be enhanced by using multiple antennas at the transmitter and the receiver. OFDM-based MIMO systems are thus promising techniques which offer high data rates with reliable transmission. MIMO-OFDM is making its way into high-speed communication technologies. However, a major drawback with OFDM is the high peak-to-average ratio (PAR), which, when not limited, would require a high power supply voltage and hence also high power dissipation. The rest of the chapter is organized as follows. In Section 2.1, we start with a brief history of OFDM, followed by the OFDM system model and its matrix representation. Section 2.2 provides an overview of MIMO systems and MIMO channel diagonalization followed by a description of the MIMO-OFDM system in Section 2.3. In Section 2.4, we will discuss the PAR problem statement, and will provide a mathematical as well as a statistical analysis of the problem. Consequences of high PAR are discussed in Section 2.5, whereas Section 2.6 provides an overview of some already existing PAR reduction approaches.

### 2.1 Orthogonal frequency division multiplexing

Orthogonal Frequency-Division Multiplexing is a multi-carrier transmission technique used for robust and reliable data transmission over noisy channels for high data rate systems. In OFDM a wide-band channel is divided into a set of ideally independent narrow-band parallel sub-channels orthogonal to each other. As the name indicates, it is a special form of Frequency Division Multiplexing (FDM) with orthogonal sub-carriers. Herein, we first provide a brief history of the development of OFDM systems before going into a detailed description. For a more comprehensive history of the development of OFDM systems, the readers are referred to [26], [27].

### 2.1.1 A brief history of OFDM

For the last two decades OFDM has gained quite some popularity in modern day communication systems. The concept of OFDM is, however, quite old with some early studies dating back to the mid sixties. The first noted paper on OFDM systems, synthesis of bandlimited orthogonal signals for multichannel data transmission, was published in 1966 by Chang [16]. Chang presented a principle of transmitting parallel data streams through linear bandlimited channels using orthogonal multiplexing without interchannel (ICI) and intersymbol interference (ISI). In 1967, Saltzberg [17] extended Chang's principle using Offset Quadrature Amplitude Modulation (OQAM) with multicarrier systems, i.e., OQAM-OFDM. Kineplex [18], KATHRYN [19], and ANDEFT [20] are few examples of the earliest modems which deployed OFDM.

A major breakthrough in the development of OFDM systems was the paper presented in 1971 by Weinstein and Ebert [21]. The authors applied the Discrete Fourier Transform (DFT) for modulation and demodulation of the baseband OFDM signal. Using DFT for modulation and demodulation reduced the complexity by eliminating the subcarrier oscillator bank. Another important milestone in the development of OFDM systems was the paper by Peled and Ruiz in 1980 [22]. The authors filled the empty guard space with a cyclic extension (cyclic prefix (CP)) of the OFDM signal, thus solving the orthogonality problem.

In 1980, Hirosaki [23] proposed per-carrier equalization in order to eliminate intersymbol interference and crosstalk for OQAM-OFDM systems. In 1981, Hirosaki [24] extended Saltzberg's work [17] OQAM-OFDM by a DFT implementation. In the late 80's, Alard and Lasalle [25] deployed OFDM for digital broadcasting for mobile receivers.

OFDM has seen a sudden increase in implementations in practical systems in the past 20 years. It has been deployed for broadband data communication in different technologies, e.g., Asymmetric Digital Subscriber Lines (ADSL), Very High-speed Digital Subscriber Lines (VHDSL). It is also adopted as a standard for Institute of Electrical and Electronic Engineers (IEEE) 802.11 a/ g/ n Wireless Local Area Networks (WLANs), IEEE 802.16 Wireless Metropolitan Area Networks (WMAN), IEEE 802.15.3a Wireless Personal Area Networks (WPAN) (MultiBank-OFDM).

Besides point-to-point data communications, OFDM has been implemented in various broadcast technologies (Coded OFDM (COFDM)) such as Digital Audio Broadcasting (DAB), Digital Video Broadcasting (DVB), High Definition Television (HDTV), digital Terrestrial Television broadcasting (dTTb), High Definition Digital Video Narrowband Emission (HD-DIVINE), System de Television En Radiodiffusion Numerique (STERNE).

### 2.1.2 Basic principle of OFDM modulation

In multicarrier modulation, a wideband channel is divided into a set of parallel narrow-band independent subchannels centered at different frequencies [2] [3]. The number of subchannels  $N$  are chosen such that the subchannel bandwidth  $B_N$  is smaller than the coherence bandwidth  $B_c$  of the channel. This will ensure that the subchannel will experience minimum Inter Symbol Interference (ISI) [3].

OFDM is an efficient implementation of the multicarrier modulation which allows the frequency spectra of the individual subcarriers to overlap, thereby, utilizing the available bandwidth much more efficiently. The transmitter model of an OFDM implementation

of the multicarrier modulation is shown in Fig. 2.1. The input data stream  $\mathbf{I}$  is arranged into  $N$  small data chunks. Each data chunk is mapped into an  $\mathcal{M}$ -ary QAM symbol  $X_n$ , ( $X_n = X_I(n) + jX_Q(n)$ , where  $n = 1, 2, \dots, N$ ) and  $\mathcal{M}$  is the constellation size. The sequence of QAM symbols is then passed through a serial-to-parallel converter. The parallel QAM symbols are modulated by a carrier frequency centered at  $f_n$ , occupying a bandwidth  $B_N$ . For an OFDM symbol of duration  $T$ , the spacing between two adjacent carriers is  $B_N = \Delta f = 1/T$ , thus, the total bandwidth is  $N\Delta f$ .

As shown in Fig. 2.1, the final OFDM signal is obtained by adding the  $N$  QAM symbols

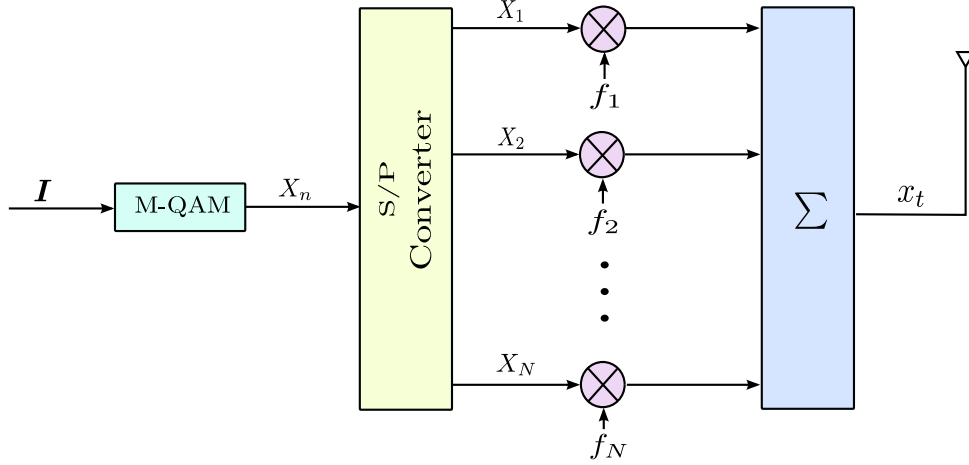


**Figure 2.1:** OFDM system

$[X_1, X_2, \dots, X_N]$ . With the  $n$ th QAM symbol at a carrier frequency  $f_n$ , i.e.,  $X_n e^{j2\pi f_n t}$ , the output OFDM signal can be written as

$$x(t) = \sum_{n=1}^N X_n e^{j2\pi f_n t} \quad t \in [0, T], \quad (2.1)$$

where  $x(t) = x_I(t) + jx_Q(t)$  is the complex OFDM symbol envelope with a symbol duration  $T$ .

### Orthogonality in OFDM

Two signals  $x_i(t)$  and  $x_j(t)$  are said to be orthogonal over a time period  $T$  if

$$\int_0^T x_i(t) x_j^*(t) dt = 0 \quad i \neq j, \quad (2.2)$$

In order to utilize the available bandwidth more efficiently, OFDM allows the individual subcarriers to overlap in an orthogonal fashion. The subcarriers will be orthogonal if the frequency spacing between the adjacent subchannels is  $\Delta f = 1/T$ , where  $T$  is the OFDM symbol duration. The  $n$ th orthogonal subcarrier is obtained as [3]

$$f_n = f_0 + \frac{n}{T}, \quad \text{where} \quad n = 0, 1, \dots, N-1, \quad (2.3)$$

with  $f_0$  being the reference carrier frequency. During the rectangular time window of duration  $T$ , each of the subcarriers is equivalent to a sinc function ( $\sin x/x$ ) in frequency domain as shown in Fig. 2.2 [32]. As shown in Fig. 2.2, at orthogonal frequencies, the individual subcarriers have maxima that line up with the nulls of the other subcarriers.

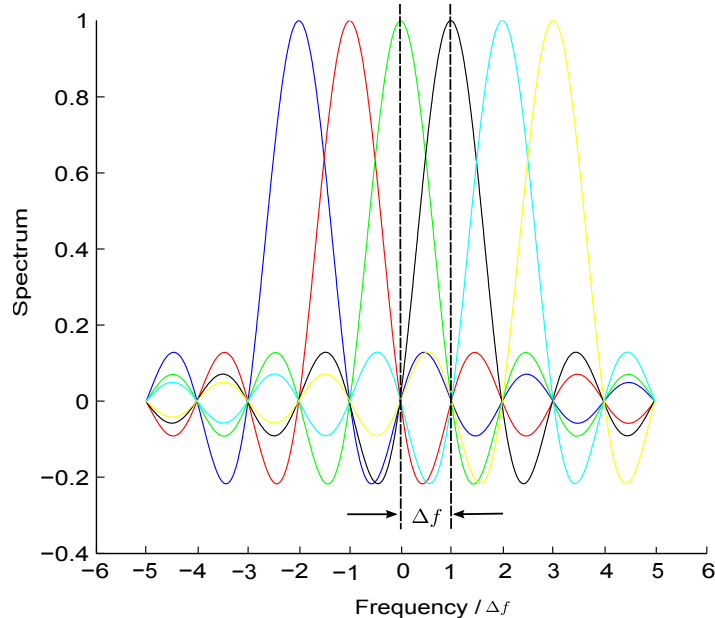


**Figure 2.2:** OFDM symbol

### Pros and cons of OFDM

A major advantage of OFDM is that the symbol duration is much greater than the delay spread of the channel, alternatively the subchannel bandwidth is much smaller than the coherence bandwidth of the channel, thus making each subchannel less susceptible to channel-induced dispersions. A disadvantage of multicarrier transmission, which stopped it to be deployed in practical systems, was the complexity of the system as compared to the conventional single carrier systems. For the  $N$  subchannels, it required a number of  $N$  modulators and transmit filters at the transmitter and  $N$  number of demodulators and receive filters at the receiver. It was till 1971 when Weinstein and Ebert [21] proposed-DFT based OFDM system. The authors employed DFT for modulation and demodulation of baseband OFDM signals. This approach considerably reduced the complexity. The complexity is even further reduced from  $N^2$  operations into  $N/2 \log N$  operations, using Fast Fourier Transform (FFT) algorithm [11]. The next section provides a brief overview of DFT (FFT) based OFDM.

### 2.1.3 Discrete-time OFDM system model

Hereafter, we will consider a discrete-time OFDM system deploying Inverse Discrete Fourier Transform (IDFT) and Discrete Fourier Transform (DFT) for modulation and demodulation, respectively. Before going into the system model, we recall the formulas for DFT/IDFT transformations.

## Discrete and Inverse Discrete Fourier Transform

DFT and IDFT are transformation techniques used to transform a signal from time domain to frequency domain and vice versa. The IDFT (Inverse Fast Fourier Transform (IFFT)) of an information sequence  $\mathbf{X} = [X_n]$ ,  $n = 1, 2, \dots, N$  in frequency domain<sup>1</sup> is given as

$$[x_k] = \text{IDFT}\{[X_n]\} = \frac{1}{\sqrt{N}} \sum_{n=1}^N X_n e^{j \frac{2\pi nk}{N}}, \quad 1 \leq k \leq N, \quad (2.4)$$

where  $x_k$  is the  $k$ th sample of the discrete time sequence  $\mathbf{x} = [x_k]$ ,  $k = 1, 2, \dots, N$ , and  $N$  is the frame size. The frequency domain information sequence  $[X_n]$  can be recovered from the discrete time sequence  $[x_k]$  by taking the DFT (Fast Fourier Transform (FFT)) over  $[x_k]$  given as,

$$[X_n] = \text{DFT}\{[x_k]\} = \frac{1}{\sqrt{N}} \sum_{k=1}^N x_k e^{-j \frac{2\pi nk}{N}}, \quad 1 \leq n \leq N. \quad (2.5)$$

The DFT modulator is used to correlate the sinusoidal basis functions to the input signal. The correlation of the input signal with the basis functions results in a peak at a particular frequency while nullify the energies from other subcarriers at that frequency [2].

## System model

A block diagram of a baseband DFT-based OFDM system is shown in Fig. 2.3, the information bit stream  $\mathbf{I}$  is mapped to a set of size  $N$   $\mathcal{M}$ -ary QAM symbols,  $\mathbf{X} = [X_n]$ ,  $n = 1, 2, \dots, N$ , sent over each subchannel. The elements  $X_n$  are complex numbers, i.e.,  $X_n = X_I(n) + jX_Q(n)$ , which specifies an  $\mathcal{M}$ -ary QAM constellation with  $\mathcal{M}$  signal points

$$X_n \in \{\pm X_I(n) \pm jX_Q(n)\}, \quad \text{where} \quad X_{I/Q}(n) \in \left\{ \frac{1}{2}, \frac{3}{2}, \dots, \frac{\sqrt{M}-1}{2} \right\}. \quad (2.6)$$

The selection of the  $\mathcal{M}$ -ary QAM constellation solely depends on the data rate and the channel properties. An important feature of OFDM is that it is not necessarily required to use the same QAM constellation for all data symbols  $[X_n]$ . Different modulation schemes can be used for the subchannels using optimization algorithms known as *bit loading and power loading* [30, 36] (and the references therein).

After mapping, the  $\mathcal{M}$ -ary QAM symbols  $[X_n]$  are passed through a serial-to-parallel (S/P) converter. The S/P converter, converts the serial symbol stream  $[X_n]$  (row vector) into a parallel stream  $[X_n]$  (column vector), i.e.,  $[X_n] \rightarrow [X_n]^T$ , where  $T$  stands for transpose. The OFDM frame is transformed into time domain using an IDFT (IFFT) modulator, defined as

$$[x_k] = \text{IDFT}\{[X_n]\} = \frac{1}{\sqrt{N}} \sum_{n=1}^N X_n e^{j \frac{2\pi nk}{N}}, \quad k = 1, 2, \dots, N, \quad (2.7)$$

---

<sup>1</sup>we will talk about “frequency” domain instead of the formally correct “DFT” domain, since it is very common.

where  $x_k$  is the  $k$ th sample and  $N$  is the block length of the OFDM frame,  $\mathbf{x} = [x_k] = [x_1, x_2, \dots, x_N]$ .

After the IDFT (IFFT), the time domain samples are converted into a serial data stream using a parallel-to-serial (P/S) converter. A Cyclic Prefix (CP) of length  $\mu$  is then appended to the front of the serial data stream. The CP is a periodic extension of the time domain OFDM signal obtained by prepending the last  $\mu \geq l_{ch} - 1$ , where  $l_{ch}$  is the assumed channel length (delay spread), samples of the signal to the front of the symbol as shown in Fig. 2.4, i.e.,

$$\tilde{\mathbf{x}} = [\tilde{x}_k] = [x_{N-\mu}, x_{N-\mu+1}, \dots, x_N, x_1, x_2, \dots, x_N]. \quad (2.8)$$

The use of the CP is two fold beneficial,

1. helps to mitigate the effect of channel dispersion which results in Inter Symbol Interference (no ISI),
2. converts the linear convolution of the input signal with the channel impulse response equivalent to a circular convolution (converts the convolution of the input signal with the channel impulse response to a multiplication in DFT domain).

After prepending the CP, the OFDM symbol  $[\tilde{x}_k]$  is transmitted over a discrete-time channel, with a channel impulse response  $H(z)$  (discussed in Section 2.1.4). The channel adds Additive White Gaussian Noise (AWGN)  $\mathbf{w} \sim \mathcal{CN}(0, \sigma_n^2)$ .

As shown in Fig. 2.3, the receiver first removes the cyclic prefix from the received signal  $[\tilde{y}_k]$ , resulting in  $\mathbf{y} = [y_k]$ . After serial-to-parallel conversion, the time domain signal is demodulated via the DFT (FFT), i.e.,

$$[Y_n] = \text{DFT}\{[y_k]\} = \frac{1}{\sqrt{N}} \sum_{k=1}^N [y_k] e^{-j \frac{2\pi nk}{N}}, \quad n = 1, 2, \dots, N, \quad (2.9)$$

where  $[Y_n] = \mathbf{Y} = [Y_1, Y_2, \dots, Y_N]$  is the DFT vector of the received symbols. As mentioned earlier, with a CP longer than the channel impulse response, the linear convolution of the input signal with the discrete-time channel having a finite impulse response is converted into a circular convolution (according to the DFT properties, a convolution in time domain equals to a multiplication in frequency domain). After the DFT (FFT), the received symbols are demodulated (de-mapped) using a frequency domain equalizer (EQ) which equalizes the received data by a multiplication with the inverse complex channel coefficients.

### 2.1.4 Channel model

Throughout this work, if not otherwise stated, we will consider perfect Channel State Information (CSI) both at the transmitter and the receiver. We consider a discrete-time channel, as chosen by the authors in [33], defined by a polynomial in the  $z$  domain as

$$H(z) = \sum_{k=0}^{l_H-1} h_k \cdot z^{-k}, \quad (2.10)$$

where  $l_H$  is the channel length and  $h_k$  is the  $k$ th channel tap.

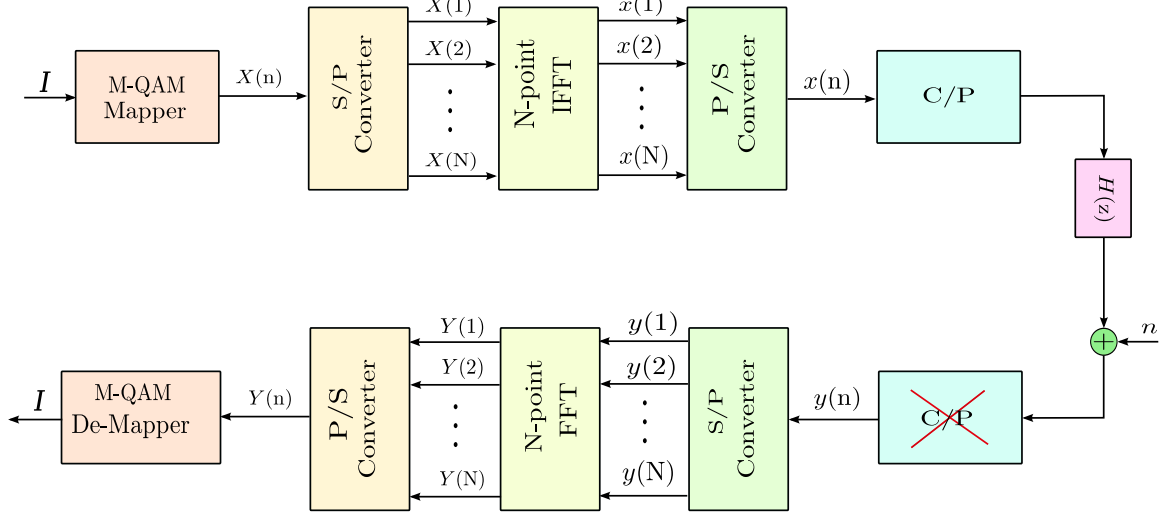


**Figure 2.3:** Transmitter and receiver structures of an OFDM system

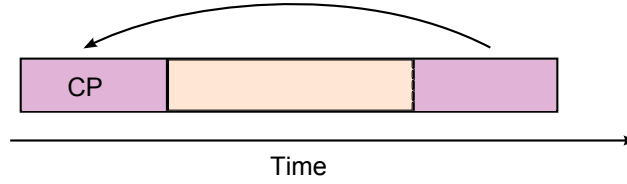


**Figure 2.4:** Cyclic extension of an OFDM symbol

### 2.1.5 OFDM matrix representation

A matrix representation will provide a deeper insight into the channel orthogonalization using a CP. As shown in the Fig. 2.3, the input data sequence  $\mathbf{X} = [X_n]$  is transformed into a time domain sequence  $\mathbf{x}$  using an IDFT (IFFT) modulator, defined as

$$\mathbf{x} = \mathbf{F}^H \mathbf{X}, \quad (2.11)$$

where  $(\cdot)^H$  stands for Hermitian, and  $\mathbf{F}$  is the  $N \times N$  Vandermonde DFT matrix (normalized),

$$\mathbf{F} = 1/\sqrt{N} \begin{pmatrix} 1 & 1 & 1 & 1 & 1 \\ 1 & \omega_N & \omega_N^2 & \dots & \omega_N^{N-1} \\ 1 & \omega_N^2 & \omega_N^4 & \dots & \omega_N^{2(N-1)} \\ \vdots & \ddots & \ddots & \dots & \dots \\ 1 & \omega_N^{N-1} & \dots & \dots & \omega_N^{(N-1)^2} \end{pmatrix}, \quad (2.12)$$

where  $\omega = e^{j\frac{2\pi}{N}}$ , and  $1/\sqrt{N}$  is to make  $\mathbf{F}$  a unitary matrix such that

$$\mathbf{F} \cdot \mathbf{F}^H = \mathbf{I}. \quad (2.13)$$

After appending a cyclic prefix of length  $\mu \geq l_{ch} - 1$  to  $\mathbf{x}$ ,  $\tilde{\mathbf{x}} = [\tilde{x}_k]$  is transmitted over the channel, where it is filtered by the channel with the channel impulse response  $h_n$ ,  $n = 1, 2, \dots, \mu$ , and adds additive noise  $\mathbf{w}$ . The convolutional equation for the received

vector  $\tilde{\mathbf{y}}$ , in matrix form can be written as

$$\tilde{\mathbf{y}} = \begin{pmatrix} h_\mu & h_{\mu-1} & \dots & h_0 & 0 & \dots & 0 \\ 0 & h_\mu & h_{\mu-1} & \dots & h_0 & \dots & 0 \\ \vdots & \vdots & \ddots & \vdots & \ddots & \ddots & \vdots \\ \vdots & \ddots & \vdots & \ddots & \vdots & \ddots & \vdots \\ \vdots & \vdots & \ddots & \vdots & \ddots & \ddots & \vdots \\ \vdots & \ddots & \vdots & \ddots & \vdots & \ddots & \vdots \\ \vdots & \ddots & \vdots & \ddots & \vdots & \ddots & \vdots \\ 0 & \dots & 0 & h_\mu & h_{\mu-1} & \dots & h_0 \end{pmatrix} \begin{pmatrix} x_{N-1-\mu} \\ \vdots \\ x_{N-2} \\ x_{N-1} \\ x_0 \\ x_1 \\ \vdots \\ x_{N-1} \end{pmatrix} + \begin{pmatrix} w_{N-1-\mu} \\ \vdots \\ \vdots \\ w_{N-2} \\ w_{N-1} \\ w_0 \\ \vdots \\ w_{N-1} \end{pmatrix}, \quad (2.14)$$

which in more compact form can be written as

$$\tilde{\mathbf{y}} = \mathbf{H} \tilde{\mathbf{x}} + \mathbf{w}. \quad (2.15)$$

Discarding the first  $\mu$  samples of the received sequence  $\tilde{\mathbf{y}}$ , i.e.,  $y_{N-\mu}, y_{N-\mu+1} \dots y_N$ , which are corrupted from the previous block, the received symbols  $\mathbf{y} = [y_k]$  in matrix notation can equivalently be written as

$$\begin{pmatrix} y_1 \\ y_2 \\ \vdots \\ \vdots \\ \vdots \\ \vdots \\ y_N \end{pmatrix} = \begin{pmatrix} h_0 & 0 & \dots & 0 & h_\mu & \dots & h_1 \\ h_1 & h_0 & 0 & \dots & h_{\mu-1} & \dots & \vdots \\ \vdots & \vdots & \ddots & & \ddots & \ddots & h_\mu \\ \vdots & \vdots & \ddots & & \ddots & \ddots & \vdots \\ h_\mu & \dots & h_0 & 0 & 0 & \dots & 0 \\ \vdots & \vdots & \ddots & & \ddots & \ddots & \vdots \\ 0 & 0 & \dots & h_{\mu-1} & \dots & h_0 & 0 \\ 0 & 0 & \dots & h_\mu & \dots & h_1 & h_0 \end{pmatrix} \begin{pmatrix} x_1 \\ x_2 \\ x_3 \\ \vdots \\ \vdots \\ x_{N-1} \\ x_N \end{pmatrix} + \begin{pmatrix} w_1 \\ w_2 \\ w_3 \\ \vdots \\ \vdots \\ w_{N-1} \\ w_N \end{pmatrix}, \quad (2.16)$$

which in a compact form can be formulated as

$$\mathbf{y} = \tilde{\mathbf{H}} \mathbf{x} + \mathbf{w}, \quad (2.17)$$

where  $\tilde{\mathbf{H}}$  is an  $N \times N$  circulant convolution channel matrix over the  $N$  samples. Using DFT and IDFT, the circulant channel matrix  $\tilde{\mathbf{H}}$  can be diagonalized as

$$\tilde{\mathbf{H}} = \mathbf{F}^H \mathbf{\Lambda} \mathbf{F}. \quad (2.18)$$

where  $\mathbf{\Lambda}$  is an  $N \times N$  diagonal matrix with the complex channel gains.  $\mathbf{y}$  is then transformed into frequency domain using the DFT to get  $\mathbf{Y}$ , i.e.,

$$\mathbf{Y} = \text{DFT}\{\mathbf{y}\} = \mathbf{F} \mathbf{y}. \quad (2.19)$$

$$\mathbf{Y} = \mathbf{F} \left[ \tilde{\mathbf{H}} \mathbf{x} + \mathbf{w} \right], \quad (2.20)$$

putting the values of  $\mathbf{x} = \mathbf{F}^H \mathbf{X}$  (from Eq. (2.11)), and  $\tilde{\mathbf{H}} = \mathbf{F}^H \mathbf{\Lambda} \mathbf{F}$  (from Eq. (2.18)), Eq. (2.19) can be reformulated as

$$\mathbf{Y} = \underbrace{\mathbf{F} \cdot \mathbf{F}^H}_{\mathbf{H}} \cdot \underbrace{\mathbf{\Lambda} \cdot \mathbf{F} \cdot \mathbf{F}^H}_{\mathbf{x}} \cdot \mathbf{X} + \mathbf{F} \mathbf{w}, \quad (2.21)$$

Simplifying Eq. (2.21) with  $\mathbf{F}\mathbf{F}^H = \mathbf{F}^H\mathbf{F} = \mathbf{I}$ , we have

$$\mathbf{Y} = \mathbf{\Lambda} \mathbf{X} + \tilde{\mathbf{w}}, \quad (2.22)$$

where  $\mathbf{X}$  is the input sequence and  $\mathbf{\Lambda}$  is a diagonal matrix with complex channel coefficients in DFT domain, which in matrix form can be written as

$$\mathbf{Y} = \begin{pmatrix} \lambda_1 & 0 & 0 & 0 \\ 0 & \lambda_2 & 0 & \vdots \\ \vdots & \ddots & \dots & 0 \\ 0 & 0 & \dots & \lambda_N \end{pmatrix} \begin{pmatrix} X_1 \\ X_2 \\ \vdots \\ X_N \end{pmatrix} + \tilde{\mathbf{w}}, \quad (2.23)$$

$\mathbf{F}$  is unitary thus  $\tilde{\mathbf{w}}$  has the same circularly symmetric distribution as  $\mathbf{w}$ . OFDM thus decomposes a wide-band channel into a set of  $N$  orthogonal independent narrow-band subchannels with the help of an IDFT/DFT pair and the cyclic prefix.

Besides the available spectrum, modern day communication systems are trying to use other available resources, e.g., space and time, as well. One of such techniques which has gained a lot of popularity is Multiple-Input Multiple-Output (MIMO) transmission. MIMO systems deploy multiple antennas at the transmitter and the receiver. OFDM together with MIMO is making its way into current communication systems. The next section will provide a brief overview of MIMO systems, followed by an OFDM based MIMO system model.

## 2.2 Multi-antenna systems

Multi-antenna systems mean to provide multiple antennas at the transmitters and/or at the receivers. Multiple antennas yield spatial diversity, which is used to enhance the system performance by reliable data transmission with high data rates, increased diversity, and reduced interference. Subsequently, we will consider multi-antenna systems equipped with  $M_t$  transmit and  $M_r$  receive antennas, respectively. The multiple antennas are practically deployed in three different scenarios,

1. Multiple-Input Multiple-Output (MIMO) or Point-to-Point (P2P) scenario.
2. Multiple-Input Single-Output (MISO), e.g., in a multi-user uplink scenario.
3. Single-Input Multiple-Output (SIMO), e.g., in a multi-user downlink scenario.

### 2.2.1 Point-to-point scenario

A point-to-point P2P MIMO system deploying  $M_t$  transmit and  $M_r$  receive antennas, respectively, as shown in Fig. 2.5. For P2P scenarios, signal processing is possible both at the transmitter and the receiver ends. Subsequently, we will consider a single user P2P MIMO system equipped with an equal number of antennas at both ends, i.e.,  $M_t = M_r$ . With perfect CSI at the transmitter, we will consider transmitter-sided precoding and receiver-sided post processing of the received data. For precoding and postprocessing, diagonalization of the channel gain matrix  $\mathbf{H}$  is discussed subsequently.

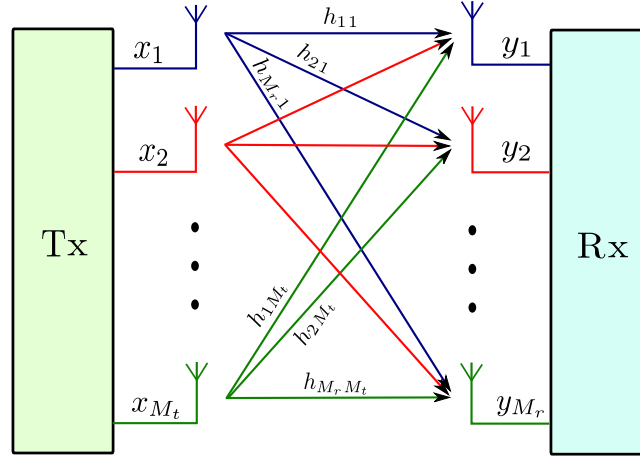


Figure 2.5: Point-to-point MIMO system model



Figure 2.6: Signal flow diagram of a P2P MIMO system model

#### P2P MIMO system model and channel diagonalization

Consider a P2P MIMO system with  $M_t$  transmit and  $M_r$  receive antennas as shown in Fig. 2.5. Let  $\mathbf{x} = [x_t] = [x_1, x_2, \dots, x_{M_t}]^T$  be the input data symbols to the MIMO system.  $\mathbf{x}$  is transmitted through the channel with channel impulse response  $\mathbf{H}(z)$ . In matrix form, the output vector  $\mathbf{y} = [y_r] = [y_1, y_2, \dots, y_{M_r}]^T$  at the receiver is formulated as

$$\begin{pmatrix} y_1 \\ y_2 \\ \vdots \\ y_{M_r} \end{pmatrix} = \begin{pmatrix} h_{11} & h_{12} & \dots & h_{1M_t} \\ h_{21} & h_{22} & \dots & h_{2M_t} \\ \vdots & & \ddots & \vdots \\ h_{M_r 1} & h_{M_r 2} & \dots & h_{M_r M_t} \end{pmatrix} \begin{pmatrix} x_1 \\ x_2 \\ \vdots \\ x_{M_t} \end{pmatrix} + \begin{pmatrix} w_1 \\ w_2 \\ \vdots \\ w_{M_r} \end{pmatrix} \quad (2.24)$$

In more compact form, we write

$$\mathbf{y} = \mathbf{H} \mathbf{x} + \mathbf{w}, \quad (2.25)$$

where  $\mathbf{H}$  is the  $M_r \times M_t$  channel gain matrix with coefficients  $h_{ij}$  from the  $j$ th transmit antenna to the  $i$ th receive antenna,  $\mathbf{x}$  and  $\mathbf{y}$  are  $M_t$ - and  $M_r$ -dimensional column vectors,

respectively, and  $\mathbf{w} \sim \mathcal{CN}(0, \sigma_r^2)$  is an  $M_r \times 1$  complex white Gaussian noise vector with zero mean and variance  $\sigma_r^2$ . Using singular value decomposition (SVD), the channel gain matrix  $\mathbf{H}$  can be rephrased as

$$\mathbf{H} = \mathbf{U}\mathbf{\Lambda}\mathbf{V}^H, \quad (2.26)$$

where  $\mathbf{U}$  and  $\mathbf{V}$  are unitary matrices such that  $\mathbf{U}^H\mathbf{U} = \mathbf{V}^H\mathbf{V} = \mathbf{I}$  and  $\mathbf{\Lambda}$  is a diagonal matrix with singular values  $\delta_{ij} = [\delta_{11}, \delta_{22}, \dots, \delta_{R_H R_H}, 0, \dots, 0]$  of  $\mathbf{H}$  where  $R_H \leq \min(M_r M_t)$  is the rank of the  $\mathbf{H}$  matrix. The singular values are usually sorted in a descending order, i.e.,  $\delta_{11} \geq \delta_{22} \geq \dots \geq \delta_{R_H R_H}$ .

For a P2P MIMO system with perfect CSI, to diagonalize the channel, the input data vector to the transmit antennas is obtained by precoding the input data symbols  $\tilde{\mathbf{x}}$  using the preprocessing matrix  $\mathbf{V}$ , i.e.,  $\mathbf{x} = \mathbf{V} \tilde{\mathbf{x}}$ . The received signal is postprocessed by  $\mathbf{U}^H$  as shown in Fig. 2.6, i.e.,

$$\tilde{\mathbf{y}} = \mathbf{U}^H \mathbf{y} = \mathbf{U}^H (\mathbf{H} \mathbf{x} + \mathbf{w}). \quad (2.27)$$

Herewith, Eq. (2.27) is reformulated as

$$\tilde{\mathbf{y}} = \underbrace{\mathbf{U}^H \cdot \mathbf{U}}_{\mathbf{I}} \cdot \underbrace{\mathbf{\Lambda} \cdot \mathbf{V}^H \cdot \mathbf{V}}_{\mathbf{H}} \cdot \tilde{\mathbf{x}} + \mathbf{U}^H \mathbf{w}, \quad (2.28)$$

which simplifies to

$$\tilde{\mathbf{y}} = \mathbf{\Lambda} \cdot \mathbf{x} + \tilde{\mathbf{w}}, \quad (2.29)$$

where  $\mathbf{\Lambda}$  is a diagonal matrix containing the singular values  $\delta_k$  of  $\mathbf{H}$  on the diagonals and zeros elsewhere and  $\tilde{\mathbf{w}}$  is the noise vector having the same statistical properties as  $\mathbf{w}$  [3]. For an  $M \times M$  channel matrix, omitting  $\tilde{\mathbf{w}}$ , Eq. (2.29) in matrix notation can be expressed as

$$\begin{pmatrix} \tilde{y}_1 \\ \tilde{y}_2 \\ \vdots \\ \tilde{y}_M \end{pmatrix} = \begin{pmatrix} \delta_{1,1} & 0 & 0 & 0 \\ 0 & \delta_{2,2} & 0 & 0 \\ 0 & 0 & \ddots & 0 \\ 0 & 0 & 0 & \delta_{M,M} \end{pmatrix} \begin{pmatrix} \tilde{x}_1 \\ \tilde{x}_2 \\ \vdots \\ \tilde{x}_M \end{pmatrix}, \quad (2.30)$$

where  $\tilde{x}_i$ , and  $\tilde{y}_i$  are the input and the output at the  $i$ th antenna, respectively.  $\delta_{i,i}$  are the gains of the eigenchannels. Equation (2.30) shows a parallel decomposition of the channel gain matrix  $\mathbf{H}$  into  $M$  independent channels with  $\mathbf{\Lambda}$  being the gain matrix.

## 2.2.2 Multi-user uplink and downlink scenarios

Multi-user uplink and downlink scenarios are shown in figures 2.7 and 2.8, respectively. As is obvious from these figures, in multi-user scenarios, a central base station (BS), deploying multiple antennas, communicates with independent mobile users having one or more antennas. Subsequently, we will consider a central base station equipped with multiple antennas communicating with  $U$  users, each one equipped with a single antenna. Moreover, we assume that the number of antennas at the central base station equals the number of mobile terminals  $U$ .

In multi-user scenarios, the mobile users are usually distant from each other, thus, there will typically be no coordination amongst them. The majority of the signal processing operations are hence performed at the central base station. For the downlink scenario,

where the central base station transmits data to the mobile users (point-to-multipoint or broadcast channel (BC)), we will consider transmitter-sided precoding. In the case of uplink scenarios, where the BS is operating as a receiver of the independent data streams from the mobile stations (multipoint-to-point or multiple access channel (MAC)), we consider the receiver-sided postprocessing. Moreover, we assume perfect channel state information at the transmitter as well as at the receiver.

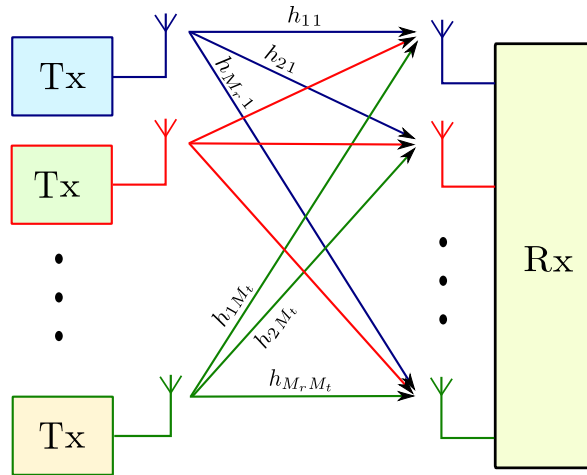


Figure 2.7: Multipoint-to-point MIMO system model

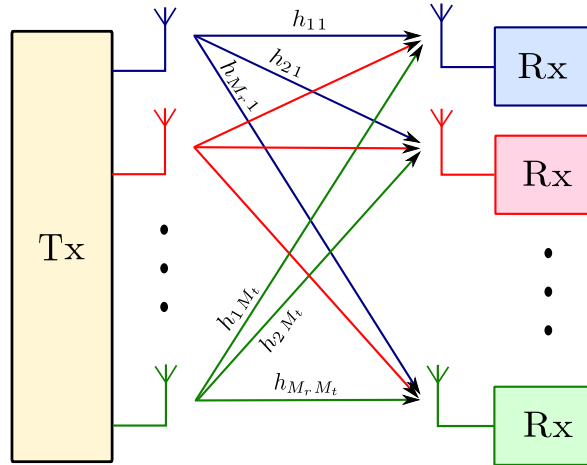


Figure 2.8: Point-to-multipoint MIMO system model

**Precoding and postprocessing for the downlink and the uplink scenarios and QR decomposition of the channel matrix  $H$**

**Multi-users Multiple Access Channel (MAC):**

Let  $M_r$  be the total number of receive antennas deployed at the central base station and let  $U$  be the total number of user supported by the base station, each one equipped with a single transmit antenna, i.e.,  $U_t = 1$ . Then, the total number of transmit antennas  $M_t$

is given as  $M_t = \sum U_t = U$ . For the uplink case, let us suppose  $\mathbf{x} = [x_1, x_2, \dots, x_{M_t}]$ , is a  $1 \times U$  vector of the input data symbol. These symbols when transmitted over the channel are filtered by the channel with a channel gain matrix  $\mathbf{H}$  and the channel adds additive noise  $\mathbf{w}$ . The received signal  $\mathbf{y} = [y_1, y_2, \dots, y_{M_r}]$  at the base station can be written as

$$\mathbf{y} = \mathbf{H} \mathbf{x} + \mathbf{w} , \quad (2.31)$$

where  $\mathbf{w}$  is complex additive white Gaussian noise with zero mean and  $\sigma_n$  variance. For an  $M_t = M_r = M$ , Eq. (2.31) in matrix notation can be rephrased as

$$\begin{pmatrix} y_1 \\ y_2 \\ \vdots \\ y_M \end{pmatrix} = \begin{pmatrix} h_{11} & h_{12} & \dots & h_{1M} \\ h_{21} & h_{22} & \dots & h_{2M} \\ \vdots & & \ddots & \vdots \\ h_{M1} & h_{M2} & \dots & h_{MM} \end{pmatrix} \begin{pmatrix} x_1 \\ x_2 \\ \vdots \\ x_M \end{pmatrix} + \begin{pmatrix} w_1 \\ w_2 \\ \vdots \\ w_M \end{pmatrix} , \quad (2.32)$$

where  $\mathbf{H}$  is the  $M \times M$  channel gain matrix,  $\mathbf{x}$  is  $1 \times M$  column input vector,  $\mathbf{y}$  is  $1 \times M$  column output vector and  $\mathbf{w}$  is a  $1 \times M$  noise vector.

For the uplink scenario with  $M_t = M_r = M$ , the channel gain matrix  $\mathbf{H}_{M \times M}$  can be rephrased using QR decomposition as

$$\mathbf{H} = \mathbf{Q} \cdot \mathbf{R} , \quad (2.33)$$

where  $\mathbf{Q}$  is a unitary matrix such that  $\mathbf{Q}^H \mathbf{Q} = \mathbf{I}$  and  $\mathbf{R}$  is an upper triangular matrix which can be expressed as

$$\begin{pmatrix} R_{11} & R_{12} & \dots & R_{1M} \\ 0 & R_{22} & \dots & R_{2M} \\ 0 & \ddots & \ddots & \vdots \\ 0 & 0 & \dots & R_{MM} \end{pmatrix} . \quad (2.34)$$

Performing a spatial equalization at the base station with a postprocessing matrix  $\mathbf{Q}^H$ , Eq. (2.31) then leads to

$$\tilde{\mathbf{y}} = \mathbf{Q}^H \mathbf{y} = \mathbf{Q}^H \mathbf{H} \mathbf{x} + \mathbf{Q}^H \mathbf{w} \quad (2.35)$$

$$\tilde{\mathbf{y}} = \underbrace{\mathbf{Q}^H \mathbf{Q}}_{\mathbf{I}} \mathbf{R} \mathbf{x} + \mathbf{Q}^H \mathbf{w} , \quad (2.36)$$

which in simple form can be written as

$$\tilde{\mathbf{y}} = \mathbf{R} \mathbf{x} + \tilde{\mathbf{w}} , \quad (2.37)$$

where  $\tilde{\mathbf{w}}$  is the noise vector after post processing, however, its distribution is the same as  $\mathbf{w}$ . Omitting  $\tilde{\mathbf{w}}$ , Eq. (2.37) in matrix form can be expressed as

$$\begin{pmatrix} \tilde{y}_1 \\ \tilde{y}_2 \\ \vdots \\ \tilde{y}_M \end{pmatrix} = \begin{pmatrix} R_{11} & R_{12} & \dots & R_{1M} \\ 0 & R_{22} & \dots & R_{2M} \\ 0 & \ddots & \ddots & \vdots \\ 0 & 0 & \dots & R_{MM} \end{pmatrix} \cdot \begin{pmatrix} x_1 \\ x_2 \\ \vdots \\ x_M \end{pmatrix} . \quad (2.38)$$

Using Eq. (2.38), the base station applies a back-substitution approach to get an estimate of the transmitted symbols.

### Multi-users Broadcast Channel (BC):

For multi-users downlink scenarios we will assume transmitter-sided (central base station) precoding. Let  $M_t$  be the total number of transmit antennas and let  $U$  be the total number of users with  $U_r = 1$ . The total number of receive antennas  $M_r = \sum U_r = U$ . Moreover, for simplicity, we consider  $M_t = M_r = M$ . For a downlink scenario with transmitter-sided precoding, QR decomposition is applied to the transpose of the channel matrix  $\mathbf{H}^H$ , i.e.,

$$\mathbf{H}^H = \mathbf{Q} \mathbf{R} \quad \Rightarrow \quad \mathbf{H} = \mathbf{R}^H \mathbf{Q}^H . \quad (2.39)$$

At the base station, the input data vector  $\tilde{\mathbf{x}}$  are preprocessed using the preprocessing matrix  $\mathbf{Q}$ , i.e.,  $\mathbf{x} = \tilde{\mathbf{x}} \mathbf{Q}$ . The received vector  $\mathbf{y}$  is given as

$$\mathbf{y} = \mathbf{H} \mathbf{x} + \mathbf{w} . \quad (2.40)$$

Now replacing  $\mathbf{x}$  and  $\mathbf{H}$ , Eq. (2.40) leads to

$$\mathbf{y} = \mathbf{R}^H \underbrace{\mathbf{Q}^H \mathbf{Q}}_{\mathbf{I}} \tilde{\mathbf{x}} + \mathbf{w} , \quad (2.41)$$

which, in a simple form, can be written as

$$\mathbf{y} = \mathbf{R}^H \tilde{\mathbf{x}} + \mathbf{w} , \quad (2.42)$$

where  $\mathbf{R}^H$  is a lower triangular matrix. In order to have interference free reception at mobile terminals, the input data vector  $\mathbf{X}$  is first precoded such that the following equality holds:

$$\text{diag}(\mathbf{R}^H) \mathbf{x} = \mathbf{R}^H \tilde{\mathbf{x}} . \quad (2.43)$$

The  $i$ th element of  $\tilde{\mathbf{x}}$ , i.e.,  $\tilde{x}_i$  is then defined as

$$\tilde{x}_i = \Gamma_M \left[ \tilde{x}_i - \sum_{j=1}^{i-1} \frac{R_{j,i}}{R_{i,i}} \cdot \tilde{x}_j \right] , \quad (2.44)$$

where  $\Gamma_M$  is the modulo operation of Tomlinson-Harashima precoding [12] [29].

## 2.3 OFDM-based MIMO systems

Due to its ease in implementation, robustness against channel impairments, and flexibility, OFDM is the choice of modern day communication systems. Moreover, the system performance can further be enhanced when considering OFDM together with MIMO. MIMO-OFDM is thus a promising technique for current high-speed communication systems offering high data rates with reliable transmissions. It uses multiple transmitters and multiple receivers for transmission and reception of OFDM frames, respectively. A general transceiver structure of a point-to-point MIMO-OFDM is shown in Fig. 2.9.

We consider a P2P MIMO-OFDM system with  $M_t$  transmit and  $M_r$  receive antennas (for

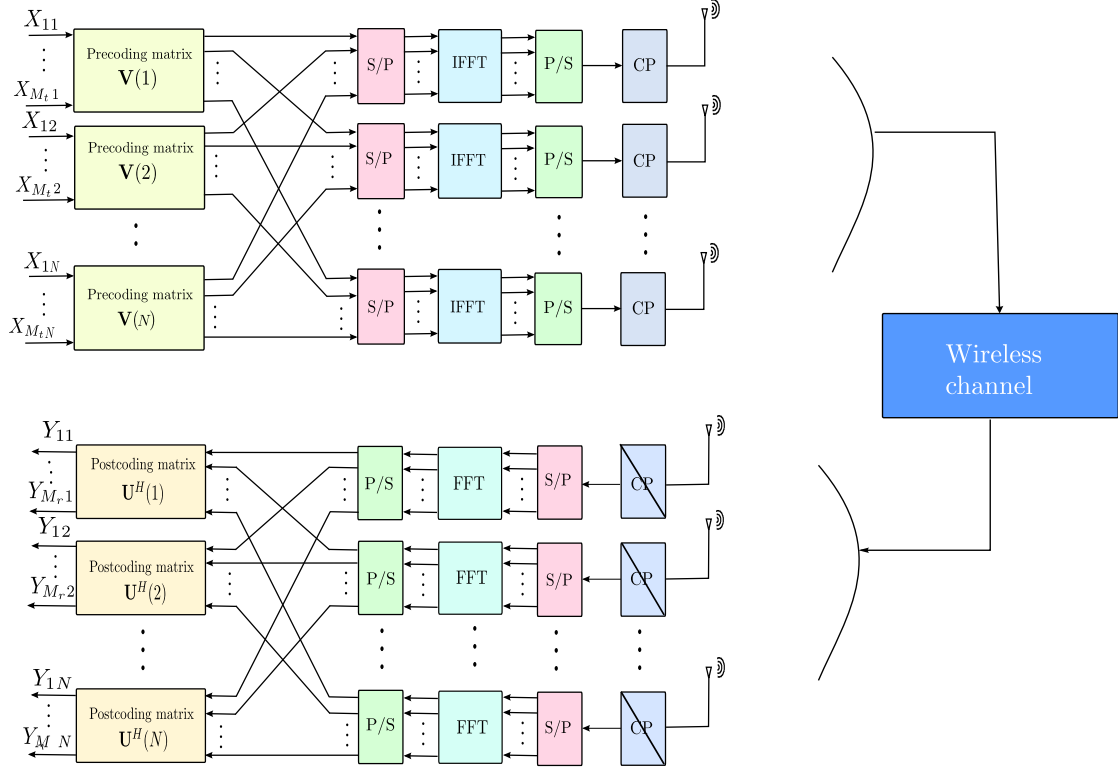


**Figure 2.9:** Block diagram of MIMO OFDM

convenience, we assume  $M_t = M_r = M$ ). Let  $\mathbf{X}(n) = [X_1(n), X_2(n), \dots, X_M(n)]^T$  be an input vector, where  $X_\mu(n)$  is the input symbol at the  $\mu$ th,  $\mu = 1, 2, \dots, M$ , spatial channel and the  $n$ th carrier. With transmitter-sided precoding,  $\mathbf{X} = [\mathbf{X}(1) \ \mathbf{X}(2) \ \dots \ \mathbf{X}(N)]$  is pre-processed using preprocessing matrices  $\mathbf{V} = [\mathbf{V}(1) \ \mathbf{V}(2) \ \dots \ \mathbf{V}(N)]$  and converted into a parallel data stream using a serial to parallel converter. After the IFFT, the time-domain signal  $\mathbf{x} = [\mathbf{x}(1) \ \mathbf{x}(2) \ \dots \ \mathbf{x}(N)]$  is padded with a cyclic prefix (CP) to mitigate the effect of inter-symbol interference (ISI). This signal is transmitted over a MIMO channel with a channel matrix  $\mathbf{H} = [\mathbf{H}(1) \ \mathbf{H}(2) \ \dots \ \mathbf{H}(N)]$ . At the receiver, reverse operations are performed to obtain an estimate of the transmitted signal. Let  $\mathbf{y}(n) = [y_1(n), y_2(n), \dots, y_M(n)]^T$  be the output vector, where,  $y_\mu(n)$  is the output symbol of the  $\mu$ th,  $\mu = 1, 2, \dots, M$ , spatial channel. At the  $n$ th tone, the transmit signal  $\mathbf{X}(n)$  is pre-multiplied by  $\mathbf{V}(n)$ , whereas the signal at the receiver after the DFT (FFT) is post-multiplied by  $\mathbf{U}^H(n)$  to obtain the output  $\mathbf{Y}(n)$ . The received symbol of the  $n$ th tone over the  $\mu$ th receive antenna  $y_\mu(n)$  can be written as [8, 38]

$$y_\mu(n) = \sum_{j=1}^M h_{\mu,j}(n)x_j(n) + w_\mu(n), \quad \mu = 1, 2, \dots, M, \quad (2.45)$$

where  $x_j(n)$  is the input symbol at the  $n$ th tone at the  $j$ th antenna,  $w_\mu(n)$  is the additive white Gaussian noise at the  $\mu$ th receive antenna for the corresponding symbol with zero mean and  $\sigma^2$  variance, and  $h_{\mu,j}$  is the channel coefficients from the  $j$ th transmit antenna

to the  $\mu$ th receive antenna. The received data vector at the  $n$ th subcarrier, i.e.,  $\mathbf{y}(n)$  is given as

$$\mathbf{y}(n) = \mathbf{H}(n)\mathbf{x}(n) + \mathbf{w}(n), \quad (2.46)$$

where  $\mathbf{w}(n) = [w_1(n), w_2(n), \dots, w_M(n)]^T$  and  $\mathbf{H}(n)$  is an  $M \times M$  channel gain matrix. The MIMO-OFDM input-output relationship for the whole frame [8, 38] can then be formulated as

$$\mathcal{Y} = \mathcal{H} \mathcal{X} + \mathcal{N}, \quad (2.47)$$

where  $\mathcal{Y} = [\mathbf{y}(1)^T \mathbf{y}(2)^T \dots \mathbf{y}(N)^T]^T$  is  $M_r N \times 1$  receive vector,  $\mathcal{X} = [\mathbf{x}(1)^T \mathbf{x}(2)^T \dots \mathbf{x}(N)^T]^T$  is  $M_t N \times 1$  transmit vector,  $\mathcal{H} = [\mathbf{H}(1) \mathbf{H}(2) \dots \mathbf{H}(N)]$  is  $M_r N \times M_t N$  block diagonal channel gain matrix and  $\mathcal{N} = [\mathbf{w}(1) \mathbf{w}(2) \dots \mathbf{w}(N)]$  is  $M_r N \times 1$  additive white Gaussian noise vector with zero mean and  $\mathcal{E}(\mathcal{N} \times \mathcal{N}) = \sigma^2 \mathbf{I}$  variance.

## 2.4 Peak-to-average ratio of an OFDM signal

Previous sections have given a brief overview of the OFDM and MIMO systems. OFDM has a number of advantages, i.e., reduced/no ISI, ease of implementation using DFT/IDFT and the optimum usage of the spectrum with overlapping orthogonal subcarrier, due to which OFDM is making its way into modern communication systems. However, a major drawback which the OFDM symbol inherit is the high dynamic range of the transmit signal, expressed by the Peak-to-Average Ratio (PAR). The QAM symbols are assumed as independent identically distributed (i.i.d.) which according to the Central Limit Theorem may result in a Gaussian like distribution. This results in a big difference between the peak power of the time domain signal to its average power. The difference between the peak power and the average power of an OFDM signal is termed as peak-to-average ratio and is defined as

$$\text{PAR}(\mathbf{x}) = \frac{\max_{k, 1 \leq k \leq N} |x_k|^2}{E\{|x_k|^2\}}, \quad (2.48)$$

where  $\max_k |x_k|^2$  represents the amplitude of the maximum peak power of the envelope and  $E\{|x_k|^2\}$  denotes the average power over an interval  $1 \leq k \leq N$  of the OFDM symbol  $\mathbf{x}$ . In literature often PAR and Crest factor ( $C_f$ ) are used interchangeably, though, there is a difference between the two. Crest factor ( $C_f$ ) is usually used for voltages and is the ratio of the peak amplitude to the root mean square (RMS) value of a waveform, defined as

$$C_f = \frac{|x|_{\text{peak}}}{x_{\text{rms}}}. \quad (2.49)$$

The PAR is obtained by squaring the Crest factor, i.e.,

$$\text{PAR} = C_f^2 \quad \text{or} \quad C_f = \sqrt{\text{PAR}}. \quad (2.50)$$

When measured in dB, PAR and Crest factor are, of course, the same. We will use the term PAR throughout this work, unless otherwise stated. Moreover, with ‘‘PAR’’ we mean the PAR of  $N$  discrete samples of a baseband OFDM (or MIMO-OFDM) symbol.

### 2.4.1 Mathematical formulation

Herein, we will provide a mathematical analysis for a discrete time baseband OFDM signal. Let  $\mathbf{X} = [X_n]$ ,  $1 \leq n \leq N$ , be the vector of input QAM symbols. Using an IDFT (IFFT), the time domain signal  $\mathbf{x} = [x_k]$ ,  $1 \leq k \leq N$ , is obtained as

$$x_k = \frac{1}{\sqrt{N}} \sum_{n=1}^N X_n e^{j \frac{2\pi nk}{N}}, \quad (2.51)$$

where  $X_n$  is the  $n$ th QAM symbol. According to the central limit theorem, due to the statistical independence of the QAM symbols, the time domain samples exhibit an almost Gaussian distribution. This results in a high difference between the peak power to the average power of the time domain signal. The PAR for baseband OFDM signal  $[x_k]$  is then defined as

$$\text{PAR}(\mathbf{x}) = \frac{\max_{k, 1 \leq k \leq N} |x_k|^2}{E\{|x_k|^2\}}, \quad (2.52)$$

where  $E\{\cdot\}$  stands for expectation. For QAM modulation, the peak power  $\hat{P}_{QAM}$  of an  $\mathcal{M}$ -ary QAM symbol is given as

$$\hat{P}_{QAM} = \frac{a^2}{2} \left( \sqrt{\mathcal{M}} - 1 \right)^2, \quad (2.53)$$

where  $a$  is the minimum Euclidean distance between two constellation points and  $\mathcal{M}$  is the constellation size. The average power  $\bar{P}_{QAM}$  of an  $\mathcal{M}$ -ary QAM constellation point is defined as

$$\bar{P}_{QAM} = \frac{a^2}{6} (\mathcal{M} - 1). \quad (2.54)$$

The PAR of a single carrier with  $\mathcal{M}$ -ary QAM modulation is then calculated as

$$\text{PAR}_{QAM} = \frac{\hat{P}}{\bar{P}} = 3 \left( \frac{\sqrt{\mathcal{M}} - 1}{\sqrt{\mathcal{M}} + 1} \right). \quad (2.55)$$

In case of OFDM with  $N$  subcarriers, the instantaneous power  $|x_k|^2$  of the time domain transmit signal  $\mathbf{x}$  is given as

$$|x_k|^2 = x_k x_k^* = \frac{1}{\sqrt{N}} \sum_{n=1}^N X_n e^{j \frac{2\pi nk}{N}} \cdot \frac{1}{\sqrt{N}} \sum_{m=1}^N X_m e^{-j \frac{2\pi mk}{N}}, \quad (2.56)$$

which, using Euler formulas, can be simplified as

$$|x_k|^2 = \frac{1}{N} \left\{ \sum_{n=1}^N |X_n|^2 + \sum_{n=1}^N \sum_{n \neq m} X_n X_m e^{j \frac{2\pi k(n-m)}{N}} \right\}. \quad (2.57)$$

According to Parseval's theorem, the relationship between the average power of a signal in time and DFT domain is given as

$$E\{|x_k|^2\} = E\{|X_n|^2\}. \quad (2.58)$$

Using Eq. (2.57), the peak power of an OFDM signal can be expressed as [32]

$$\begin{aligned}
 \max_k |x_k|^2 &= \frac{1}{N} \max_n \left\{ \sum_{n=1}^N |X_n|^2 + \sum_{n=1}^N \sum_{n \neq m} X_n X_m e^{j \frac{2\pi k(n-m)}{N}} \right\} \\
 &\leq \frac{1}{N} \left\{ \max_n \sum_{n=1}^N |X_n|^2 + \max_n \sum_{n=1}^N \sum_{n \neq m} X_n X_m e^{j \frac{2\pi k(n-m)}{N}} \right\} \\
 &\leq \frac{1}{N} \left\{ N \max_n |X_n|^2 + N(N-1) \max_n |X_n|^2 \right\} \\
 &\leq \frac{1}{N} \left\{ N^2 \max_n |X_n|^2 \right\} \\
 \max_k |x_k|^2 &\leq \left\{ N \max_n |X_n|^2 \right\}.
 \end{aligned} \tag{2.59}$$

Using equations (2.58) and (2.59), the PAR in (2.52) can be computed as

$$\text{PAR}(\mathbf{x}) \leq N \frac{\max_{1 \leq n \leq N} |X_n|^2}{E\{|X_n|^2\}}, \tag{2.60}$$

where the inequality turns into an equality when all the symbols drawn from the  $\mathcal{M}$ -ary QAM constellation have the same phase, i.e.,  $\arg\{x_1\} = \arg\{x_k\}$  for  $1 \leq k \leq N$  [31]. The PAR in that case is maximal, i.e.,  $\text{PAR}_{\max}$  and is expressed as

$$\text{PAR}_{\max}(\mathbf{x}) = N \frac{\max_{1 \leq n \leq N} |X_n|^2}{E\{|X_n|^2\}}. \tag{2.61}$$

It is clear from Eq. (2.61) that the PAR grows linearly with the number of tones. For an OFDM system with  $N$  subcarriers each one modulated by an  $\mathcal{M}$ -ary QAM constellation, using Eq. (2.61), the  $\text{PAR}_{\max}$  can then be expressed as

$$\text{PAR}_{\max}(\mathbf{x}) = N \left( 3 \frac{\sqrt{\mathcal{M}} - 1}{\sqrt{\mathcal{M}} + 1} \right). \tag{2.62}$$

Figure 2.10 shows the PAR of OFDM symbols for a different number of tones, which shows that the PAR for OFDM with a higher number of tones is larger than for a lower number of tones.

For Binary Phase Shift Keying (BPSK) modulation, the peak power  $\hat{P}_{BPSK}$  and the average power  $\bar{P}_{BPSK}$  are the same. Using Eq. (2.61) for OFDM with BPSK modulation,  $\text{PAR}_{\max}$  is given as  $\text{PAR}_{\max}(\mathbf{x}) = N$ .

Equation (2.61) defines an upper bound or the worst case PAR of an OFDM symbol. However, practically, the probability to really obtain the worst PAR is very low. Thus, a statistical analysis of the PAR distribution of the OFDM samples is usually used to evaluate the system performance. We, therefore, next provide a statistical analysis for the PAR of an OFDM signal.

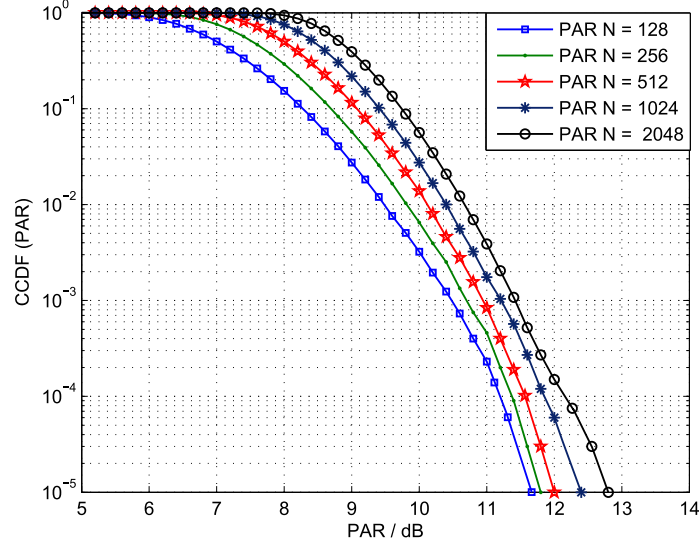


**Figure 2.10:** CCDF(PAR) for OFDM with different number of subcarriers

## 2.4.2 Statistical analysis

Statistically, the *Complementary Cumulative Distribution Function (CCDF)* is used to compare different PAR reduction schemes. The CCDF of the PAR is defined as the probability that the PAR of an OFDM frame is greater than a given threshold  $\tau$ , i.e.,  $\text{CCDF}(\text{PAR}) = P_r(\text{PAR} > \tau)$ .

In order to proceed to the statistical analysis, let  $\mathbf{X} = [X_n]$ ,  $n = 1, 2, \dots, N$ , be the vector of the input  $\mathcal{M}$ -ary QAM symbols where each element  $X_n$  of  $\mathbf{X}$  is considered as statistically independent, identically distributed complex Gaussian with zero mean and  $\sigma_k^2 = [x_k x_k^*]$  variance. Let  $\mathbf{x}$  be the time domain counter part of  $\mathbf{X}$  obtained as  $\mathbf{x} = \text{IDFT}\{\mathbf{X}\}$ . As  $\mathbf{x}$  is a linear combination of the  $N$  i.i.d. QAM symbols, therefore, the time domain samples  $\mathbf{x} = [x_k]$  are also i.i.d. complex Gaussian, i.e.,  $x_k \sim \mathcal{C}(0, \sigma_x^2)$ .

For large  $N$ , the instantaneous power  $|x_k|^2$  has a  $\chi^2$  distribution with two degrees of freedom. The square root of the power, i.e., the amplitude or the envelope of the OFDM symbols  $x_k$  follow a Rayleigh distribution with a probability density function (pdf)

$$\text{pdf}(x_k) = 2 x_k e^{-|x_k|^2}. \quad (2.63)$$

Let  $\tau_k$  be the PAR of the  $k$ th sample, then the probability that the PAR is smaller than the threshold value  $\tau$ , given as  $\text{CDF}(\text{PAR}) = P_r(\tau_k \leq \tau)$ , can be expressed as

$$\text{CDF}_{\tau_k}(\tau) = \int_0^\tau \text{pdf}(\tau_k) d(\tau_k) = \int_0^\tau 2 \tau_k e^{-|\tau_k|^2} d(\tau_k) = 1 - e^{-\tau}. \quad (2.64)$$

For an OFDM symbol of length  $N$  the time domain samples  $x_k$  are i.i.d.. Thus, the CDF for an OFDM frame with  $N$  i.i.d. samples can then be formulated as

$$\text{CDF}_\tau(\tau) = (\text{CDF}_{\tau_k}(\tau))^N = (1 - e^{-\tau})^N. \quad (2.65)$$

Using Eq. (2.65), the *Complementary Cumulative Distribution Function*, i.e., the probability that the PAR of the OFDM frame is higher than the given threshold  $\tau$ , is calculated as

$$\text{CCDF}(\text{PAR}) = P_r(\text{PAR} > \tau) = 1 - (1 - e^{-\tau})^N. \quad (2.66)$$

Equation (2.66) is the CCDF for a single-antenna OFDM system at Nyquist rate. The extension of the statistical analysis to multi-antenna systems is straight forward. In a multi-antenna system,  $M_t$  transmit antennas are used to transmit  $M_t$  OFDM frames simultaneously. However, the  $M_t$  OFDM frames at the input of all antennas are statistically independent of each other. Thus, instead of  $N$  i.i.d. samples, as in the case of a SISO system, we now have  $M_t N$  samples. The situation is comparable to a single OFDM frame of size  $M_t N$ . For MIMO-OFDM with  $M_t$  transmit antennas, the CDF can then be expressed as

$$\text{CDF}(\text{PAR}) = (\text{CDF}_{\tau_k}(\tau))^{M_t N} = (1 - e^{-\tau})^{M_t N}. \quad (2.67)$$

The CCDF of the PAR for MIMO-OFDM, using Eq. (2.67), can be calculated as

$$\text{CCDF}(\text{PAR}) = 1 - (1 - e^{-\tau})^{M_t N}. \quad (2.68)$$

## 2.5 Consequences of high PAR

A major drawback of an OFDM system is its high Peak-to-Average power Ratio (PAR). The QAM symbols are i.i.d., which according to the Central Limit Theorem (CLT) leads to a Gaussian-like distribution in the time domain and may occasionally add up constructively. This results in a big difference between the peak power of the time domain signal to the average power. However, almost all electronic circuitry, e.g., Analog-to-Digital (A/D) converters, mixers, High Power Amplifiers (HPA), etc., are peak-power limited. The most important of them is the HPA, which is used to amplify the signal before transmission. If a signal with high dynamic range is passed through an HPA without any precautionary measures, it will drive the amplifier to operate in its nonlinear (saturation) region, resulting in the signal distortion. The precautionary measures are either to operate the HPA with large input power back-off (IBO) or to reduce the peak values of the input signal. Operating an HPA with high back-offs is not an efficient use of power as it will lead to high power dissipation. In order to avoid operating amplifiers with extremely large back-offs, occasional saturation of the power amplifiers or clipping must be allowed [31]. Clipping a signal beyond a certain power value results in signal distortion referred to as in-band distortion and out-of-band radiation. The in-band distortion results in an increase in bit-error ratio (BER) at the receiver. To cope with the effects of in-band distortion, error correcting codes are often used. With the help of strong channel codes like Low-Density Parity-Codes (LDPC) or Turbo codes, the BER problem may be solved. However, the out-of-band radiation is of big concern, especially for wireless applications [33, 39, 40]. We will first start with a brief overview of high power amplifiers.

### 2.5.1 Theoretical models of high power amplifiers

Herein, we will give an overview of the transfer characteristic function of different power amplifier models typically used in literature just to give an impression. Let  $x(t)$  be the input signal to the amplifier, then in polar form, the complex envelope of the input signal can be expressed as [42]

$$x(t) = |A(t)|e^{j\arg\{x(t)\}} = |A(t)|e^{j\phi(t)}, \quad (2.69)$$

where,  $A(t)$  is the amplitude and  $\arg\{x(t)\} = \phi(t)$  is the phase of the complex value  $x$  at time instant  $t$ . The output signal  $\tilde{x}(t)$  from the high power amplifier, in polar form, is written as

$$\tilde{x}(t) = g[A(t)]e^{j\phi(t)+\psi[A(t)]}, \quad (2.70)$$

where  $g[A]$  and  $\psi[A]$  are the AM/AM and AM/PM (amplitude modulation/phase modulation) transfer characteristic of a memoryless nonlinear power amplifier, respectively. The most common amplifier models available in literature are

- Soft Limiter Amplifier (SLA) model (or ideal amplifier model)
- Traveling Wave Tube Amplifier (TWTA) model
- Solid State Power Amplifier (SSPA) model

#### Soft limiter amplifier model

The SLA amplifier model is the simplest amplifier model. It ignores the AM/PM conversion. The AM/AM conversion of SLA model is expressed as

$$g[A] = \begin{cases} A, & |A| \leq A_0 \\ A_0 e^{j\arg\{A\}}, & A > A_0 \end{cases}, \quad (2.71)$$

where  $A_0$  is the limiting level (saturation value) of the power amplifier and  $\arg\{A\}$  is the phase of the complex value  $A$ . The conversion characteristic is shown in Fig. 2.11. As can be seen, the input-output conversion is linear as long as the value of the input signal is below the saturation value of the amplifier. However, the input signal is clipped as soon as its value goes beyond the limiting value of the power amplifier.

#### Traveling-wave-tube amplifier model

The TWTA model was first proposed by Saleh [41]. The input/output transfer characteristics of a TWTA amplifier model are defined as

$$g[A] = \frac{\alpha_A A}{(1 + \beta_A A^2)} \quad (2.72)$$

and

$$\psi[A] = \frac{\alpha_\psi A}{(1 + \beta_\psi A^2)} \quad (2.73)$$

The AM/AM characteristic curve of a TWTA amplifier are as shown in Fig. 2.11, with  $\beta_A = 0.25$ . Some common parameters for the TWTA amplifier model are  $\alpha_A = 1$ ,  $\beta_\psi = 0.25$ , and  $\alpha_\psi = 0.26$  [42].

### Solid state power amplifier model (Rapp model)

The third most common power amplifier model is known as the solid state power amplifier model. It was proposed by Rapp [42]. The AM/PM for the SSPA model is very small and neglected. The AM/AM conversion characteristics of an SSPA amplifier model is given as

$$g[A] = \frac{A}{(1 + [(\frac{A}{A_0})^2]^p)^{\frac{1}{2p}}}, \quad (2.74)$$

where  $p$  is the knee factor and is used to control the transition of the amplifier from the linear region to the saturation region,  $A_0$  is the saturation value of the SSPA amplifier. Figure 2.11 shows the input-output characteristics for an SSPA model with  $p = 3$ . The Rapp model approaches the SLA model for  $p \rightarrow \infty$ .

The transfer curves can be divided into three different regions. Subsequently, we will give a brief overview to the different regions of an HPA transfer characteristic curves.

Figure 2.12 shows the transfer characteristic curve of a typical amplifier model (for example, Rapp model with  $p = 3$ ). As shown in Fig. 2.12, the characteristics curve have three prominent regions:

- **Linear Region:** In this region the value of the input signal is smaller than the limiting value of the amplifier. The HPA works as a linear device without any distortion. The output signal is proportional to the input signal.
- **Compression region:** Restricting the amplifier to the linear range is inefficient. For an efficient use of the power amplifiers, the HPA must be driven close to the saturation (limiting) value. However, the HPA exhibits a nonlinear behavior when driven close to the saturation level, resulting in a distortion of the input signal. The output signal is no more proportional to the input signal, the gain becomes smaller. The distortion increases as the HPA goes further into deep saturation.
- **Saturation Region:** When the value of the input signal to the amplifier crosses the amplifier's limiting power, the output power  $P_{out,sat}$  remains constant after a certain point. The HPA is said to be operating in the saturation region. The gain in this region is decreasing. The nonlinearities become more and more evident.

In order to characterize an amplifier, the input back-offs (IOB) and the output back-offs (OBO) of the HPA, based on the input and output to the amplifier, are considered. Let  $A_{in}$  be the limiting amplitude of the input signal and  $A$  is the limiting amplitude of the output signal, then the IOB and the OBO of the HPA amplifiers can be defined as

$$IOB = 10 \log_{10} \left( \frac{A_{in}^2}{E\{|x|^2\}} \right) \text{ in [dB]}, \quad (2.75)$$

and

$$OBO = 10 \log_{10} \left( \frac{A^2}{E\{|g(x)|^2\}} \right) \text{ in [dB]}, \quad (2.76)$$

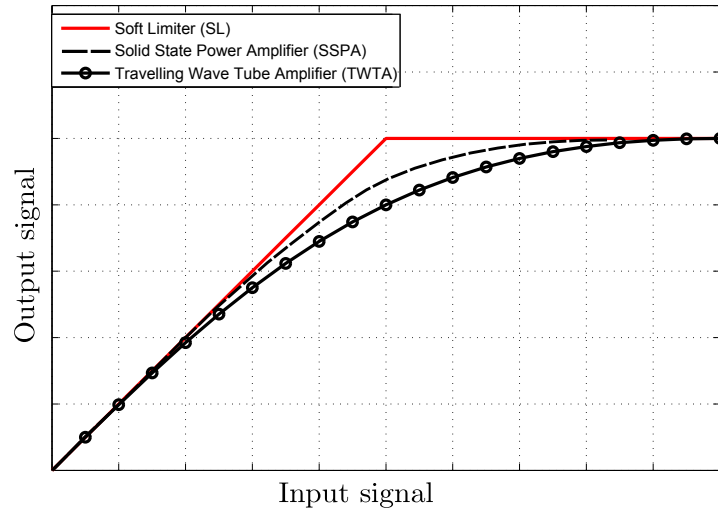


**Figure 2.11:** Characteristic curves of (a) Soft Limiter (SL), (b) Traveling Wave Tube amplifier (TWTA) with  $\beta = 0.25$ , and (c) Solid State Power amplifier (SSPA) (Rapp model) with  $p = 3$

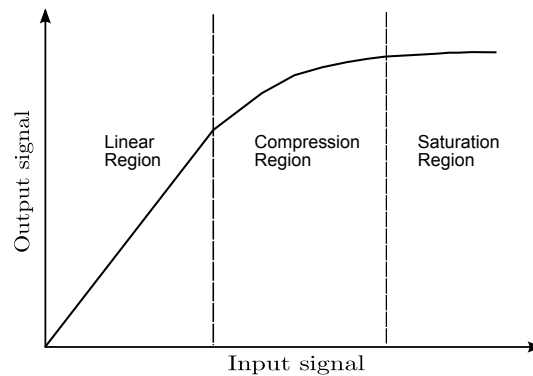


**Figure 2.12:** Characteristic curve of a typical power amplifier

where  $E\{|x|^2\}$  and  $E\{|g(x)|^2\}$  are the average powers of the input and the output signals, respectively.

## 2.6 Peak-to-average reduction techniques

In the previous sections, we discussed that all electronic circuits, especially the HPAs, are peak power limited. When an OFDM signal, with a peak value higher than the amplifiers linear operational range, is passed through the HPA, it drives the amplifier to operate in its non-linear region. This results in signal distortions which degrade the system performance. Thus, measures are usually taken to limit the peak values of the signal below the amplifiers linear operational range. In literature, a number of techniques have been proposed to lower the peak excursions of an OFDM signal. These techniques were first presented for single-input single-output (SISO) systems. Some of them have been extended, recently, for the PAR reduction of multi-antenna systems, as well. Herein,

we will discuss the most popular techniques for the PAR reduction of SISO and multi-antenna systems. We will first start with the techniques introduced for SISO systems.

## 2.6.1 Peak-to-average reduction techniques in SISO systems

### Clipping

Clipping is the simplest PAR reduction technique which is widely used. In clipping, the peak excursions are clipped beyond a predefined threshold value of the HPA linear range, simply by the D/A converter or the HPA itself. Mathematically, the clipping operation is expressed as [47–54]

$$x^c = \begin{cases} x, & |x| \leq A_0 \\ A_0 e^{j \arg\{x\}}, & |x| > A_0 \end{cases}, \quad (2.77)$$

where  $A_0$  is the predefined threshold value (saturation value of the HPA),  $\arg\{x\}$  is the phase of the complex value  $x$  and  $x^c$  is the clipped signal. Clipping is done at the transmitter. The distribution and occurrence of high peaks are random. Therefore, clipping the signal results in in-band distortion which increases the BER at the receiver and in out-of-band radiation, which leads to spectral spreading causing interference into adjacent bands. In order to solve the problem of in-band distortion and out-of-band radiation, Amström [51], introduced frequency domain filtering of the clipped signal. The filter proposed by the authors consists of two DFT (FFT) operations. The forward DFT is used to transform the signal back into the DFT domain. This helps in nullifying the out-of-band components while the in-band frequency components of the clipped signal are passed to the input of the second DFT. Then the IDFT (IFFT) transforms the signal back into time domain. This filter has little effect on the in-band frequency domain components and greatly attenuates the out-of-band components [51]. However, there is a peak regrowth, thus, the clipping and filtering operations are usually iterated to reduce the peak values into the linear region of the HPA. This result in an increase in the computational complexity of the system. In [54], the authors have optimized clipping and filtering to reach a target value with a few iterations, thus, considerably reducing the computational complexity.

An alternative approach is peak windowing, where the large signal peaks are multiplied with a time domain window function, like Hamming window [55]. This approach reduces the out-of-band radiation but unfortunately increases the BER. This increase in the BER can be compensated using error correcting codes at the expense of a reduction in the effective data rate [31]. One such approach is discussed in [56], where the author make use of the analog code (Reed solomon code over complex numbers) for clipping noise correction.

The advantage of clipping is its simple implementation at the transmitter, however, the major drawback is the added complexity resulting from the iterative clipping and filtering.

### Selected Mapping

Selected Mapping (SLM) is another well-known PAR reduction technique. The idea was first proposed by Bäuml, Fischer, and Huber in 1996 [57]. The core principles of Selected Mapping is to translate the original OFDM frame into  $U$  statistically independent OFDM frames bearing the same information. The  $U$  OFDM frames are obtained by multiplying

the original data frame with  $U$  phasor vectors. These OFDM frames are converted into time domain and the one with the lowest PAR is selected for transmission.

Let  $\mathbf{X} = [X_n]$ ,  $n = 1, 2, \dots, N$ , be the original OFDM frame, i.e.,

$$\mathbf{X} = [X_n] = [X_1 X_2 \dots X_N] .$$

Now,  $U$  independent phasor vectors are generated, expressed as

$$\mathbf{P}^{(u)} = [P_n^{(u)}] = [P_1^{(u)}, P_2^{(u)}, \dots, P_N^{(u)}] ,$$

where,  $P_n^{(u)} = e^{j\phi_n^{(u)}}$ , such that  $\phi_n^{(u)} \in [0, 2\pi)$ ,  $u = 1, 2, \dots, U$ . The phasor vectors are usually generated with four phases separated by  $\pi/2$ , i.e.,  $P_n \in (\pm 1, \pm j)$  [57]. The  $u$ th translated OFDM frame is then obtained by multiplying the OFDM frame element-wise with the  $u$ th phasor, i.e.,

$$\mathbf{X}^{(u)} = [X_n] \cdot P_n^{(u)} = [X_n] \cdot e^{j\phi_n^{(u)}} . \quad (2.78)$$

Taking the IDFT (IFFT), the time domain vector is obtained as

$$\mathbf{x}^{(u)} = \frac{1}{\sqrt{N}} \sum_{n=1}^N [X_n] \cdot e^{j\phi_n^{(u)}} e^{j\frac{2\pi nk}{N}} . \quad (2.79)$$

After the IFFT, the frame with the lowest PAR is selected for transmission.

At the receiver, the OFDM frame is recovered by sending side information about the phase vector used, protected by a channel code. At the receiver, after the DFT (FFT) and decision about the used vector, the original OFDM frame is recovered as

$$\mathbf{Y}^{(u)} = \text{FFT}\{\mathbf{x}\} \bullet e^{-j\phi^{(u)}} = \mathbf{X} \bullet e^{j\phi^{(u)}} \bullet e^{-j\phi^{(u)}} = \mathbf{X} , \quad (2.80)$$

where  $\bullet$  represent an element-wise multiplication. This is also a simple approach, however, the computational complexity increases with  $U$ , the number of translated frames.

### Partial Transmit Sequences

Partial Transmit Sequences (PTS) was first proposed by Müller and Huber [58]. The principle of PTS is the same as SLM, i.e., multiple signal representation bearing the same information. However in PTS, rather than defining  $U$  statistically independent OFDM frames as in SLM, the input data vector  $\mathbf{X}$  is subdivided into  $D$  disjoint sub-blocks as shown in Fig. 2.13. The size of each sub-block is  $N/D$ . Each sub-block is assigned a set of tones and the others are set to zero, such that

$$\mathbf{X} = \sum_{i=1}^D \mathbf{X}^i, \quad i = 1, 2, \dots, D . \quad (2.81)$$

SLM used to rotate the individual tones inside the frame, however, in PTS a rotation factor is defined for each sub-block  $\mathbf{X}^i$ , i.e.,

$$P^i = e^{j\phi_i} , \quad \phi_i \in [0, 2\pi) . \quad (2.82)$$

The translated input data vector  $\tilde{\mathbf{X}}$  can then be expressed as

$$\tilde{\mathbf{X}} = \sum_{i=1}^D P^i \mathbf{X}^i = \sum_{i=1}^D e^{j\phi_i} \mathbf{X}^i \quad (2.83)$$

Exploiting the linearity property of the IDFT, the time domain vector  $\tilde{\mathbf{x}}$  is obtained as

$$\begin{aligned} \tilde{\mathbf{x}} &= \text{IDFT}(\tilde{\mathbf{X}}) = \text{IDFT} \left\{ \sum_{i=1}^D P^i \mathbf{X}^i \right\} \\ \tilde{\mathbf{x}} &= \sum_{i=1}^D e^{j\phi_i} \text{IDFT}(\mathbf{X}^i) = \sum_{i=1}^D e^{j\phi_i} \mathbf{x}^i, \end{aligned} \quad (2.84)$$

where  $D$  partial transmit sequences have been introduced [58]. To get a transmit sequence with lowest PAR, an optimum combination of the partial sequences has to be found. The optimal combination of  $\{\tilde{P}^{(1)}, \tilde{P}^{(2)}, \dots, \tilde{P}^{(D)}\}$  can be written as

$$\{\tilde{P}^{(1)}, \tilde{P}^{(2)}, \dots, \tilde{P}^{(D)}\} = \arg \left\{ \min_{\tilde{P}^{(1)}, \tilde{P}^{(2)}, \dots, \tilde{P}^{(D)}} \right\} \left[ \max_{1 \leq k \leq N} \left| \sum_{i=1}^D P^i \mathbf{x}_k^i \right| \right], \quad (2.85)$$

where  $\arg \min(\cdot)$  denotes the arguments for which the given expression yields the minimum. The optimum sequence with the lowest PAR is then defined as

$$\tilde{\mathbf{x}} = \sum_{i=1}^D P^i \cdot \mathbf{x}^i. \quad (2.86)$$

PTS has a slightly better performance than SLM [58, 59]. However, it has high computational complexity, for searching optimum phase factors for the sub-blocks that will finally result in an output with low peak signal. In order to retrieve the useful information correctly at the receiver, the algorithm needs to send side information about the phase factors used, to the receiver or use differential encoding.

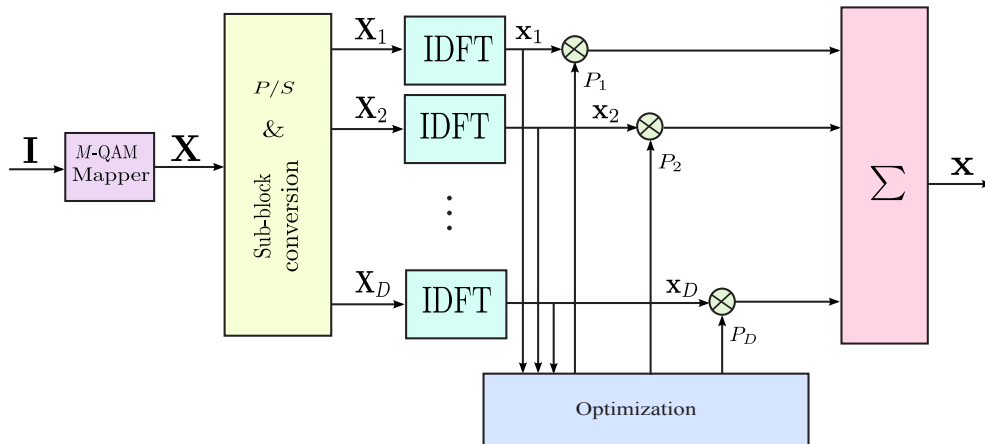


**Figure 2.13:** Block diagram of Partial Transmit Sequences

### Tone Reservation

Tone Reservation is the least complex PAR reduction technique. First proposed by Tellado [31, 60], the TR algorithm adds (subtracts) a data-dependent signal to the original signal in time domain for peak reduction. This time domain signal is generated by using a certain number of tones reserved for PAR reduction. The algorithm, thus, divides the tones in an OFDM frame into two disjoint sets, the tones used for data transmission  $\bar{\mathbf{X}}$  and the tones used for PAR reduction  $\mathbf{R}$ , as shown in Fig. 2.14, such that  $\mathbf{X} = \bar{\mathbf{X}} + \mathbf{R}$ .  $\mathbf{R}$  is used to generate a Dirac-like function  $\mathbf{r}$  which is then iteratively added to the original signal  $\mathbf{x}$  for PAR reduction in time domain, as shown in Fig. 2.15.

$$\mathbf{x} = \text{IDFT}\{\mathbf{X}\} = \text{IDFT}\{\bar{\mathbf{X}} + \mathbf{R}\}. \quad (2.87)$$

At the  $(i + 1)$ th iteration, the time domain vector  $\mathbf{x}^{(i)}$  is updated as [12]

$$\mathbf{x}^{(i+1)} = \mathbf{x}^{(i)} - \alpha(x_d^{(i)} - e^{j \arg\{x_d^{(i)}\}} \cdot \tau)(\mathbf{r}(N - m) \text{ modulo } N), \quad (2.88)$$

with the parameters:

- $\alpha$  - step size
- $i$  -  $i$ th iteration
- $d$  - peak position
- $\arg x_k$  - is the phase of the complex value  $x_k$
- $\tau$  - threshold value
- $\mathbf{r}(N - m)$  - time-shifted version of  $\mathbf{r}$
- $(x_d^{(i)} - e^{j \arg\{x_d^{(i)}\}} \cdot \tau)$  - threshold overshoot

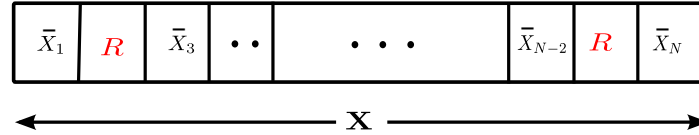


**Figure 2.14:** OFDM frame with reserved tones

The TR algorithm can be summarized as follows:

1. Initialize the information vector  $\mathbf{X}$  with the reserved tones set to zero.
2. Transform  $\mathbf{X}$  into time domain, i.e.,  $\mathbf{x} = \text{IFFT}(\mathbf{X})$ .
3. Find the peak value  $x_d^{(i)}$  and the position  $d$  for which  $|x_d^{(i)}| = \max_k |x_k^{(i)}|$ .
4. If  $|x_d^{(i)}| < \tau$  or if  $i > i_{max}$  stop and transmit  $\mathbf{x}^{(i)}$ , else
5. Modify the transmit signal  $\mathbf{x}$  according to

$$\mathbf{x}^{(i+1)} = \mathbf{x}^{(i)} - \alpha(x_d^{(i)} - e^{j \arg\{x_d^{(i)}\}} \cdot \tau)(\mathbf{r}(N - m) \text{ modulo } N) \quad (2.89)$$

$i := i + 1$   
goto 3.

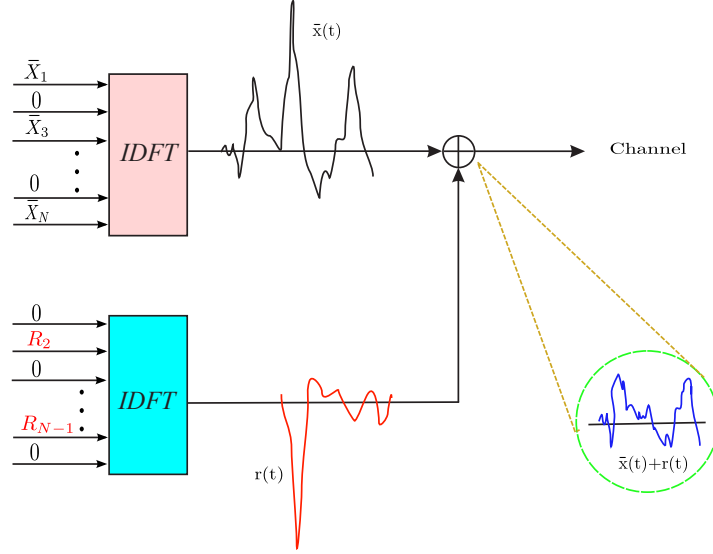


**Figure 2.15:** Block diagram of the Tone-Reservation algorithm

The TR algorithm presented by the authors in [31,60] did not take the filter response into considerations. In order to account for the filter response, an oversampled version of TR algorithm was presented in [61].

### Trellis Shaping

Forney [63] introduced Trellis Shaping for minimizing the average power of the transmit signal. However, application of the Trellis Shaping for PAR reduction was first proposed by Henkel and Wagner [64], and later the same concept has been extended in [67,68,70,99]. In order to give a brief insight to the idea, let us consider a block diagram of a trellis shaper as shown in Fig. 2.16. In there,  $\mathcal{C}_s$  is a rate- $k/n$  convolutional code (also referred to as the shaping code) with a  $k \times n$  generator matrix  $\mathbf{G}$ . Moreover,  $\mathbf{H}^T$  and  $(\mathbf{H}^{-1})^T$  represent the  $n \times (n - k)$  parity-check matrix (syndrome former) and its  $(n - k) \times n$  left inverse. For sign-bit shaping,  $\mathcal{C}_s$  is a rate-1/2 convolutional code with a  $1 \times 2$  generator matrix  $\mathbf{G}$ . The matrix dimensions of the syndrome former  $\mathbf{H}^T$  and its left inverse  $(\mathbf{H}^{-1})^T$  are  $2 \times 1$  and  $1 \times 2$ , respectively.

Let  $\mathbf{u}$  be the input data sequence prior to the constellation mapping, which will be transmitted with one  $N$ -subcarrier OFDM symbol. This sequence  $\mathbf{u}$  is comprised of two sequences  $\mathbf{m}$  and  $\mathbf{n}$ . As shown in Fig. 2.16,  $\mathbf{m}$  is used to address the MSBs (the sign bits) of the mapping constellation, as this is the bit position with the biggest possible change in the signal-point location in an  $\mathcal{M}$ -ary QAM alphabet [64], whereas  $\mathbf{n}$  are the least significant bits (LSB). To choose the MSBs, the input sequence  $\mathbf{m}$  is first preprocessed by the left inverse of the syndrome former  $(\mathbf{H}^{-1})^T$ , i.e.,  $\mathbf{z} = \mathbf{m} \cdot (\mathbf{H}^{-1})^T$ . As we know that for a valid code sequence  $\mathbf{y}$ , we obtain  $\mathbf{y} \cdot \mathbf{H}^T = 0$ , the information at the receiver can be retrieved as

$$\mathbf{z}' \cdot \mathbf{H}^T = (\mathbf{z} \oplus \mathbf{y}) \cdot \mathbf{H}^T = (\mathbf{z} \cdot \mathbf{H}^T) \oplus \underbrace{(\mathbf{y} \cdot \mathbf{H}^T)}_{=0} = \mathbf{z} \cdot \mathbf{H}^T = \mathbf{m}. \quad (2.90)$$

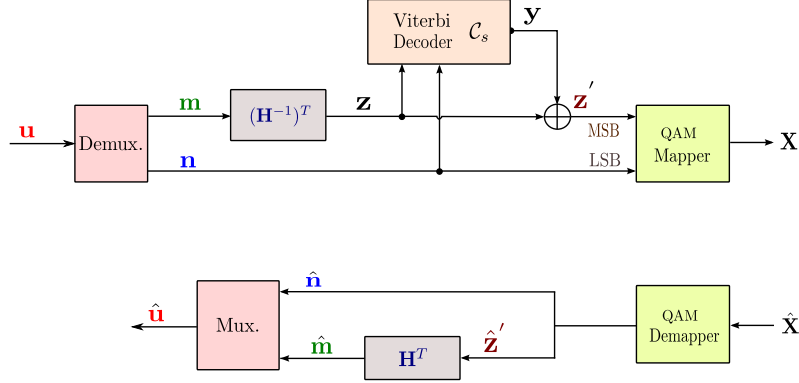


**Figure 2.16:** Block diagram of Trellis Shaping

The  $i$ th QAM symbol is then determined by the following mapping rule

$$X_i = \mathcal{M}(\mathbf{z}_i \oplus \mathbf{y}_i; \mathbf{n}) \quad (2.91)$$

For PAR reduction using Trellis Shaping, different metrics have been proposed for the search in the Viterbi algorithm [64, 67, 68, 70]. The metric proposed by Ochiai [70] is based on the autocorrelation of the sidelobes of an OFDM signal and is expressed as

$$\mu^i = \mu^{i-1} + \sum_{m=1}^{i-2} 2\Re e (R_m^{(i-1)*} \delta_m^{i-1}) + \sum_{m=1}^{i-1} |\delta_m^{i-1}|^2, \quad (2.92)$$

where  $R_m^i$  is the aperiodic autocorrelation function,  $\mu^i = \sum_{m=1}^i |R_m^i|^2$ , and  $\delta_m^i = X_i X_{i-m}^*$ . A detailed description of Trellis shaping is provided in Chapter 5.

So far, we have discussed some PAR reduction schemes for single antenna systems. In the next section, these techniques will be extended to multiple antenna systems.

## 2.6.2 Peak-to-average reduction techniques in MIMO systems

The previous section provided a brief overview of the most popular PAR reduction techniques for SISO systems available in literature. These techniques are well optimized with good performances. However, modern communication systems deploy multiple antennas at the transmitter and the receiver, as discussed in Section 2.2. Thus, current research is extending the existing techniques for PAR reduction of MIMO-OFDM systems. However, with the deployment of multiple antennas at the transmitter, the complexity of the aforementioned algorithms, of course, increases linearly with the number of transmit antennas. Besides the number of transmit antennas, the complexity and gain of these algorithms depend on the type of MIMO scenario under considerations. For example, for a single-user point-to-point MIMO-OFDM system, where joint signal processing is possible at both ends, these algorithm can directly be extended to each transmit antenna. However, the complexity of the algorithm is then  $M_t$ -fold that of the SISO systems, where  $M_t$  is the total number of transmit antennas. Similarly, for the multi-user MAC scenarios with each user being equipped with a single transmit antenna, these algorithm is just a direct extension of the SISO case, hence, it will not be considered any further, unless stated otherwise.

However, limiting the peak values become challenging when considering the multi-user point-to-multipoint scenarios (broadcast channel). In the broadcast scenario, beside the number of transmit antennas, the algorithm has to consider the effect of precoding at the central base station, which further increases the computational complexity of these algorithms. In the literature, different approaches have been proposed for the PAR reduction of MIMO-OFDM systems. Herein, we will give an overview of the techniques used for PAR reduction in MIMO systems.

### **Selected Mapping / Partial Transmit Sequences**

For MIMO systems, SLM (PTS) can be extended in the same way as applied to the SISO systems, i.e., to generate multiple copies of the same frame at each transmit antenna. Different variants of SLM (PTS) have been proposed in [74–83]. In [74], the authors extended SLM for the PAR reduction of Space Time Block Coded (STBC) MIMO-OFDM systems. Moreover, in [75] Baek et al. proposed two different variants of SLM for P2P MIMO-OFDM systems, the ordinary SLM (oSLSM) and a simplified SLM (sSLM). For the two variants, the computational complexity was the same, i.e.,  $U \cdot M_t$  IFFTs, however, sSLM uses the same phasor vectors for all transmit antennas as compared to the oSLM which is a direct extension of the SISO SLM into the MIMO topology. The authors also presented oPTS and sPTS with the same basic principle as presented for SLM. In [77], the authors proposed directed SLM (dSLM) for P2P MIMO-OFDM systems. In dSLM, the focus is on the antenna with the worst PAR. dSLM has better performance than oSLM and sSLM, as the algorithm concentrates on the antenna with the highest PAR, whereas, in oSLM and sSLM, all antennas are dealt equally likely. The directed approach was applied to PTS, i.e., dPTS. In [80], Siegel presented selected sorting (SS) for the PAR reduction of the multi-user broadcast scenarios. One thing to mention is that the basic principle in all variants are the same, i.e., to generate multiple copies of the same signal, thus the complexity in PAR reduction using SLM/PTS is very high.

### **Tone Reservation**

Like SLM and PTS, the Tone Reservation algorithm can also be extended for PAR reduction of MIMO-OFDM systems. One such approach has been proposed in [87], where the authors generate the corrective signal on the unused tones with the assumption that they are below a given power mask. The corrective signal is optimized using a second order cone programming (SOCP). Simulation results have been presented for a  $2 \times 2$  MIMO-OFDM system with Alamouti space time block coding (STBC, IEEE 802.16 WiMAX standard). However, there is a limitation of the scheme used as the relative mean power increase is very high. With a constraint on the relative mean power in the optimization algorithm, the results obtained are not very promising.

In the next chapters we present different approaches for the PAR reduction in MIMO-OFDM systems.

## Chapter 3

# PAR Reduction with Tone Reservation in MIMO and Multi-user OFDM

In the previous chapter, we showed that Partial Transmit Sequences (PTS), Selected Mapping (SLM), and Tone Reservation (TR) algorithms were extended by different authors for the PAR reduction in MIMO OFDM systems, which are well-optimized techniques for SISO systems. In case of a point-to-point MIMO-OFDM systems, these algorithms can be applied in a straight forward manner. However, the situation becomes more challenging when considering a multi-user broadcast channel (BC). In multi-user BC, the precoding block at the transmitter additionally affects the performance of PAR reduction schemes. In [33, 80], Siegel proposed Selected Sorting, a variant of SLM, for the PAR reduction in multi-user MIMO-OFDM systems, however, the algorithm is much more complex without prominent results.

Herein, we extend the Tone Reservation algorithm for PAR reduction in point-to-point and multi-user (broadcast channel) MIMO-OFDM scenarios. In Section 3.1, we first consider a P2P MIMO-OFDM scenario. Here, a joint signal processing is possible both at the transmitter as well as the receiver ends. Thus, we will use transmitter-sided precoding and receiver-sided postprocessing. In case of a P2P scenario, we assume that the last eigenchannel(s) are too weak to be used for data transmission. Not using them for data transmission will offer redundancy for the PAR reduction of a MIMO-OFDM system. In Section 3.1.3, we will show how to design an optimum spiky function using the reserved eigenchannels, which, like the TR algorithm, can be iteratively added to the transmitted signal for PAR reduction. Section 3.1.5 is devoted to simulation results obtained with the proposed algorithm.

We next extend the TR algorithm for the PAR reduction of a BC-scenario in Section 3.2. For the BC scenario, as discussed in Section 2.2.2, we will consider a transmitter-sided precoding. Herewith, the situation for PAR reduction becomes very challenging. However, we will show that Tone Reservation is very suited for this situation. For the BC scenario, we will reserve a small percentage of the total number of tones on all spatial dimensions. Thus, no implications due to precoding need to be taken into consideration at the receiver. We start with the system model and precoding performed using Tomlinson Harashima (TH) precoding in Section 3.2.1. Section 3.2.2 provides the simulation results for the BC scenarios.

### 3.1 PAR reduction with TR in point-to-point MIMO-OFDM systems

Tone Reservation is the simplest and computationally the least complex technique used for PAR reduction of the OFDM systems. For brevity, we recall from Section 2.6.1 that, in tone reservation, the algorithm reserves a certain percentage of the total number of tones. These tones are used to generate a spiky function, which is then iteratively added to the transmitted signal to reduce the peak excursion crossing a certain threshold value  $\tau$ . The idea first presented for Single-Input Single-Output (SISO) OFDM systems, can as well be extended to MIMO-OFDM systems. A first approach has been made by the authors in [87], for a  $2 \times 2$  P2P MIMO-OFDM system using Alamouti coding. The authors reserved the tones on all spatial dimensions, falling under the spectral mask, for PAR reduction.

Herein, we extend the Tone Reservation algorithm, however, with an alternative approach for generating the spiky function. In conventional TR, an optimum spiky function is generated on the reserved tones over all spatial dimensions. In contrast to the conventional method, we generate an optimum spiky function on the the weakest eigenchannels not suitable for data transmission. The motivation and key idea behind our approach is discussed subsequently.

#### 3.1.1 Key idea

Consider a point-to-point MIMO-OFDM scenario where a joint signal processing is possible at both the transmitter and the receiver ends. As discussed in Section 2.2.1, we consider a transmitter-sided precoding and receiver-sided postprocessing. Moreover, we consider perfect channel state information (CSI) at both ends. For simplicity, we will assume that the number of transmit antennas  $M_t$  is equal to the number of receive antennas  $M_r$ , i.e.,  $M_t = M_r = M$ . The channel gain matrix between the  $i$ th,  $i = 1, 2, \dots, M_t$ , transmit and  $j$ th,  $j = 1, 2, \dots, M_r$ , receive antenna at the  $n$ th,  $n = 1, 2, \dots, N$ , frequency bin can then be defined as

$$\mathbf{H}(n) = \begin{pmatrix} h_{1,1} & h_{1,2} & \dots & h_{1,M} \\ h_{2,1} & h_{2,2} & \dots & h_{2,M} \\ \vdots & \dots & \ddots & \vdots \\ h_{M,1} & h_{M,2} & \dots & h_{M,M} \end{pmatrix} \quad (3.1)$$

Using singular value decomposition (SVD), the channel gain matrix  $\mathbf{H}(n)$  in DFT domain at the  $n$ th carrier can be rephrased as

$$\mathbf{H}(n) = \mathbf{U}(n) \cdot \mathbf{\Lambda}(n) \cdot \mathbf{V}^H(n), \quad (3.2)$$

where  $\mathbf{U}(n)$  and  $\mathbf{V}(n)$  are unitary postprocessing and preprocessing matrices, respectively, ( $\mathbf{U}^H \cdot \mathbf{U} = \mathbf{V}^H \cdot \mathbf{V} = \mathbf{I}$ ) and  $\mathbf{\Lambda}(n)$  is a diagonal matrix of the singular values of  $\mathbf{H}(n)$ ,

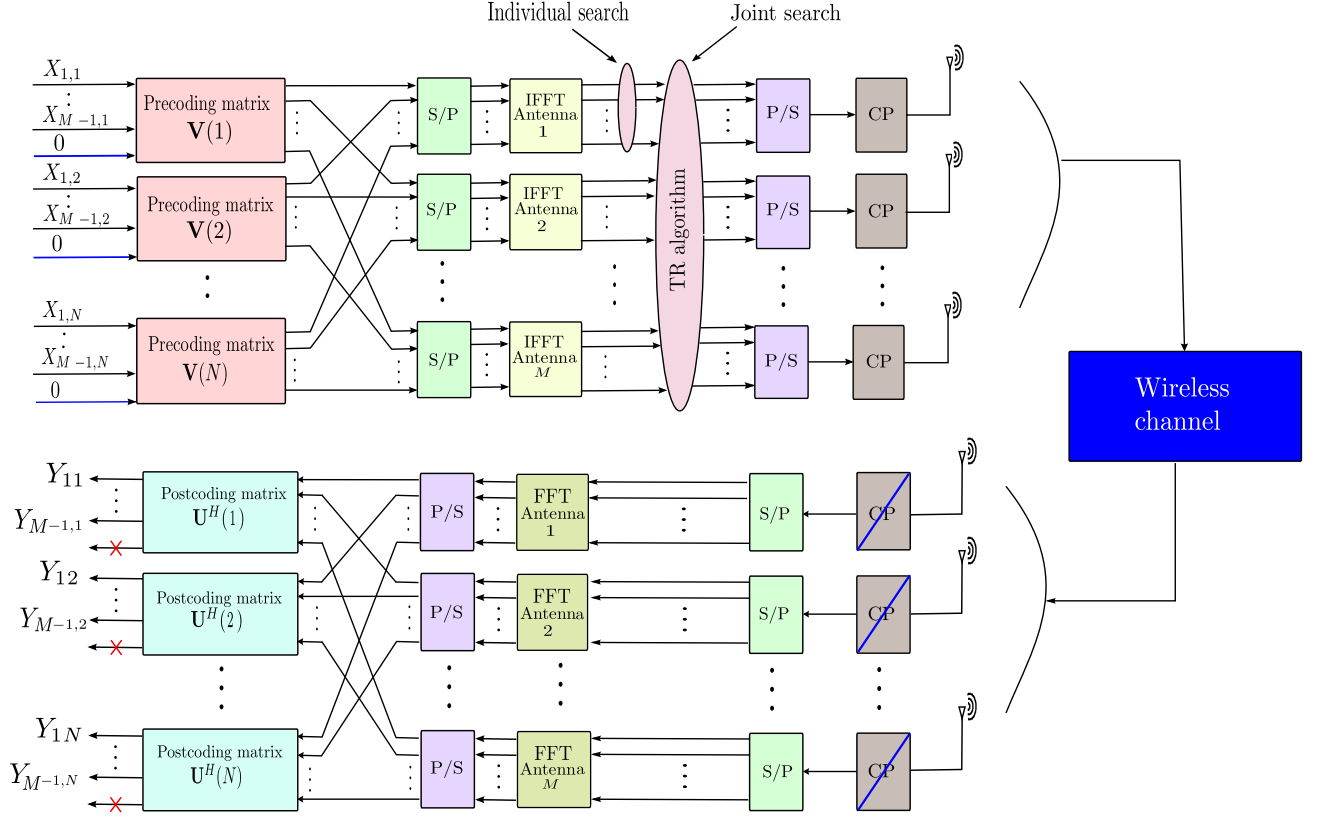


**Figure 3.1:** Block diagram of point-to-point MIMO-OFDM system with TR algorithm

i.e.,

$$\mathbf{\Lambda}(n) = \begin{pmatrix} \sigma_{1,1}(n) & 0 & 0 & 0 \\ 0 & \sigma_{2,2}(n) & 0 & 0 \\ \vdots & \dots & \ddots & \vdots \\ 0 & 0 & 0 & \sigma_{M,M}(n) \end{pmatrix} \quad (3.3)$$

Usual SVD algorithms sort the singular values in a descending order, i.e.,  $\sigma_{1,1} \geq \sigma_{2,2} \geq \dots \geq \sigma_{M,M}$ . Typically, the last singular value, i.e.,  $\sigma_{M,M}$  is so small that the corresponding eigenchannels are hardly suited for data transmission. Not using them would offer redundancy for peak-to-average ratio (PAR) reduction without a lot of cost in data rate. Thus, we will reserve the last eigenchannel to generate a spiky function, which will then be used for PAR reduction of the transmitted signal.

### 3.1.2 System model and pre-coding

We consider a point-to-point MIMO-OFDM system with  $M_t$  transmit and  $M_r$  receive antennas, as shown in Fig. 3.1. Let  $\mathbf{X}(n) = (X_{1,n}, X_{2,n}, \dots, X_{M,n})^T$  be the  $n$ th input data vector, where  $X_{\mu,n}$  is the input symbol on the  $\mu$ th ( $\mu = 1, 2, \dots, M$ ) spatial channel and the  $n$ th tone. At the transmitter,  $\mathbf{X}(n)$  is preprocessed using preprocessing matrices  $\mathbf{V}(n)$  and converted into a parallel data stream using a serial to parallel converter. The time-domain signal is obtained taking IFFTs. Then, the time-domain TR method follows. The time-domain signal is then padded with a cyclic prefix (CP) to mitigate the effect of

inter-symbol interference (ISI). This signal is transmitted over a MIMO channel with a channel gain matrix  $\mathbf{H}$ . At the receiver, reverse processes are used to obtain an estimate of the transmitted signal. For a better understanding, we write the input-output relation in DFT domain. Let  $\mathbf{Y}(n) = (Y_{1,n}, Y_{2,n}, \dots, Y_{M,n})^T$  be the output vector, where,  $Y_{\mu,n}$  is the  $n$ th output symbol of the  $\mu$ th ( $\mu = 1, 2, \dots, M$ ) spatial channel. The transmit signal  $\mathbf{X}(n)$  is pre-multiplied by  $\mathbf{V}(n)$ , whereas the signal at the receiver is post-multiplied by  $\mathbf{U}^H(n)$  to obtain the output  $\mathbf{Y}(n)$  as shown in Fig. 3.2. At the  $n$ th bin, input and output of the MIMO system can be related as

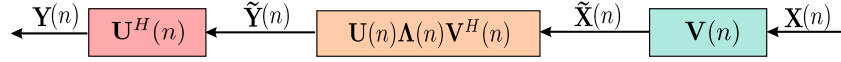


**Figure 3.2:** MIMO channel diagonalization using SVD

$$\tilde{\mathbf{Y}}(n) = \mathbf{H}(n) \cdot \tilde{\mathbf{X}}(n) + \mathbf{w}(n), \quad (3.4)$$

where  $\mathbf{w}(n)$  is additive white Gaussian noise. After postprocessing with  $\mathbf{U}^H(n)$ , Eq. (3.4) can be written as

$$\mathbf{Y}(n) = \mathbf{U}^H(n) \cdot \tilde{\mathbf{Y}}(n) = \mathbf{U}^H(n) \cdot \mathbf{H}(n) \cdot \tilde{\mathbf{X}}(n) + \tilde{\mathbf{w}}(n), \quad (3.5)$$

with  $\tilde{\mathbf{w}}(n) = \mathbf{U}^H(n) \cdot \mathbf{w}(n)$ , since  $\mathbf{U}^H(n)$  is unitary thus the statistical properties of  $\tilde{\mathbf{w}}(n)$  are the same as that of  $\mathbf{w}(n)$ . With  $\tilde{\mathbf{X}}(n) = \mathbf{V}(n) \cdot \mathbf{X}(n)$ , also applying the SVD to the channel matrix  $\mathbf{H}(n)$ , i.e.,  $\mathbf{H}(n) = \mathbf{U}(n) \cdot \mathbf{\Lambda}(n) \cdot \mathbf{V}^H(n)$  and omitting  $\tilde{\mathbf{w}}(n)$ , Eq. (3.5) can be rephrased as

$$\mathbf{Y}(n) = \underbrace{\mathbf{U}(n)^H \cdot \mathbf{U}(n)}_{\mathbf{I}} \cdot \underbrace{\mathbf{\Lambda}(n) \cdot \mathbf{V}^H(n) \cdot \mathbf{V}(n)}_{\mathbf{H}(n)} \cdot \underbrace{\mathbf{X}(n)}_{\tilde{\mathbf{X}}(n)}, \quad (3.6)$$

With the identities  $\mathbf{U}^H(n) \cdot \mathbf{U}(n) = \mathbf{V}^H(n) \cdot \mathbf{V}(n) = \mathbf{I}(n)$ , where  $\mathbf{I}(n)$  is an identity matrix of size  $M \times M$ , Eq. (3.6) simplifies to

$$\mathbf{Y}(n) = \mathbf{\Lambda}(n) \cdot \mathbf{X}(n). \quad (3.7)$$

For an  $M \times M$  (with  $M_t = M_r = M$ ) case, Eq. (3.7) can be rephrased in matrix notation as

$$\mathbf{Y}(n) = \begin{pmatrix} \sigma_{1,1}(n) & 0 & 0 & 0 \\ 0 & \sigma_{2,2}(n) & 0 & 0 \\ 0 & 0 & \ddots & 0 \\ 0 & 0 & 0 & \sigma_{M,M}(n) \end{pmatrix} \begin{pmatrix} X_{1,n} \\ X_{2,n} \\ \vdots \\ X_{M,n} \end{pmatrix}. \quad (3.8)$$

It is assumed that only the last spatial dimension is reserved for PAR reduction while the other dimensions are used for data transmission. Let  $\mathbf{S}(n)$  denote the first dimensions used for data transmission, i.e.,

$$\mathbf{S}(n) = (X_{1,n} \ X_{2,n} \ \dots \ X_{M-1,n} \ 0)^T,$$

where  $X_{\mu,n}$  is the QAM symbol at the  $\mu$ th spatial dimension and the  $n$ th frequency bin. We also define  $\mathbf{R}(n)$ , for the last/reserved eigenchannels, i.e.,

$$\mathbf{R}(n) = ( 0 \ 0 \ \dots \ 0 \ R_n )^T .$$

In conventional TR algorithms, a spiky function is generated on a small number of reserved tones. Likewise, we will use  $\mathbf{R}(n)$ , the last eigenchannel, to generate a spiky function. As shown in Fig. 3.1, the input data vector  $\mathbf{S}(n)$  and the spiky function  $\mathbf{R}(n)$  are preprocessed as

$$\tilde{\mathbf{S}}(n) = \mathbf{V}(n) \cdot \mathbf{S}(n) = \mathbf{V}(n) \cdot ( X_{1,n} \ \dots \ X_{M-1,n} \ 0 )^T \quad (3.9)$$

and

$$\tilde{\mathbf{R}}(n) = \mathbf{V}(n) \cdot \mathbf{R}(n) = \mathbf{V}(n) \cdot ( 0 \ \dots \ 0 \ R_n )^T . \quad (3.10)$$

Transforming both into time domain by applying the block diagonal IFFT modulator, i.e.,  $\tilde{\mathbf{s}}^T = \mathbf{F}^{-1}\tilde{\mathbf{S}}^T$  and  $\tilde{\mathbf{r}}^T = \mathbf{F}^{-1}\tilde{\mathbf{R}}^T$ , where  $\mathbf{F}^{-1}$  is a block-IDFT matrix with blocks of diagonal submatrices with  $M$  identical diagonal elements  $w_{n,k}$ . This spiky function  $\tilde{\mathbf{r}}^T$  is then iteratively added to the original signal  $\tilde{\mathbf{s}}^T$  in time domain for PAR reduction. The two sum up to

$$\tilde{\mathbf{x}} = \tilde{\mathbf{s}} + \tilde{\mathbf{r}} = \mathbf{F}^{-1}\mathbf{V}\mathbf{X} = \mathbf{F}^{-1}\mathbf{V}(\mathbf{S} + \mathbf{R}) . \quad (3.11)$$

Now, the goal is to design an optimum spiky function using the reserved eigenchannels  $\mathbf{R}$ , such that it will reduce the peak excursions crossing a predefined threshold  $\tau$ .

### 3.1.3 Designing an optimum spiky function

#### Designing a spiky function using $R_n = 1/V_{\mu,M}(n)$

An optimum prototype spiky function would mean a spike at time zero resulting from a constant in frequency domain at the corresponding antenna  $\mu$ . Herein, we will generate  $M$  spiky functions, one at each antenna (since an  $M \times M$  P2P system is considered). First let us assume that we like to produce a spiky function at one antenna only, not caring about the others for now.

In Eq. (3.10), every component (column) of the  $M$  spatial dimensions is multiplied by  $\mathbf{V}(n)$ , where  $n$  is the frequency index. Essentially, Eq. (3.10) cuts out the last column of  $\mathbf{V}(n)$ .

A spiky function at time zero would mean a constant in frequency domain at the corresponding antenna  $\mu$ , i.e., all ones for example. Now, we can easily compute the necessary  $R_n$ , since we know the weighting factor out of the last column of  $\mathbf{V}(n)$  that corresponds to the selected antenna, i.e., one chooses

$$R_n = 1/V_{\mu,M}(n) . \quad (3.12)$$

We do not know, of course, how the other antennas are affected at the same time, however, we will select antenna  $\mu$  with the highest peak. Using (3.12) in Eq. (3.10), and applying an IFFT, we obtain the modification matrix in time domain for all antennas and all times

$1, 2, \dots, N$  by

$$\tilde{\mathbf{r}}^\mu = \mathbf{F}^{-1} \cdot \mathbf{V} \cdot \begin{bmatrix} 0 & \dots & 0 \\ 0 & \dots & 0 \\ 0 & \dots & 0 \\ R_1^\mu & \dots & R_N^\mu \end{bmatrix}, \quad (3.13)$$

A spiky function corresponding to  $R^1(n) = 1/V_{1,4}(n)$ , i.e., a spike at the first antenna of a  $4 \times 4$  system is as shown in Fig. 3.3.

Figure 3.3 shows a spike on first antenna while having some very low peaks on the

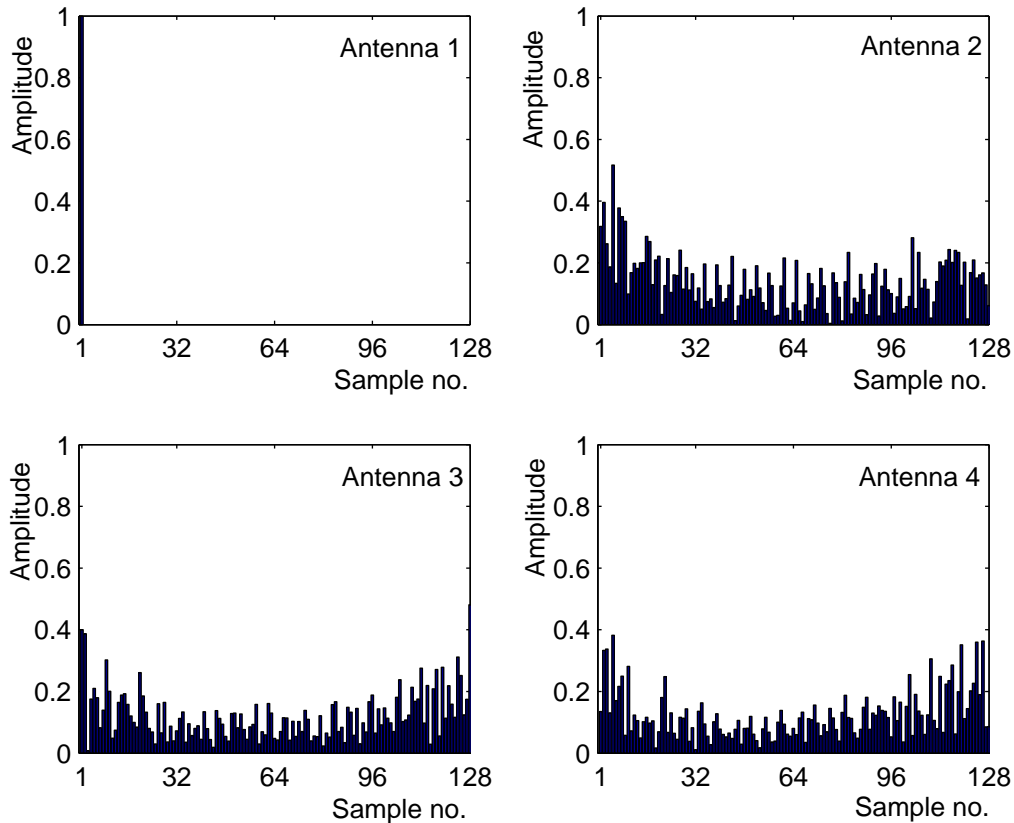


**Figure 3.3:** Absolute values of the spiky time domain vectors, with a highest peak at the 1st antenna using  $R^1(n) = 1/V_{1,4}(n)$

remaining dimensions, where we have considered a  $4 \times 4$  P2P MIMO-OFDM system. In case of an  $M \times M$  MIMO-OFDM system, we will generate  $M$  such spiky function, one for each dimension, with each optimum spiky function having a perfect spike at a particular antenna/dimension while not taking into account other dimensions in the choice of the reserved components. However, it might then occur that besides the optimum spike at a specific antenna, there are higher peaks on the remaining dimensions as well, as shown in Fig. 3.4. We will call such a spiky function *bad* further on, where there are high peaks on the remaining dimensions besides the optimum spike on the intended dimension. Such spiky functions are challenging to the performance of the proposed algorithm due to overshoots on the remaining dimensions resulting in a peak regrowth. Herein, we propose

an alternative approach for generating a spiky function on the reserved eigenchannels  $\mathbf{R}$ .

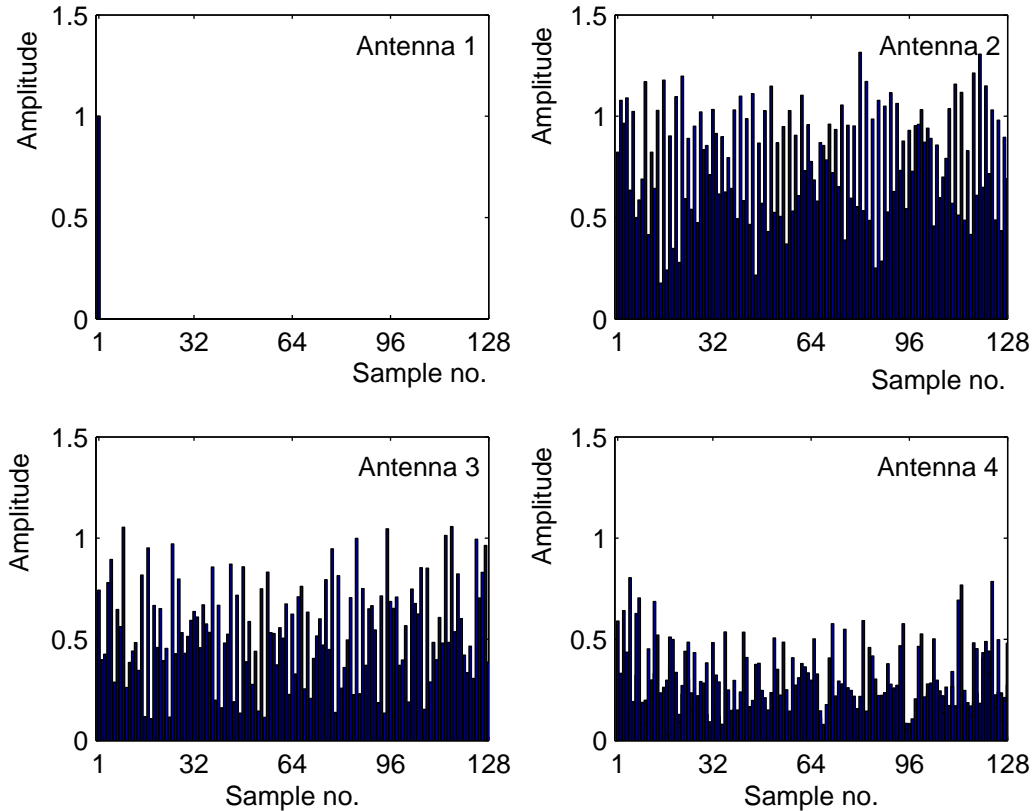


**Figure 3.4:** Bad spiky function with highest peak on the remaining dimensions beside a peak at the 1st antenna,  $R^1(n) = 1/V_{1,4}(n)$

### Designing a spiky function using $R_n = V_{\mu,M}^*(n)$

In the previous section, we used the weighting factor based on the last column of  $\mathbf{V}(n)$  to have a spiky function at the intended dimension. However, because of the occurrence of possibly *bad* spiky functions, there might be a peak regrowth on the remaining dimensions. The occurrence of the *bad* spiky function might be due to very small components  $V_{\mu,M}$  of the preprocessing matrix  $\mathbf{V}$ , which when used as  $1/V_{\mu,M}$ , results in big values. These big values when multiplied with big components of the  $\mathbf{V}$  matrix associated with the remaining spatial dimensions results in even larger values. This may cause higher peaks on remaining dimensions than the intended dimension when such high values pops up on them. This is, however, not a formal proof. The occurrence of the *bad* spiky function is still not completely investigated.

Subsequently, we present an alternative approach for designing an optimum spiky function on the reserved eigenchannels. As stated earlier, we know the weighting factors from the last column of  $\mathbf{V}(n)$ . Now, for computing  $R_n$ , we choose  $V_{\mu,M}^*(n)$  instead of  $1/V_{\mu,M}(n)$ .

Equation (3.12) can then be rephrased as

$$R_n = V_{\mu,M}^*(n), \quad (3.14)$$

where  $(\cdot)^*$  stands for complex conjugate. Multiplying a particular dimension with its conjugate will result in real values at that dimension, which will yield a spiky function at time zero at the corresponding dimension. The optimum spiky function generated with this approach has a lower peak at time zero on the intended dimension, however, an advantage of this approach is that the peaks on the remaining dimensions never exceed the intended peak on the specific dimension for which the spiky function is generated. Replacing Eq. (3.14) in Eq. (3.10), and applying an IFFT, the time domain signal can be obtained as

$$\tilde{\mathbf{r}}^\mu = \mathbf{F}^{-1} \cdot \mathbf{V} \cdot \begin{bmatrix} 0 & \dots & 0 \\ 0 & \dots & 0 \\ 0 & \dots & 0 \\ R_1^\mu & \dots & R_N^\mu \end{bmatrix}, \quad (3.15)$$

which is of course the same as Eq. (3.13) with  $R_n^\mu = V_{\mu,M}^*(n)$ . A normalized spiky function with  $R^1(n) = V_{1,4}^*(n)$ , i.e., a spike at the first antenna of a  $4 \times 4$  system is shown in Fig. 3.5.

This spiky function  $\tilde{\mathbf{r}}$  is then iteratively added to the transmit signal  $\tilde{\mathbf{s}}$  in time domain

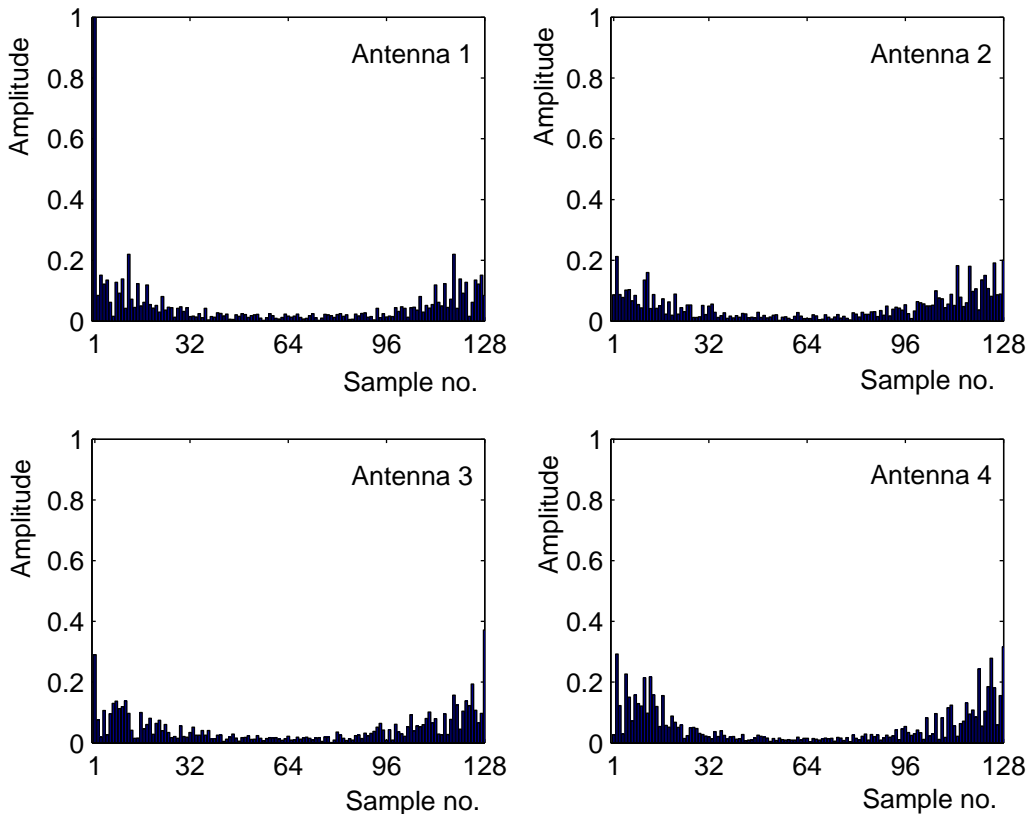


**Figure 3.5:** Absolute values of the spiky time domain vectors, with a highest peak at first antenna using  $R^1(n) = V_{1,4}^*(n)$

for PAR reduction. The algorithm used for the PAR reduction is presented next.

### 3.1.4 Tone Reservation algorithm

The necessary steps required to reduce the peak values crossing a predefined threshold  $\tau$  are

1. Initialize  $\mathbf{S}$  to be the DFT-domain information matrix, with the reserved dimensions set to zero, likewise, initialize  $\mathbf{R}$  to be the DFT-domain spiky matrix with the dimensions used for information set to zero.
2. Preprocess  $\mathbf{S}$  and  $\mathbf{R}$  using the preprocessing matrix  $\mathbf{V}$ , i.e.,  $\tilde{\mathbf{S}} = \mathbf{V}\mathbf{S}$  and  $\tilde{\mathbf{R}} = \mathbf{V}\mathbf{R}$
3. Transform  $\tilde{\mathbf{S}}$  and  $\tilde{\mathbf{R}}$  into time domain using the block-diagonal IFFT modulator  $\mathbf{F}^{-1}$ , i.e.,  $\tilde{\mathbf{s}} = \mathbf{F}^{-1}\tilde{\mathbf{S}}$  and  $\tilde{\mathbf{r}} = \mathbf{F}^{-1}\tilde{\mathbf{R}}$ . Set the iteration counter  $i$  to zero, i.e.,  $i = 0$
4. For the time-domain signal  $\tilde{\mathbf{s}}$ , find the value  $s_{m,\mu}^i$  and position  $m$  for which  $|s_{m,\mu}^i| = \max_k |s_k^i|$ .
5. If  $s_{m,\mu}^i < \tau$  or  $i > i_{max}$  then stop and transmit  $\tilde{\mathbf{s}}^i$ , otherwise
6. Update the time-domain vector

$$\tilde{\mathbf{s}}^{i+1} = \tilde{\mathbf{s}}^i - \alpha \cdot \left( s_{\mu,m}^i - e^{j \arg(s_{\mu,m}^i)} \cdot \tau \right) \cdot (\tilde{\mathbf{r}}^\mu \rightarrow m), \quad (3.16)$$

$i = i + 1$  and go to Step 4.

The last step is the time-domain Tone Reservation processing for a peak at transmit antenna  $\mu$ , where  $\mu = 1, 2, \dots, M_t$ , and location  $m$  using the  $\mu$ th spiky function  $\tilde{\mathbf{r}}^\mu$ . The iteration counter is  $i$  and  $\tilde{\mathbf{s}}$  denotes the  $M_t \times N$  time-domain matrix, where  $M_t$  is the total number of transmit antennas and  $N$  is the IFFT length.

### 3.1.5 Results and discussion

For a P2P MIMO-OFDM system with transmitter-sided precoding, the average power is distributed over all spatial dimensions. Moreover, we add a time-domain signal  $\tilde{\mathbf{r}}$  to the original signal  $\tilde{\mathbf{s}}$  for PAR reduction, thus, the average power is slightly increased with every iteration. The PAR after applying the TR algorithm is defined in here as

$$\text{PAR} = \frac{\max_{\forall \mu, \forall k} |s_{\mu,k} + r_{\mu,k}|^2}{\sigma^2}, \quad (3.17)$$

where  $k$  is the sample index, and  $\sigma^2 = E_{\forall \mu, \forall k} \{|x_{\mu,k}|^2\}$  is chosen to be the average power (averaged over all spatial dimensions) without any PAR reduction measures, i.e., with an unused spatial dimension and without an increase in the average power after the algorithm.

The channel matrix is chosen as in [80], however, with a channel length of  $l_h = 20$ . Moreover, it is assumed that the transmitter has perfect channel state information. For simulation, we chose a  $4 \times 4$  MIMO-OFDM system with 128 carriers and a 16-QAM modulation. To check and evaluate the performance, the complementary cumulative

distribution function (CCDF) is considered, which is the probability that the current PAR exceeds a certain threshold  $\tau$ , i.e.,  $Pr\{PAR > \tau\}$  [80], determined as,

$$Pr\{PAR > \tau\} = 1 - (1 - e^{-\tau})^{NM}, \quad (3.18)$$

assuming a complex Gaussian distribution.  $N$  is the total number of sub-carriers,  $M$  is the number of transmit antennas used, and  $\tau$  is the PAR target value (threshold value). For PAR reduction of the MIMO-OFDM transmit signal, the algorithm searches for the peak excursion on all spatial dimensions crossing a given target value  $\tau$  in time domain. The algorithm then cyclically shifts the corresponding  $\mu$ th spiky function to the appropriate location and is added to the transmitted signal  $\tilde{\mathbf{s}}$  according to Eq. (3.16). However, as the algorithm processes one peak at a time, the procedure is thus iterated to process the leftover peaks exceeding the threshold value  $\tau$ . Given a maximum number of iterations  $i_{max}$ , the algorithm searches for the highest peak in two ways,

1. Individual search on each spatial dimension by dividing the maximum iteration equally amongst all antennas, i.e.,  $i_{max}/M$ . The algorithm thus processes one antenna at a time for the given number of iterations, without considering any peak regrowth on the remaining antennas. For the  $\mu$ th antenna it then uses the corresponding spiky function for PAR reduction.
2. A joint search on all spatial dimension, the algorithm thus searches for the highest peak on all spatial dimension. It thus finds the antenna  $\mu$ , the position  $k$  and the value  $s$ , i.e.,  $s_{\mu,k}^i$  at the  $i$ th iteration and adds the corresponding  $\mu$ th spiky function to the transmitted signal for PAR reduction.

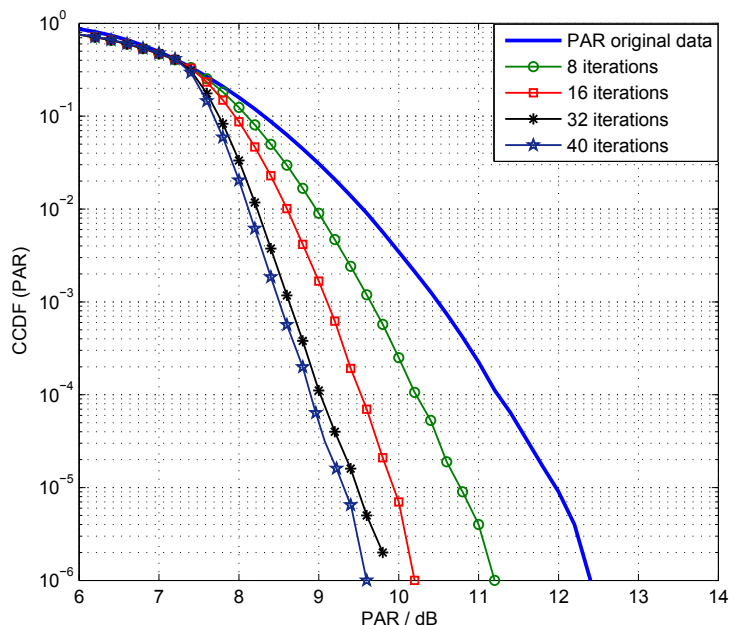


**Figure 3.6:** CCDF (PAR) of the proposed Tone Reservation algorithm for a  $4 \times 4$  P2P MIMO-OFDM, PAR target value  $\tau = 7.5$  dB,  $R_n^\mu = 1/V_{\mu,4}(n)$ , with a joint search algorithm

Figure 3.6 shows the simulation results for the first approach, i.e., designing the spiky function using Eq. (3.12), which for a  $4 \times 4$  MIMO-OFDM systems can be rephrased as  $R_n^\mu = 1/V_{\mu,4}(n)$ ,  $\mu = 1, \dots, 4$ . We have considered a joint search with a target PAR value  $\tau$  of 7.5 dB. Here, additionally one should be aware of a possible peak regrowth at the other dimensions during the reduction of peaks at one of them due to the occurrence of the *bad* spiky functions, as obvious from from Fig. 3.3. Due to a possible peak regrowth, the target value is chosen high, i.e., 7.5 dB as compared to 5.5 dB. Figure 3.6 shows that a gain of approximately 2.8 dB is obtained at  $10^{-6}$  with 40 iterations. However, this method is more sensitive to the choice of the number of iterations, the step size  $\alpha$ , and the PAR target value  $\tau$ . Easily, a non-converging situation can result with a flooring of the CCDF.

Figures 3.7 and 3.8 shows the simulation results for a  $4 \times 4$  P2P MIMO-OFDM system

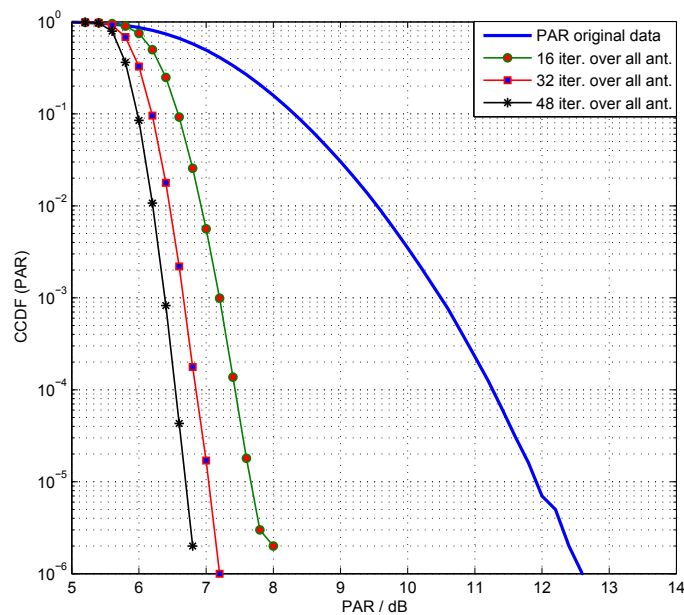


**Figure 3.7:** CCDF (PAR) of the proposed Tone Reservation algorithm for a  $4 \times 4$  P2P MIMO-OFDM, PAR target value  $\tau = 5.5$  dB,  $R_n^\mu = V_{\mu,4}^*(n)$ , with a joint search algorithm

using the second approach, i.e., using Eq. (3.14), which for a  $4 \times 4$  MIMO-OFDM system can be written as  $R_n^\mu = V_{\mu,4}^*(n)$ . Figure 3.7 shows the results for a joint processing, searching for the highest peak among all transmit antennas, and Fig. 3.8 shows the simulation results for individual search, i.e., searching for a peak on a particular antenna for a given number of iterations. In both cases, the PAR target value  $\tau$  is 5.5 dB. Figure 3.7 shows that a gain of approximately 5.8 dB can be obtained with 48 iterations at a CCDF of  $10^{-6}$  with a joint search. With as few as 16 iterations, already a gain of 4.6 dB can be obtained. In the case of an individual search, a gain of approximately 3.8 dB can be obtained with a total of 10 iterations per antenna at a CCDF of  $10^{-6}$  as shown in Fig. 3.8. The joint search is, of course, more efficient than the individual search.

As stated earlier, we add a time domain signal to the transmit signal for PAR reduction. In doing so, the mean transmit power of the signal is increased. It is thus necessary to consider the effect of the increase in the mean power and analyze the performance gain of the given algorithm under a mean power constraint.

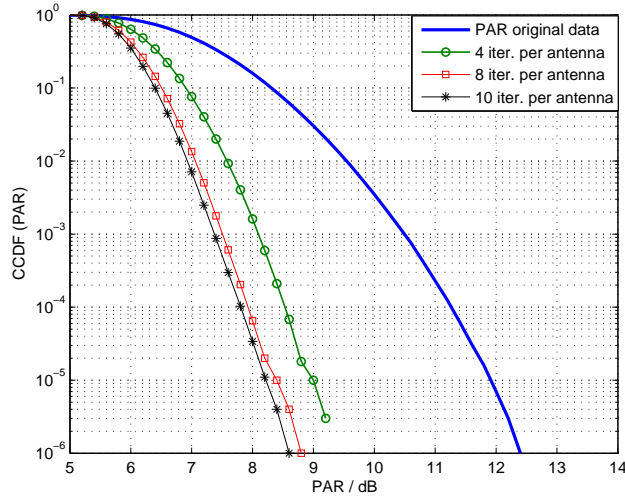


**Figure 3.8:** CCDF (PAR) of the proposed Tone Reservation algorithm for a  $4 \times 4$  PtP MIMO-OFDM, PAR target value  $\tau = 5.5$  dB,  $R_n^\mu = V_{\mu,4}^*(n)$  with an individual search algorithm

### Relative mean power increase $\Delta E$

In order to reduce the clipping probability of the signal  $\tilde{\mathbf{s}}$ , a time-domain signal  $\tilde{\mathbf{r}}$  is added to  $\tilde{\mathbf{s}}$  for PAR reduction. However, in doing so, the mean transmit power is increased. Thus, the relative mean transmit power increase  $\Delta E$  for the transmit signal  $\tilde{\mathbf{s}}$  can be defined as

$$\Delta E = 10 \log_{10} \frac{E\{\|\tilde{\mathbf{s}}^i + \tilde{\mathbf{r}}^i\|_2^2\}}{E\{\|\tilde{\mathbf{s}}\|_2^2\}}, \quad (3.19)$$

where  $E\{\|\tilde{\mathbf{s}}\|_2^2\} = \sigma^2$  is the nominal average power and  $E\{\|\tilde{\mathbf{s}}^i + \tilde{\mathbf{r}}^i\|_2^2\}$  is the average power at the  $i$ th iteration.

The simulation results are obtained with a small change in the TR algorithm presented in Sec. 3.1.4. In order to put a constraint on the mean power of the transmit signal, i.e.,  $\Delta E$ , Step 5 of the TR algorithm stated in Sec. 3.1.4 can be re-written as

- If  $s_{\mu,m}^i < \tau$  or  $i > i_{max}$  or  $\Delta E > \Delta E_{Th}$  then stop and transmit  $\tilde{\mathbf{s}}^i$ ,

where  $\Delta E_{Th}$  is the threshold value, i.e., the maximum relative mean power increase in the nominal average power of the transmit signal. Besides checking for the maximum number of iterations  $i_{max}$  and the PAR target value  $\tau$ , the algorithm now also checks an increase in the mean transmit power  $\Delta E$ . Using Eq. (3.19), the algorithm thus calculates the relative mean power increase  $\Delta E$  in each iteration.

Figure 3.9 presents the simulation results of the transmitted signal  $\tilde{\mathbf{s}}$  with limited  $\Delta E$ . The results are obtained for a P2P MIMO-OFDM with a joint search and PAR target value  $\tau = 5.5$  dB. It can be seen from Fig. 3.9 that a gain of approximately 4.2 dB can be obtained at  $10^{-6}$  for a slight increase in the mean power of  $\Delta E = 0.25$  dB.

For a point-to-point MIMO OFDM system, we applied the TR algorithm for PAR reduction. We next extend this TR approach for the PAR reduction of a point-to-multipoint

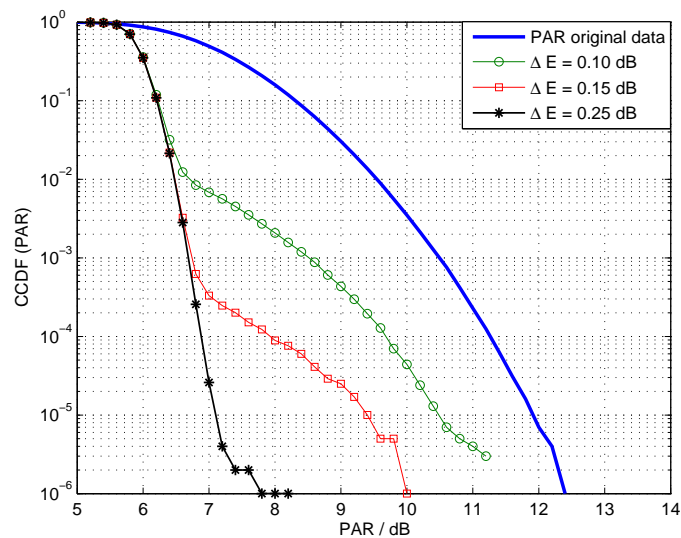


**Figure 3.9:** CCDF(PAR) of the TR algorithm with different mean power constraints  $\Delta E$ ,  $\tau = 5.5$  dB,  $R_n^\mu = V_{\mu,4}^*(n)$ , and a joint search algorithm with 40 iterations.

(broadcast channel) scenario. For a BC scenario, we will use the conventional approach of reserving a certain number of tones on all spatial dimensions. These tones are then used to generate a spiky function which is iteratively added to the transmit signal for PAR reduction. The PAR reduction of a multi-user broadcast scenario using the TR algorithm is presented in the following section.

## 3.2 PAR reduction in multi-user MIMO-OFDM systems

Next, we consider PAR reduction of a multi-user MIMO-OFDM, i.e., multipoint to point (Uplink or MAC) and point-to-multipoint (Downlink or BC) scenario. In the uplink scenario, let us consider the case of  $U$  users, each equipped with a single transmit antenna, communicating with a central base station having  $M_r$  antennas, where  $M_r$  is the total number of receive antennas. As the users are far apart and are considered to communicate independently, no joint signal processing nor any joint PAR reduction algorithms are possible at the transmitter sides, i.e., the mobile terminals. For a MAC scenario, where each user deploys a single antenna, the SISO PAR reduction schemes (as discussed in Section 2.6.1) can be applied. Tone reservation might be the best option, as it is the simplest and computationally the least complex PAR reduction technique. An alternative approach for the MAC scenario might also be Trellis shaping, where promising results can be obtained with a marginal loss in the channel capacity.

Secondly, we consider PAR reduction in a multi-user broadcast scenarios (BC, Downlink or point-to-multipoint scenario). In BC, a central base station, equipped with  $M_t$  transmit antennas, communicates with  $U$  users equipped with  $U_r$  receive antennas. For simplicity, we will consider  $U_r = 1$ , i.e., each user is equipped with a single antenna, only. Let  $M_r$  represent the total number of receive antennas deployed for all users, i.e.,  $M_r = \sum U_r$ .

Moreover, for convenience we assume  $M_t = M_r = M$ . Again, as stated earlier, the mobile stations (users) are independent and usually lie far apart. Thus, a joint signal processing is performed at the transmitter, for, e.g., spatial interference cancelation using preprocessing of the transmit data. It is thus possible to reduce the peak excursions of the transmit signals for each user at the central base station. However, the complexity of the PAR reduction schemes increases with the number of antennas. Besides the number of transmit antennas, precoding of the input data additionally influences the performance and complexity of the PAR reduction algorithms. A first approach for the PAR reduction of multi-user broadcast scenarios was made in [33, 80]. The authors proposed a variant of Selected Mapping (Selected Sorting). However, the algorithm is complex, requiring many FFTs.

Herein, we will try to extend TR for PAR reduction in a multi-user broadcast scenario. The reason to extend TR is two-fold. First, it is the least complex PAR reduction algorithm. Secondly, it reserves tones on all spatial dimensions so no additional implication has to be considered at the transmitter/receiver. In the previous section, we used the weakest eigenchannels to design an optimum spiky function, however, for the multi-user broadcast system, we will extend the conventional technique of the TR algorithm to generate the spiky function on a number of reserved tones. In the next section we will discuss the system model along with Tomlinson-Harashima (TH) precoding.

### 3.2.1 System model and TH precoding for multi-user broadcast

Figure 3.10 shows the system model for the MU MIMO-OFDM broadcast scenario. The base station (BS) has  $M_t$  transmit antennas and is transmitting  $\mu$  spatially multiplexed streams to  $U$  users. Each user has  $U_r = 1$  receive antenna. The number of transmit antennas is  $M_t$ , whereas  $M_r$  is used for the total number of receive antennas, and not for the number of antennas per user.

The signal flow diagram for our proposed algorithm is shown in Fig. 3.11. The in-

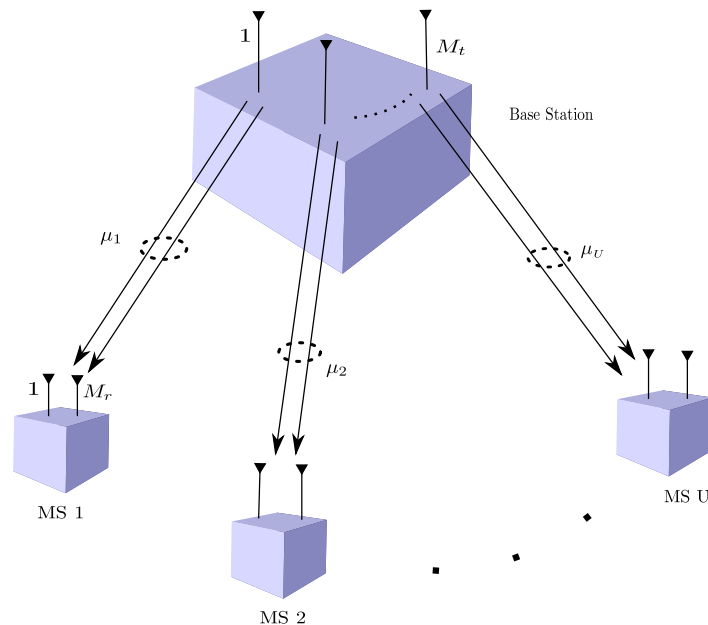


**Figure 3.10:** System model for multi-user broadcast scenarios

formation symbols are first encoded using Tomlinson-Harashima precoding as shown in Fig. 3.12.

Using TH precoding for the BC downlink, one first considers the conjugate transpose<sup>1</sup>

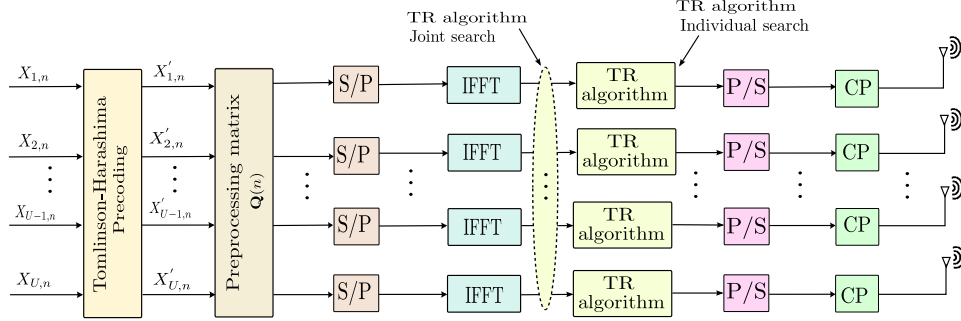


**Figure 3.11:** Multi-user broadcast scenario deploying TR algorithm

of the channel matrix [29]. Using QR decomposition, the channel matrix at the  $n$ th tone can then be rephrased as

$$\mathbf{H}^H(n) = \mathbf{Q}(n)\mathbf{R}(n) . \quad (3.20)$$

Let  $\mathbf{X}(n)$  be the input information vector at the  $n$ th tone. Using the preprocessing  $\mathbf{Q}(n)$ ,  $\mathbf{X}(n)$  is preprocessed to get  $\tilde{\mathbf{X}} = \mathbf{Q}(n)\mathbf{X}'(n)$ . After preprocessing,  $\tilde{\mathbf{X}}(n)$  is transmitted over the channel with a channel gain matrix  $\mathbf{H}(n)$ . After being filtered by the channel, the received vector  $\mathbf{Y}$  can be written as

$$\mathbf{Y}(n) = \mathbf{H}(n)\tilde{\mathbf{X}}(n) + \mathbf{w}(n) , \quad (3.21)$$

where  $\mathbf{w}(n)$  is additive white Gaussian noise. With Eq. (3.20), replacing  $\tilde{\mathbf{X}}$  and omitting the frequency index  $n$ , Eq. (3.21) can then be rephrased as

$$\mathbf{Y} = \mathbf{R}^H \underbrace{\mathbf{Q}^H \mathbf{Q}}_{\mathbf{I}} \mathbf{X}' + \mathbf{w} , \quad (3.22)$$

where  $\mathbf{Q}^H \mathbf{Q} = \mathbf{I}$ ,  $\mathbf{I}$  being an identity matrix. Omitting  $\mathbf{w}$ , Eq. (3.22) can thus be simplified as

$$\mathbf{Y} = \mathbf{R}^H \mathbf{X}' . \quad (3.23)$$

In order to have interference-free reception at the receiver, the data for each user at the central base station is pre-distorted such that the following equation holds:

$$\text{diag}(\mathbf{R}^H) \mathbf{X} = \mathbf{R}^H \mathbf{X}' , \quad (3.24)$$

which in a matrix form can be written as

$$\begin{bmatrix} r_{11}x_1 \\ r_{22}x_2 \\ \vdots \\ r_{UU}x_U \end{bmatrix} = \begin{bmatrix} r_{11} & 0 & \cdots & 0 \\ r_{21} & r_{22} & \cdots & 0 \\ \vdots & \vdots & \ddots & \vdots \\ r_{U1} & r_{U2} & \cdots & r_{UU} \end{bmatrix} \cdot \begin{bmatrix} x'_1 \\ x'_2 \\ \vdots \\ x'_U \end{bmatrix} . \quad (3.25)$$

<sup>1</sup> $H$  denotes Hermitian, i.e., conjugate transpose

As shown in Eq. (3.25),  $\mathbf{R}^H$  is a lower triangular matrix, the input data vector  $\mathbf{X}$  can thus be precoded as

$$\begin{aligned} x'_1 &= x_1 \\ x'_2 &= x_2 - \frac{r_{21}}{r_{22}}x'_1 \\ &\vdots \\ x'_U &= x_U - \frac{r_{UU-1}}{r_{UU}}x'_{U-1} - \cdots - \frac{r_{U1}}{r_{UU}}x'_1. \end{aligned}$$

The typical modulo operation of Tomlinson-Harashima precoding is used to limit the peak power, leading to the following solution

$$\begin{aligned} x'_1 &= x_1 \\ x'_2 &= \Gamma_{M_2} \left[ x_2 - \frac{r_{21}}{r_{22}}x'_1 \right] \\ &\vdots \\ x'_U &= \Gamma_{M_U} \left[ x_U - \frac{r_{UU-1}}{r_{UU}}x'_{U-1} - \cdots - \frac{r_{U1}}{r_{UU}}x'_1 \right], \end{aligned} \quad (3.26)$$

where  $\Gamma_{M_i}[x]$  is a two-dimensional modulo operation which can be rephrased with one-dimensional modulo operations as,

$$\Gamma_{\sqrt{M_i}}[x] = \Gamma_{\sqrt{M_i}}^{1D}[\text{Re}(x)] + j\Gamma_{\sqrt{M_i}}^{1D}[\text{Im}(x)] \quad (3.27)$$

with

$$\Gamma_{\sqrt{M_i}}^{1D}[x] = x - \sqrt{M_i}d \left\lfloor \frac{x + \frac{\sqrt{M_i}d}{2}}{\sqrt{M_i}d} \right\rfloor, \quad (3.28)$$

where  $\sqrt{M_i}$  is the PAM constellation size corresponding to an  $M_i$ -QAM of user  $i$ ,  $d$  is the constellation point spacing, and  $x$  is the complex value.

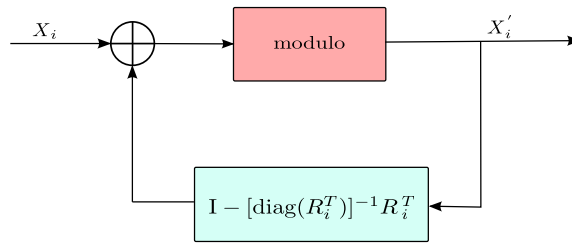


**Figure 3.12:** Block diagram of a TH precoder

### 3.2.2 Results and discussion for the multi-user BC

For BC scenarios, as in the conventional way, we reserve a certain percentage of the total number of tones on all spatial dimensions. These tones are used to generate a spiky function  $\mathbf{r}$ , which is then iteratively used in time domain to lower peak excursions crossing

a certain threshold value  $\tau$ . The algorithm used for PAR reduction of the BC systems is the same as the one presented for the point-to-point MIMO-OFDM system in Sec. 3.1.4, however with a slight modification in the first step of the algorithm, which is

- Initialize  $\mathbf{X}$  to be the DFT domain input data symbol, with the reserved bins set to zero. Pre-distort  $\mathbf{X}$  using TH precoding (Eq. (3.26)) to obtain  $\mathbf{X}'$

After TH precoding,  $\mathbf{X}'$  is preprocessed using  $\mathbf{Q}$  to obtain  $\tilde{\mathbf{X}}$ . The rest of the steps are the same as presented in Sec. 3.1.4.

For simulations, we considered a BC system with a central base station equipped with  $M_t = 4$  transmit antennas communicating with  $U = 4$  users, each one equipped with a single receive antenna  $U_r = 1$ . The total number of receive antennas thus equals 4, i.e.,  $M_r = \sum U_r = 4$ . Again, the channel matrix  $\mathbf{H}$  is adopted from [80] with a channel length  $l_{ch} = 5$ , where the channel coefficients are i.i.d. complex Gaussian distributed with zero mean and variance  $= 1/l_{ch}$ . We consider a 16-QAM constellation with Grey mapping and the number of subcarriers to be 128.

As stated earlier, the proposed algorithm searches for a peak excursion on all spatial dimensions. The spiky function is then cyclically shifted to that location and is added to the transmit signal for PAR reduction. However, the hunt for the peak excursion on all spatial dimensions is carried out in two ways, 1) individually, where the algorithm considers one antenna at a time and processes it for the defined number of iterations or 2) a joint search, where the algorithm searches for the highest peak among all spatial dimensions for a given maximum number of iterations. In the joint search, the  $M$ -fold iterations are applied to all dimensions and is thus more efficient than the individual search.

The algorithm adds a time-domain spiky function  $\mathbf{r}$  to the transmit signal  $\mathbf{x}$  for PAR reduction, thus, the average power increases slightly at each iteration. However, in the calculation of the PAR of the transmit signal after the algorithm, we consider a nominal average power. The PAR after the maximum number of iterations  $i_{\max}$  is thus defined as

$$\text{PAR} = \frac{\max_{\forall \mu, \forall k} |x_{\mu,k} + r_{\mu,k}|^2}{\sigma^2}, \quad (3.29)$$

where  $k$  is the sample index, and  $\sigma^2 = E_{\forall \mu, \forall k} \{|x_{\mu,k}|^2\}$  is chosen to be the average power (averaged over all spatial dimensions) without any PAR reduction measures. To check and evaluate the performance, the CCDF is used, again.

For simulation results, we consider 5 % and 10 % redundancy of the total subcarriers. The tones are used to generate a spiky function, which is then iteratively used for PAR reduction. The selection of the tones to be reserved is random. A spiky function generated on 5 % reserved tones is as shown in Fig. 3.13.

Figure 3.14 and 3.15 show the simulation results for MU broadcast using the TR algorithm with 5 % and 10 % redundancy, respectively, with separate and joint search for a PAR target value  $\tau = 7.0$  dB. For 5 % redundancy, a gain of 4 dB and 4.6 dB is obtained with individual and joint search at a CCDF (PAR)  $10^{-6}$ , respectively. The number of iterations for the individual search are 12 iterations per antenna while a total of 48 iterations are used in case of the joint search. In the joint search, the four-fold iterations are applied to all antennas. With 10 % redundancy, a gain of as much as 5.2 dB and 6 dB can be obtained at a CCDF of  $10^{-6}$  with an individual search with 8 iteration per antenna and a joint search with 32 iterations in total, respectively. If the latency of the system

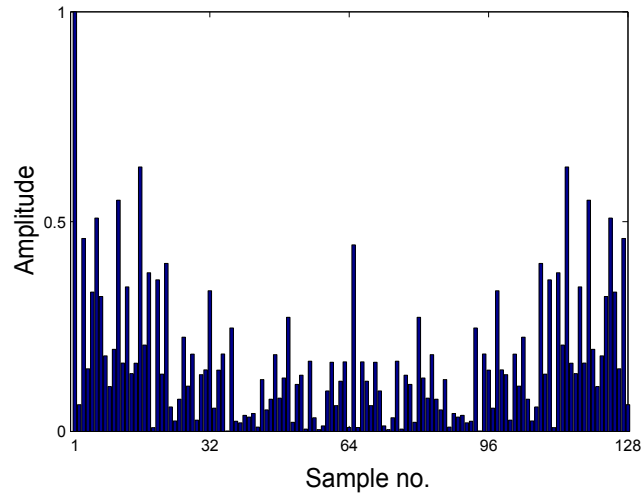


**Figure 3.13:** Absolute values of an exemplary time-domain spiky function for 5 % redundant tones

has to be taken into considerations, then a gain of 4 dB and 5.6 dB can be obtained with as few as 4 iteration per antenna and 16 iterations in total using individual and joint search algorithms, respectively.

Next, we consider the relative mean power increase  $\Delta E$  due to the addition of the time

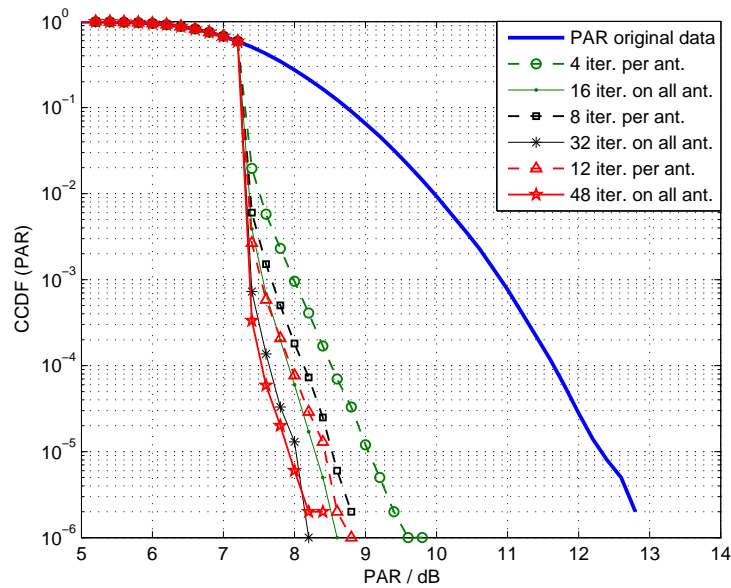


**Figure 3.14:** CCDF(PAR) of the TR algorithm for multi-user broadcast with 5 % redundancy, for separate and joint processing

domain signal  $\mathbf{r}$  for PAR reduction using Eq. (3.19). Figures 3.16 and 3.17 show the simulation results for 5 % and 10 % redundant tones for different  $\Delta E$  with a joint search algorithm,  $\tau = 7.0$  dB, and 32 iterations. A gain of approximately 3.2 dB can be obtained for 5 % redundancy with a marginal increase in the relative mean power  $\Delta E = 0.5$  dB as shown in Fig. 3.16. However, with 10 % redundancy the gain is as high as 5.4 dB at

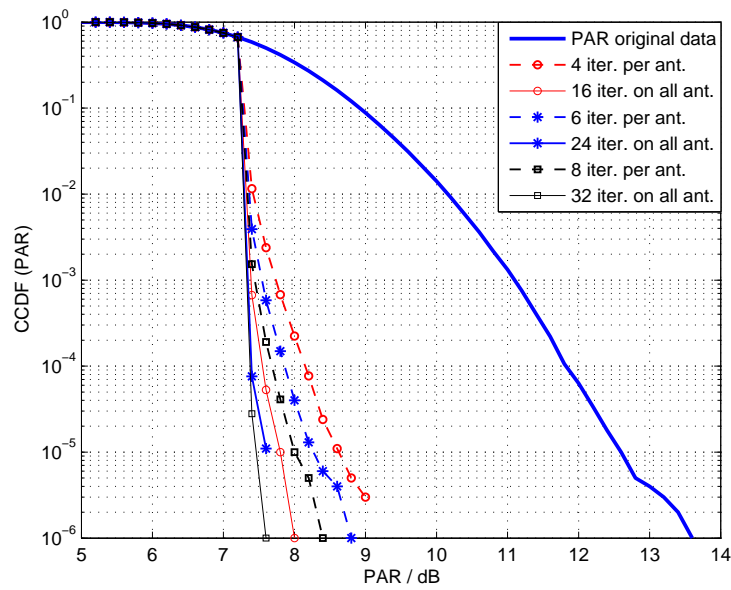


**Figure 3.15:** CCDF(PAR) of the TR algorithm for multi-user broadcast with 10 % redundancy, for separate and joint processing

a CCDF of  $10^{-6}$  for  $\Delta E = 0.3$  dB with  $\tau = 7.0$  dB, and 32 iterations. The simulation results show that the mean power increase is almost negligible for 10 % redundancy, with a high gain.

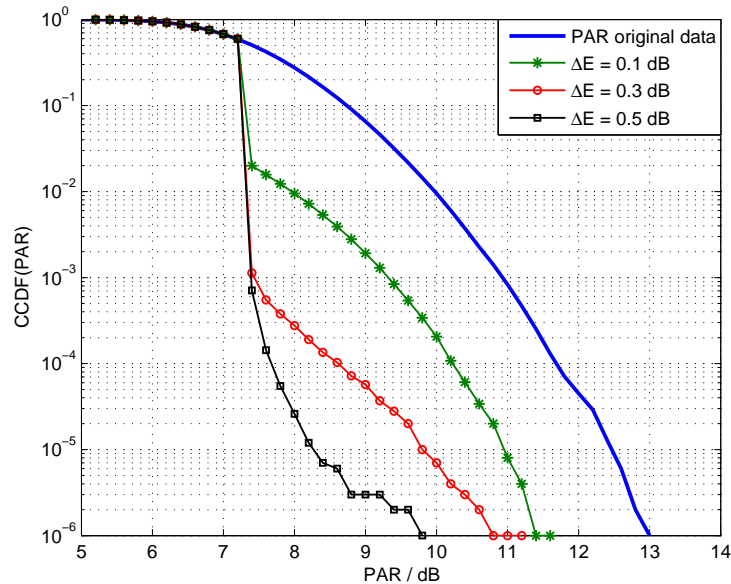


**Figure 3.16:** CCDF(PAR) of the TR algorithm for multi-user broadcast with 5 % redundancy depending on  $\Delta E$  with a joint processing

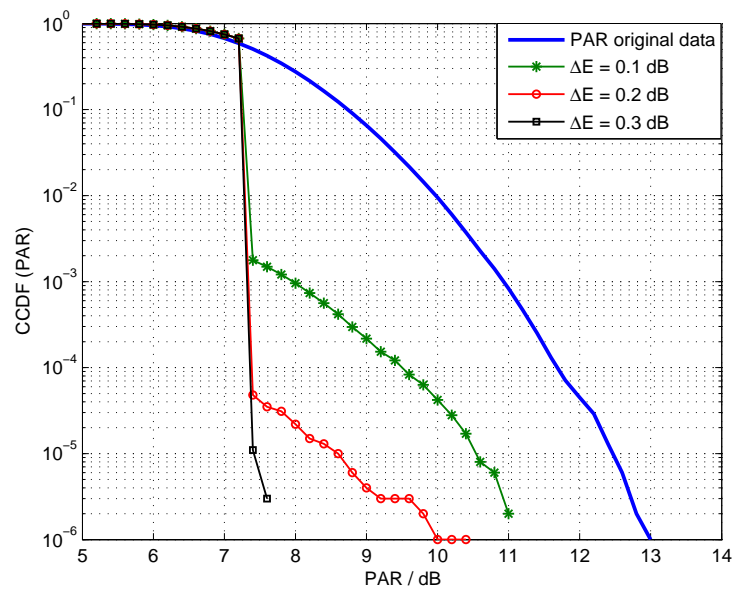


**Figure 3.17:** CCDF(PAR) of the TR algorithm for multi-user broadcast with 10 % redundancy depending on  $\Delta E$  with a joint processing

# Chapter 4

## Least-Squares Iterative PAR Reduction for MIMO and Multi-user OFDM Systems

In the previous chapter, we extended the Tone Reservation algorithm for point-to-point and multi-user MIMO-OFDM systems. Herein, we propose a novel Least-Squares iterative approach for the PAR reduction of point-to-point and multi-user MIMO-OFDM systems. For the P2P MIMO case, we will again consider that the last singular values of the channel are weak, such that the associated eigenchannels are hardly suited for data transmission. Thus, reserving them would offer redundancy for the PAR reduction on the remaining dimensions. These eigenchannels are then used to approximate the peak excursions on the remaining spatial dimensions in a least-squares fashion in DFT domain. The estimated function is transformed into time domain using an IDFT modulator and is added to the transmit signal for PAR reduction. The procedure can be iterated in order to reach a certain target value  $\tau$ .

Furthermore, we extend the Least-Squares approach for PAR reduction for multi-users broadcast scenarios. However, for a BC scenario, we will consider medium to large scale multi-user MIMO systems. For large scale MIMO systems, there is a high probability that one of the users is inactive. Subsequently, we will assume that one user is inactive and the channel associated with that user at the central base station is used to approximate the peak excursion of the remaining dimensions in DFT domain. Using an IDFT, the modeled function is transformed into time domain and added to the transmit signal for PAR reduction. The rest of the chapter is structured as follows. First, we start with P2P MIMO-OFDM systems. For the P2P scenario, in Section 4.1.1, we recall the key idea as already presented in Chapter 3 for a P2P MIMO systems followed by the system model in Section 4.1.2. Section 4.1.3 presents the idea of approximating the peak excursions by the reserved spatial dimension. The Least-Squares algorithm itself is also discussed in Section 4.1.3. The simulation results for the proposed algorithm along with comparison to some existing PAR reduction techniques are outlined in Section 4.1.4. Section 4.2 is devoted to the extension of the Least-Squares approach for multi-user broadcast scenarios.

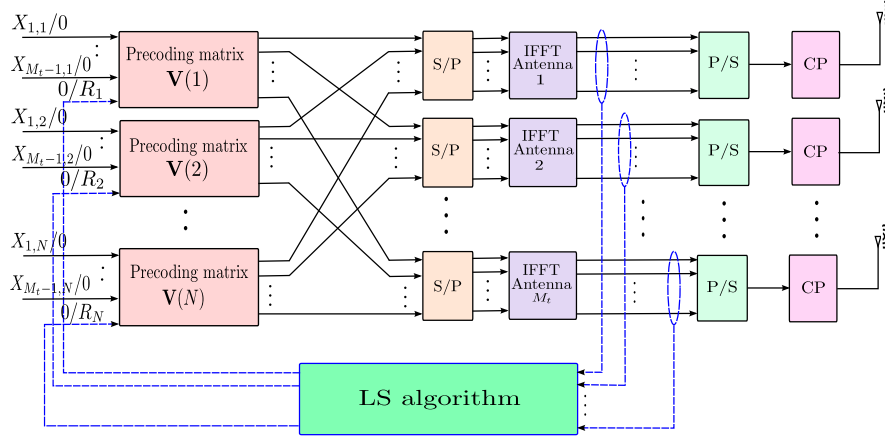


Figure 4.1: MIMO-OFDM system model with LS algorithm

## 4.1 Least-Squares iterative PAR reduction for P2P MIMO-OFDM systems

### 4.1.1 Key idea

Let us recall from Sec. 3.1.1 that the channel matrix in DFT domain at the  $n$ th carrier  $\mathbf{H}(n)$ , of a P2P MIMO-OFDM system, can be rephrased using the singular value decomposition (SVD) as

$$\mathbf{H}(n) = \mathbf{U}(n) \cdot \mathbf{\Lambda}(n) \cdot \mathbf{V}^H(n), \quad (4.1)$$

where  $\mathbf{U}(n)$  and  $\mathbf{V}(n)$  are unitary postprocessing and preprocessing matrices, respectively and  $\mathbf{\Lambda}(n)$  is a diagonal matrix of the singular values of  $\mathbf{H}(n)$ . For  $M_t = M_r = M$ , in matrix form,  $\mathbf{\Lambda}(n)$  can be expressed as

$$\mathbf{\Lambda}(n) = \begin{pmatrix} \sigma_{1,1}(n) & 0 & 0 & 0 \\ 0 & \sigma_{2,2}(n) & 0 & 0 \\ \vdots & \dots & \ddots & \vdots \\ 0 & 0 & 0 & \sigma_{M,M}(n) \end{pmatrix} \quad (4.2)$$

Herein, we will again consider that the last singular value to be very weak such that the associated eigenchannels are hardly suitable for data transmission and are thus reserved to be utilized to approximate the peak excursions on the remaining dimensions.

### 4.1.2 System model and pre coding

Figure 4.1 shows a block diagram of the point-to-point MIMO-OFDM system using our Least-Squares algorithm. We will again consider transmitter side precoding and receiver side post-processing. Let  $\mathbf{X}(n)$  be the input data vector at the  $n$ th tone, which is precoded using the preprocessing matrix  $\mathbf{V}(n)$  as  $\tilde{\mathbf{X}} = \mathbf{V}(n) \cdot \mathbf{X}(n)$ , with  $\mathbf{X}(n) = [X_{1,n}, X_{2,n}, \dots, X_{M,n}]^T$  where  $X_{\mu,n}$  is the input data symbol at the  $\mu$ th,  $\mu = 1, 2, \dots, M$ , spatial channel and the  $n$ th carrier. After the IFFT modulator, the input data vector is padded with a cyclic prefix (CP) and is transmitted over a channel with channel gain

matrix  $\mathbf{H}$ . At the receiver, the CP is stripped off from the received data and is followed by the DFT. Let  $\tilde{\mathbf{Y}}(n)$  be the  $n$ th received vector in the DFT domain given as

$$\tilde{\mathbf{Y}}(n) = \mathbf{H}(n)\tilde{\mathbf{X}}(n) + \mathbf{w}(n), \quad (4.3)$$

where  $\mathbf{w}(n)$  is additive white Gaussian noise. After the DFT, the received data vector  $\tilde{\mathbf{Y}}(n)$  at the  $n$ th frequency bin is postprocessed by  $\mathbf{U}^H(n)$  to obtain the output  $\mathbf{Y}(n)$  as shown in Fig. 4.2. Mathematically, we write

$$\mathbf{Y}(n) = \mathbf{U}^H \tilde{\mathbf{Y}}(n) = \mathbf{U}^H \mathbf{H}(n) \tilde{\mathbf{X}}(n) + \tilde{\mathbf{w}}(n), \quad (4.4)$$

where,  $\tilde{\mathbf{w}}(n) = \mathbf{U}^H \cdot \mathbf{w}(n)$  has the same statistical distribution as  $\mathbf{w}(n)$ . Expanding Eq. (4.4) and omitting  $\tilde{\mathbf{w}}(n)$ , we get

$$\mathbf{Y}(n) = \overbrace{\mathbf{U}(n)^H \cdot \mathbf{U}(n)}^{\mathbf{I}} \cdot \underbrace{\mathbf{\Lambda}(n)}_{\mathbf{H}(n)} \cdot \underbrace{\mathbf{V}^H(n) \cdot \mathbf{V}(n)}_{\tilde{\mathbf{X}}(n)} \cdot \mathbf{X}(n), \quad (4.5)$$

which simplifies to

$$\mathbf{Y}(n) = \mathbf{\Lambda}(n) \cdot \mathbf{X}(n), \quad (4.6)$$

where  $\mathbf{Y}(n) = [Y_{1,n}, Y_{2,n}, \dots, Y_{M,n}]^T$  is the output vector, with  $Y_{\mu,n}$  being the  $n$ th output symbol at the  $\mu$ th,  $\mu = 1, 2, \dots, M$ , spatial channel. Equation (4.6) in matrix notations can be written as

$$\begin{pmatrix} Y_{1,n} \\ Y_{2,n} \\ \vdots \\ Y_{M,n} \end{pmatrix} = \begin{pmatrix} \sigma_{1,1}(n) & 0 & 0 & 0 \\ 0 & \sigma_{2,2}(n) & 0 & 0 \\ 0 & 0 & \ddots & 0 \\ 0 & 0 & 0 & \sigma_{M,M}(n) \end{pmatrix} \begin{pmatrix} X_{1,n} \\ X_{2,n} \\ \vdots \\ X_{M,n} \end{pmatrix}. \quad (4.7)$$

We again represent  $\mathbf{X}(n)$  by two disjoint sets,  $\mathbf{S}(n)$  and  $\mathbf{R}(n)$ , such that  $\mathbf{X}(n) = \mathbf{S}(n) + \mathbf{R}(n)$ . Let  $\mathbf{S}(n)$  denote the first dimensions used for data transmission, i.e.,

$$\mathbf{S}(n) = ( X_{1,n} \ X_{2,n} \ \dots \ X_{M-1,n} \ 0 )^T.$$

where  $X_{\mu,n}$  is the signal at the  $\mu$ th spatial dimension and the  $n$ th frequency. Likewise, let us define  $\mathbf{R}(n)$ , which will be used for modeling the excursions above a chosen threshold, i.e.,

$$\mathbf{R}(n) = ( 0 \ 0 \ \dots \ 0 \ X_{M,n} )^T,$$

whereas  $X_{M,n}$  should not be confused with the input data, it contains the modeled corrective signal that is used for PAR reduction. As shown in Fig. 4.1, the input data vector  $\mathbf{S}(n)$  and corrective signal  $\mathbf{R}(n)$  are preprocessed as

$$\tilde{\mathbf{S}}(n) = \mathbf{V}(n) \cdot \mathbf{S}(n) = \mathbf{V}(n) \cdot ( X_{1,n} \ \dots \ X_{M-1,n} \ 0 )^T \quad (4.8)$$

and

$$\tilde{\mathbf{R}}(n) = \mathbf{V}(n) \cdot \mathbf{R}(n) = \mathbf{V}(n) \cdot ( 0 \ \dots \ 0 \ X_{M,n} )^T. \quad (4.9)$$

We combine both components and move them into time domain,

$$\tilde{\mathbf{x}} = \tilde{\mathbf{s}} + \tilde{\mathbf{r}} = \mathbf{F}^{-1} \mathbf{V} \mathbf{X} = \mathbf{F}^{-1} \mathbf{V} (\mathbf{S} + \mathbf{R}) , \quad (4.10)$$

using a block-IDFT matrix  $\mathbf{F}^{-1}$  with blocks of diagonal submatrices of  $M$  identical diagonal elements  $w_{n,k}$ . All vectors  $\mathbf{X}, \tilde{\mathbf{X}}, \dots$  are obtained by concatenating the vectors  $\mathbf{X}(n), \tilde{\mathbf{X}}(n), \dots$ . Now, the goal is to estimate and model the exceedence values by  $\mathbf{R}$  in DFT domain to finally subtract that model from the signal.

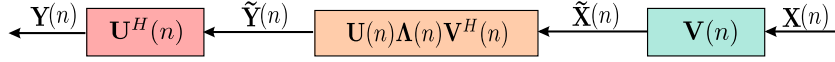


**Figure 4.2:** SVD MIMO diagonalization

### 4.1.3 Exceedence spike representation

Let  $\tilde{\mathbf{s}}$  be the transmitted signal in time domain with no data transmission on the reserved eigenchannels. The proposed algorithm searches for peak values that exceed a PAR target value. These exceedence excursions are then represented and modeled by the last spatial dimension in frequency domain. As illustrated in Fig. 4.3, let  $\mathbf{e}$  be a vector representing the exceeding excursions in time domain on all spatial dimensions of a MIMO-OFDM transmitted signal, i.e.,

$$\mathbf{e} = ((e_{1,1}e_{2,1} \cdots e_{M,1}), \cdots, (e_{1,n}e_{2,n} \cdots e_{M,n}))^T, \quad (4.11)$$

where

$$e_{\mu,k} = \begin{cases} 0 & \text{for } x_{\mu,k} \leq x_{target} , \\ x_{\mu,k} - e^{j\angle(x_{\mu,k})} \cdot x_{target} & \text{for } x_{\mu,k} > x_{target} . \end{cases} \quad (4.12)$$

Let  $\mathbf{E}$  be the DFT-domain counterpart of  $\mathbf{e}$ , i.e.,  $\mathbf{E} = \mathbf{F} \cdot \mathbf{e}$ , where  $\mathbf{F}$  is a block DFT matrix. Now, we use the Least-Squares approach for estimating the exceedence values above the chosen threshold by the last (weakest) spatial dimension.

#### Least-Squares approach

In order to estimate the exceedence excursions by the reserved spatial dimension, Eq. (4.9) can be reformulated as

$$\begin{pmatrix} \mathbf{V}(1) & \mathbf{0} & \cdots & \mathbf{0} \\ \mathbf{0} & \mathbf{V}(2) & \cdots & \mathbf{0} \\ \vdots & \cdots & \ddots & \vdots \\ \mathbf{0} & \cdots & \cdots & \mathbf{V}(N) \end{pmatrix} \begin{pmatrix} 0 \\ \vdots \\ X_{M,1} \\ \vdots \\ 0 \\ \vdots \\ X_{M,N} \end{pmatrix} = \boldsymbol{\varphi} , \quad (4.13)$$

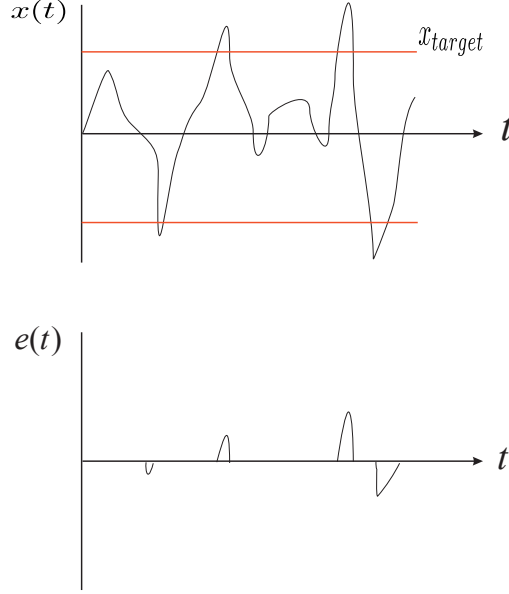


**Figure 4.3:** Representation of exceedence values

for all frequency bins  $1, \dots, N$ . As shown, Eq. (4.13) essentially only addresses the last columns of the blocks  $\mathbf{V}(n)$  inside the  $\mathbf{V}$  matrix. Thus, Eq. (4.13) can be rephrased as

$$\begin{pmatrix} \mathbf{V}_{:M}(1) & \mathbf{0} & \dots & \mathbf{0} \\ \mathbf{0} & \mathbf{V}_{:M}(2) & \dots & \mathbf{0} \\ \vdots & \dots & \ddots & \vdots \\ \mathbf{0} & \mathbf{0} & \dots & \mathbf{V}_{:M}(N) \end{pmatrix} \begin{pmatrix} X_{M,1} \\ X_{M,2} \\ \vdots \\ X_{M,N} \end{pmatrix} = \boldsymbol{\varphi}, \quad (4.14)$$

where  $\mathbf{V}_{:M}(n)$  represents the  $M$ th column ( $:$  stands for all rows) of the  $n$ th  $\mathbf{V}$  matrix, which can be represented in a compact form as

$$\boldsymbol{\varphi} = \mathbf{V}_{:M} \cdot \mathbf{R}_M, \quad (4.15)$$

where  $\mathbf{V}_{:M}$  is a block diagonal matrix with the  $M$ th column of  $\mathbf{V}(n)$  at the  $n$ th diagonal, and  $\mathbf{R}_M$  contains only the last spatial components. In a least-squares sense, the column vector  $\boldsymbol{\varphi}$  shall approximate  $\mathbf{E}$  according to

$$\min_{\mathbf{R}_M} \|\boldsymbol{\varphi} - \mathbf{E}\|_2^2. \quad (4.16)$$

In Eq. (4.16), the number of equations is higher than the number of unknowns. Thus, this leads to a pseudo-inverse solution. Eq. (4.16) is rewritten as

$$\|\boldsymbol{\varphi} - \mathbf{E}\|_2^2 = (\mathbf{V}_{:M} \mathbf{R}_M - \mathbf{E})^H (\mathbf{V}_{:M} \mathbf{R}_M - \mathbf{E}), \quad (4.17)$$

where  $H$  stands for Hermitian (conjugate transpose). Equation (4.17) can further be simplified as

$$\|\boldsymbol{\varphi} - \mathbf{E}\|_2^2 = \mathbf{R}_M^H \mathbf{V}_{:M}^H \mathbf{V}_{:M} \mathbf{R}_M - 2\mathbf{R}_M^H \mathbf{V}_{:M}^H \mathbf{E} + \mathbf{E}^H \mathbf{E}. \quad (4.18)$$

Now computing the gradient with respect to  $\mathbf{R}_M$  and equating to zero, we obtain

$$\frac{\partial}{\partial \mathbf{R}_M} (\mathbf{R}_M^H \mathbf{V}_{:M}^H \mathbf{V}_{:M} \mathbf{R}_M - 2\mathbf{R}_M^H \mathbf{V}_{:M}^H \mathbf{E} + \mathbf{E}^H \mathbf{E}) = 0, \quad (4.19)$$

with the identities,  $\frac{\partial}{\partial \mathbf{R}_M} (\mathbf{R}_M^H \mathbf{\Theta} \mathbf{\Lambda}) = \mathbf{\Theta} \mathbf{\Lambda}$  and  $\frac{\partial}{\partial \mathbf{R}_M} (\mathbf{R}_M^H \mathbf{\theta} \mathbf{R}_M) = 2 \mathbf{\theta} \mathbf{R}_M$ , Eq. (4.19) can be simplified as

$$2 (\mathbf{V}_{:M}^H \mathbf{V}_{:M} \mathbf{R}_M - \mathbf{V}_{:M}^H \mathbf{E}) = 0, \quad (4.20)$$

which for  $\mathbf{R}_M$  can be solved as

$$\mathbf{R}_M = (\mathbf{V}_{:M}^H \cdot \mathbf{V}_{:M})^{-1} \cdot \mathbf{V}_{:M}^H \cdot \mathbf{E}. \quad (4.21)$$

The procedure is iterated, as the peaks exceeding the target value are not estimated exactly by the Least-Squares approach in one iteration, as shown in Fig. 4.4.

The least squares algorithm is described as follows.

### Least Squares algorithm

1. Initialize  $\mathbf{S}$  to be the DFT-domain information vector, with the reserved dimension set to zero. Precode it using the pre-processing matrix as shown in Eq. (4.8).
2. Initialize the time-domain solution  $\tilde{\mathbf{s}}$ , i.e.,  $\tilde{\mathbf{s}} = \text{IFFT}(\tilde{\mathbf{S}})$ . Set  $i = 0$ .
3. If  $i > i_{max}$ , stop and transmit  $\tilde{\mathbf{s}}^i$ , otherwise
4. Initialize  $\mathbf{e}$  to represent the exceedence excursion according to Eq. (4.12) and transform it into DFT domain, i.e.,  $\mathbf{E} = \text{FFT}(\mathbf{e})$ .
5. Approximate  $\mathbf{E}$  by the last spatial dimension using Eq. 4.21. Precode it using the preprocessing matrix  $\mathbf{V}$  and transform it into time domain applying the IFFT modulator, i.e.,  $\tilde{\mathbf{r}} = \mathbf{F}^{-1} \tilde{\mathbf{R}}$ .
6. Update the time-domain vector

$$\tilde{\mathbf{s}}^{(i+1)} = \tilde{\mathbf{s}}^{(i)} - \tilde{\mathbf{r}}, \quad (4.22)$$

$i = i + 1$  and go to Step 3.

$i$  is the iteration counter and  $\tilde{\mathbf{s}}$  denotes the  $M \cdot N$  long time-domain vector, where  $M$  is the number of transmit antennas and  $N$  is the IFFT length. The structure follows Eq. (4.11). After having presented the least-squares procedure, we will right away modify it by introducing a weight factor which equals the number of antennas. One should note that it is very unlikely for reasonable antenna numbers (no massive MIMO) that more than one antenna channel will see a value exceeding the threshold at the same time. Hence, the least-squares approach will not approximate the peak, but yield a result reduced by a factor of  $M$ , since it tries, at the same time, to approximate the zeros (no exceedences) in the other antenna channels.<sup>1</sup> This is the drawback of an  $l_2$  norm instead of  $l_\infty$ . We introduce a weighting factor  $\gamma$  in the algorithm, which leads to optimum performance for

---

<sup>1</sup>Illustration: Assume  $e$  and  $M - 1$  zeros to be approximated in least-squares sense. This means  $\frac{d}{dx} [(x - e)^2 + (M - 1)(x - 0)^2] = 0 \implies x = e/M$ .

$\gamma = M$ . The weighting can be realized by modifying steps 3 or 5 of the presented LS algorithm. Modifying Step 4 means weighting the peak excursions before mapping them onto the last spatial dimension. Equation (4.12) becomes

$$e_{\mu,k} = \begin{cases} 0 & \text{for } x_{\mu,k} \leq x_{target} , \\ \gamma (x_{\mu,k} - e^{j\angle(x_{\mu,k})} \cdot x_{target}) & \text{for } x_{\mu,k} > x_{target} . \end{cases} \quad (4.23)$$

Alternatively, one could instead write Step 6, Eq. (4.22) as

$$\tilde{\mathbf{s}}^{(i+1)} = \tilde{\mathbf{s}}^{(i)} - \gamma \tilde{\mathbf{r}} . \quad (4.24)$$

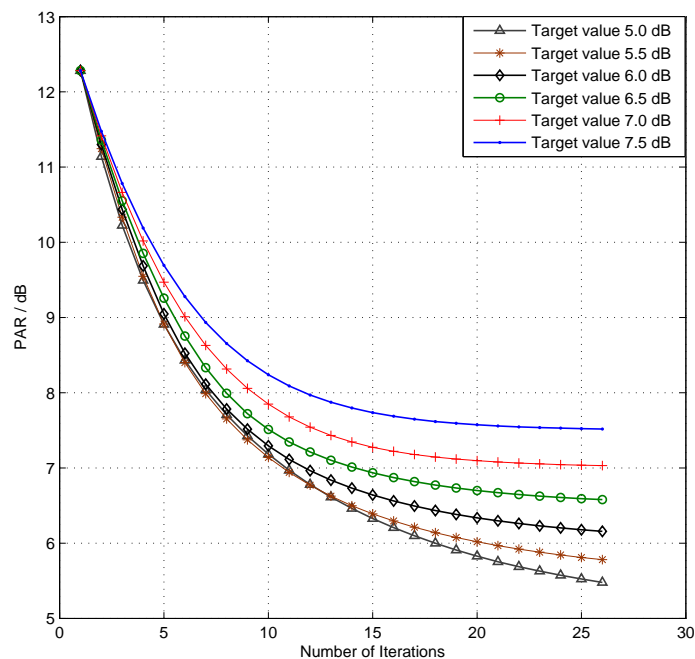


**Figure 4.4:** Exemplary PAR reduction with increasing number of iterations using our LS algorithm with different target values

#### 4.1.4 Results and discussion

For simulation results, we consider a  $4 \times 4$  MIMO-OFDM system with 128 sub-carriers each modulated by a 16-QAM constellation. We have considered transmitter-sided precoding, thus, the average power is distributed over all spatial dimensions. Moreover, it is also necessary to point out that in our LS algorithm we add a time-domain signal  $\tilde{\mathbf{r}}$  to the transmit signal  $\tilde{\mathbf{s}}$  for PAR reduction, thus, the average power is slightly increased with every iteration. However, in the PAR calculation of the transmit signal after the LS algorithm, we consider the initial mean power without any increase due to the corrective signal. The PAR of the transmit signal after applying the LS algorithm is defined in here

as

$$\text{PAR} = \frac{\max_{\forall \mu, \forall k} |x_{\mu,k} + \gamma r_{\mu,k}|^2}{\sigma^2}, \quad (4.25)$$

where  $k$  is the sample index, and  $\sigma^2 = E_{\forall \mu, \forall k} \{|x_{\mu,k}|^2\}$  is chosen to be the average power without any PAR measures, i.e., with an unused spatial dimension and without any increase in the average power after the algorithm. We first consider no additional weighting, i.e.,  $\gamma = 1$ .

Figure 4.5 shows the simulation results for a target PAR value ( $\tau$ ) of 5.0 dB. A gain of approximately 6.4 dB is obtained already at  $10^{-5}$  with 25 iterations. It is also clear from Fig. 4.5 that a sufficient gain is already obtained with 5-10 iterations (approx. 3.8 - 4.8 dB, respectively).

Figure 4.6 shows simulation results for *weighted LS* with a weighting factor  $\gamma = 4$  and a

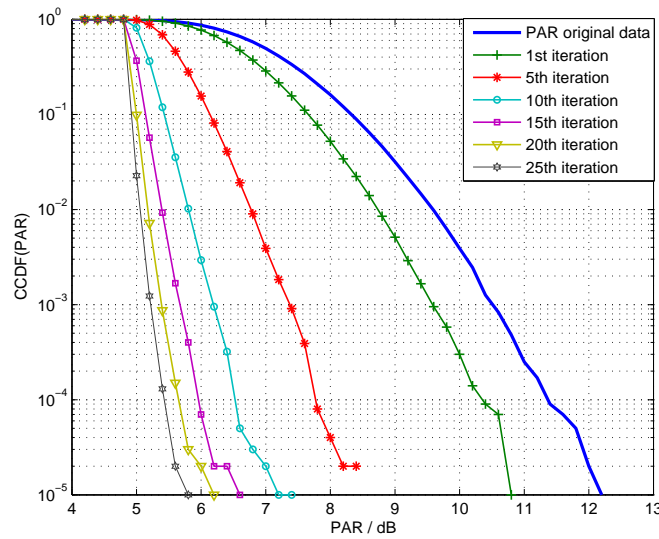
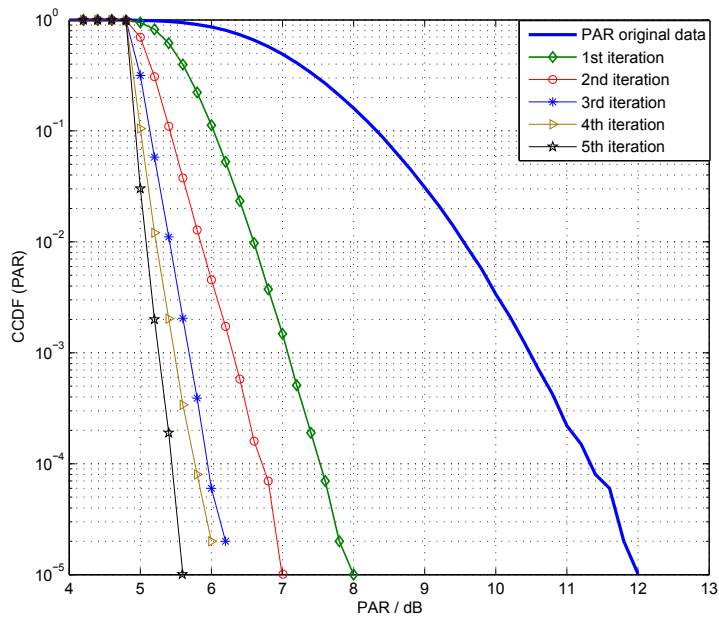


**Figure 4.5:** CCDF(PAR) of the LS algorithm for a PAR target value of 5.0 dB without mean power constraints ( $\gamma = 1$ )

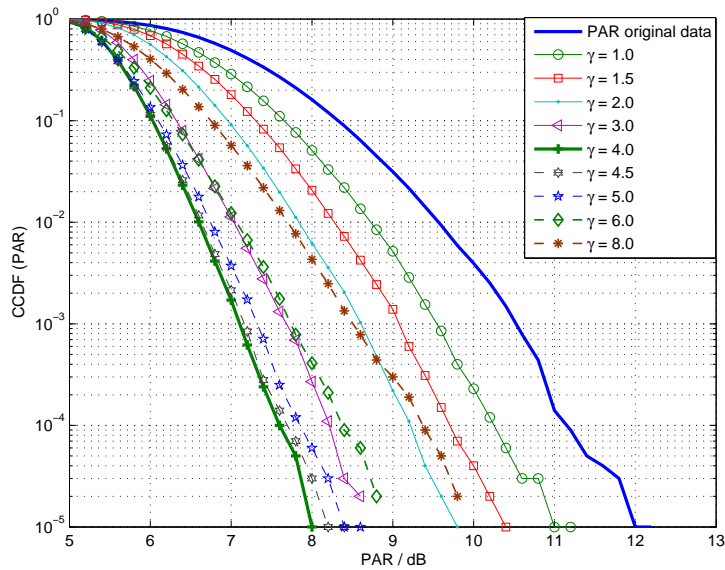
target PAR of 5.0 dB. A gain of 6.4 dB is obtained at  $10^{-5}$  with as few as 5 iterations. As can be seen from the figure, a gain of approximately 4 dB is already obtained with the first iteration and as much as 5 dB with only two iterations.

Figure 4.7 shows simulation results for different weighting factors after the first iteration at a target PAR value of 5.0 dB. It is obvious that indeed  $\gamma = M = 4$  leads to the optimum performance.

Figure 4.8 shows simulation results for different target values after 15 iterations with a weighting factor of  $\gamma = 1$ . The results demonstrate a performance gain for lower target values, however, at the expense of a slight increase in the average power. As mentioned earlier, for modeling the exceedence excursions, our algorithm searches for the peak values that exceed a given target value on all spatial dimensions in time domain. These values are transformed into DFT domain, and are estimated by the last spatial dimension. The estimated model is re-transformed into time domain and subtracted from the original signal for PAR reduction. However, in doing so, two facts need to be taken into consideration for the LS algorithm:



**Figure 4.6:** CCDF(PAR) of the weighted LS algorithm with a weighting factor  $\gamma = 4.0$  and a PAR target value of 5.0 dB without mean power constraints



**Figure 4.7:** CCDF(PAR) of the weighted LS algorithm with different weighting factors  $\gamma$ 's after the first iteration for a PAR target of 5.0 dB

1. Capacity loss: Loss in channel capacity due to the reserved eigenchannels.
2. Relative mean power increase  $\Delta E$ : Increase in the average power per iteration due to adding the corrective signal. One should hence investigate the performance of

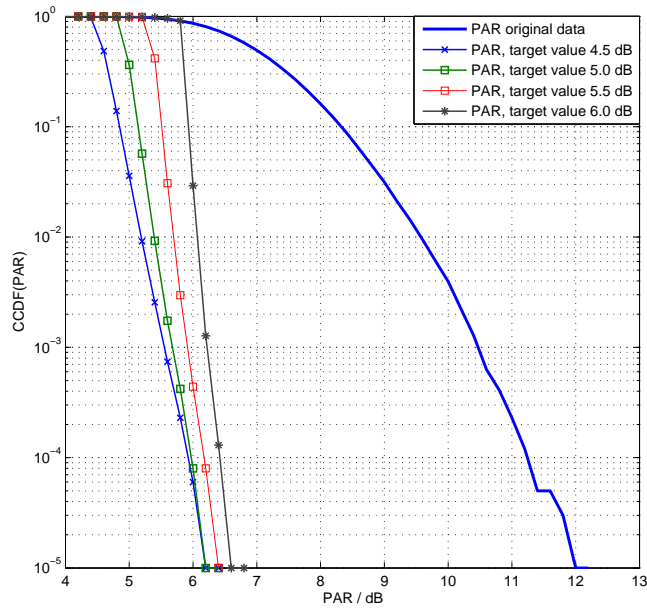


**Figure 4.8:** CCDF(PAR) of the LS algorithm for for different target values after 15 iterations ( $\gamma = 1$ )

the algorithm under a mean power constraint.

### 1. Capacity analysis of the proposed algorithm

The proposed algorithm reserves the weakest eigenchannel (spatial dimension) to model the peak excursion due to the other spatial dimensions. Thus, there is a slight loss in the channel capacity. The capacity of a MIMO channel is equal to the sum of the capacities of the independent parallel channels,

$$C_{MIMO} = \sum_{i=1}^{\min(M_r, M_t)} \log_2(1 + \alpha_i \sigma_i^2), \quad (4.26)$$

where  $\sigma_i^2$  is the  $i$ th singular value of the channel matrix  $\mathbf{H}$ ,  $\min(M_r, M_t)$  is the minimum of the number of receive or transmit antennas, and  $\alpha_i = \Phi_i / \zeta^2$  denotes signal-to-noise ratio (SNR) of the  $i$ th parallel subchannel. For a point-to-point MIMO-OFDM channel, with  $M_r = M_t = M$ , Eq. (4.26) is extended as

$$C_T = \sum_{n=1}^N \sum_{i=1}^M \log_2(1 + \alpha_i(n) \sigma_i^2(n)), \quad (4.27)$$

where  $\sigma_i^2(n)$  and  $\alpha_i(n) = \Phi_i / \zeta^2(n)$  are the singular value and the SNR at the  $n$ th subcarrier, respectively.

For our LS algorithm, Eq. (4.27) becomes

$$C_{LS} = \sum_{n=1}^N \sum_{i=1}^{M-1} \log_2(1 + \alpha_i(n)\sigma_i^2(n)) , \quad (4.28)$$

omitting the weakest (reserved) eigenchannel. The capacity curves for a  $4 \times 4$  MIMO-OFDM channel with and without reserved eigenchannels (using equations (4.27) and (4.28), respectively) are shown in Fig. 4.9. We observe that the capacity loss is almost negligible at low SNR and very little at high SNR.

Now, it is assumed that the transmitter has a perfect channel state information, thus, the power can be optimally allocated to the parallel subchannels. The channel capacity in terms of the power allocation  $\Phi_i(n)$  to the  $i$ th parallel channel at the  $n$ th subcarrier is given as [3]

$$C_T = \max_{\Phi_i: \sum_i \Phi_i \leq \Phi} \sum_{n=1}^N \sum_{i=1}^M \log_2 \left( 1 + \frac{\Phi_i(n)\sigma_i^2(n)}{\zeta^2} \right) . \quad (4.29)$$

For the LS algorithm, omitting the last spatial dimension leads to

$$C_{LS} = \max_{\Phi_i: \sum_i \Phi_i \leq \Phi} \sum_{n=1}^N \sum_{i=1}^{M-1} \log_2 \left( 1 + \frac{\Phi_i(n)\sigma_i^2(n)}{\zeta^2} \right) . \quad (4.30)$$

Using an SVD [115], the MIMO channel is decomposed into parallel single input single output (SISO) channels. The optimization solution then leads to a water-filling power allocation for the MIMO-OFDM channel as,

$$\Phi_i(n) = \left( \omega - \frac{\zeta^2}{\sigma_i^2(n)} \right)^+ , \quad (4.31)$$

where  $\omega$  is the water level chosen such that

$$\sum_{n=1}^N \sum_{i=1}^M \Phi_i(n) = \Phi ,$$

$\Phi_i(n)$  is the power at the  $i$ th eigenmode and  $n$ th bin of the channel, and  $(x)^+$  is defined as  $\max(x, 0)$ .

Figure 4.10 shows the capacity curves for a  $4 \times 4$  MIMO-OFDM channel with and without reserved eigenchannels using water filling. The capacity curves are similar to the ones in Fig. 4.10, with a negligible capacity loss at low SNR values and a still small capacity loss at high SNR values, however, the capacity gap is somewhat widened for water filling at higher SNR values.

## 2. Mean power effect of the proposed algorithm

In order to reduce the clipping probability of the transmit signal  $\tilde{\mathbf{s}}$ , a time-domain signal  $\tilde{\mathbf{r}}$  is added to  $\tilde{\mathbf{s}}$  for PAR reduction. However, in doing so, the mean transmit power is increased. Thus, the relative mean transmit power increase  $\Delta E$  of the

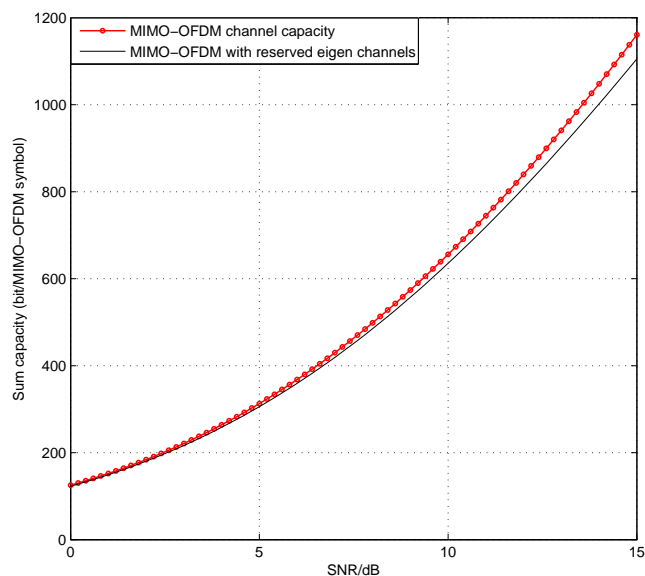


**Figure 4.9:** Capacity curve of  $4 \times 4$  MIMO-OFDM with and without reserved eigenchannels, 128 carriers, averaged over 100,000 channel models

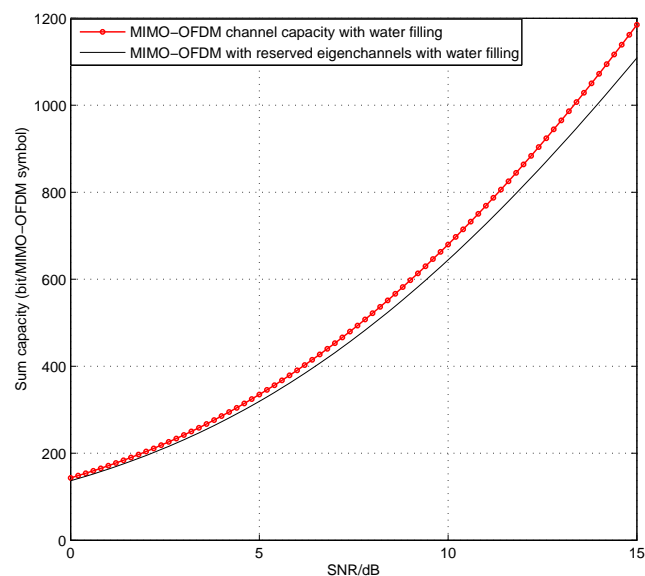


**Figure 4.10:** Capacity curve of  $4 \times 4$  MIMO-OFDM system with and without reserved eigenchannels, 128 carriers, averaged over 100,000 channel models

transmit signal  $\tilde{\mathbf{s}}$ , is defined as

$$\Delta E = 10 \log_{10} \frac{E\{\|\tilde{\mathbf{s}}^i + \gamma \tilde{\mathbf{r}}^i\|_2^2\}}{E\{\|\tilde{\mathbf{s}}\|_2^2\}}, \quad (4.32)$$

where  $E\{\|\tilde{\mathbf{s}}\|_2^2\} = \sigma^2$  is the nominal average power,  $E\{\|\tilde{\mathbf{s}}^i + \tilde{\mathbf{r}}^i\|_2^2\}$  is the average power at the  $i$ th iteration, and  $\gamma$  is the weighting factor.

In order to check the system performance using our LS algorithm (Section 4.1.3) under a mean power constraint, we modify Step No. 3 as

- if  $i > i_{max}$  or  $\Delta E > \Delta E_{Th}$ , stop and transmit  $\tilde{\mathbf{s}}^i$ .

The algorithm thus also checks for an increase in the mean power of the transmit signal. If  $\Delta E$  of the transmit signal increases beyond a threshold  $\Delta E_{Th}$ , the algorithm breaks the loop and transmits the signal.

Figure 4.11 shows the simulation results for limiting  $\Delta E$ . It can be recognized that approximately a 6 dB gain can be obtained at  $10^{-5}$  for a slight increase in the mean power of only  $\Delta E = 0.25$  dB.

Figure 4.12 shows the relative mean power increase per iteration in dB. The curves show that  $\Delta E$  is, of course, higher for lower target values, as more peaks have to be approximated. Still, the results show that the average power increase is marginal.

*Mean power effects of weighted LS:*

Figure 4.13 shows the simulation results for weighted LS ( $\gamma = 4$ ) with different mean power constraints. A gain of approximately 4 dB is obtained with a 0.1 dB increase in the average power which is almost negligible and almost 6.4 dB are reached for a marginal increase in the mean power of  $\Delta E = 0.35$  dB.

Figure 4.14 shows the relative mean power increase per iteration in dB for weighted LS with a weighting factor  $\gamma = 4$  and different target values. It is obvious that the increase in the average power of weighted LS is approximately the same as with the unweighted algorithm. In both cases, the average power increase is only marginal.

In Fig. 4.15 we provide an analysis of  $\Delta E$  per iteration for different weighting factors at a target value = 5 dB. It is clear from the figure that  $\Delta E$  per iteration is higher for larger weighting factors  $\gamma$ , however, the algorithm converges faster to the target values with a higher weighting factor. Thus, there is a compromise between weighting factor  $\gamma$  and mean power increase  $\Delta E$ .

### Comparison to the tone-reservation algorithm

The Tone Reservation (TR) algorithm reserves a set of tones to generate a corrective function, which is iteratively subtracted from the transmitted signal for PAR reduction. Similarly, the LS algorithm proposed herein reserves the weakest eigenchannels to model the peak excursion for PAR reduction. Nevertheless, the proposed algorithm is different from the TR. The TR algorithm operates completely in time domain, but in the LS algorithm, the peak values crossing a target value in time domain are transformed into DFT domain and are mapped onto the reserved spatial dimension. This model function is re-transformed into time domain and is subtracted from the transmitted signal to limit its peak values. The algorithm thus alternates between time and DFT domain in each iteration.

We compare our approach to the tone reservation algorithm regarding the following facts:

1. PAR reduction capability,
2. capacity loss due to the reserved tones (TR algorithm) / weakest eigenchannels (LS algorithm),

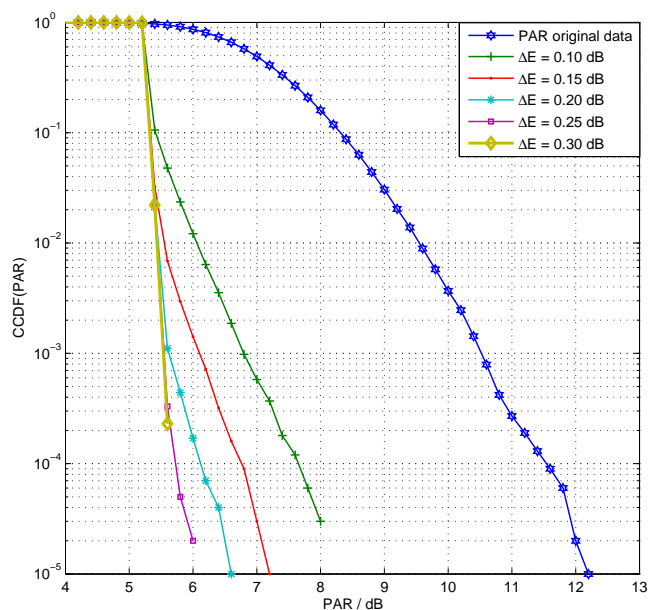


**Figure 4.11:** CCDF(PAR) of the LS algorithm for a PAR target value of 5.0 dB with different mean power constraints  $\Delta E$  and a weighting factor of  $\gamma = 1.0$

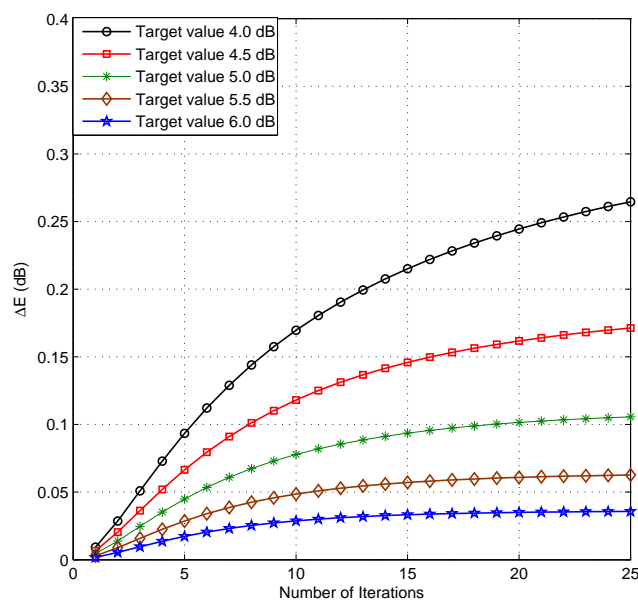


**Figure 4.12:** Mean power increase  $\Delta E$  in dB of the LS algorithm depending on the number of iterations for different PAR target values and  $\gamma = 1.0$

3. increase in the average power due to adding corrective signals for peak power limitation.

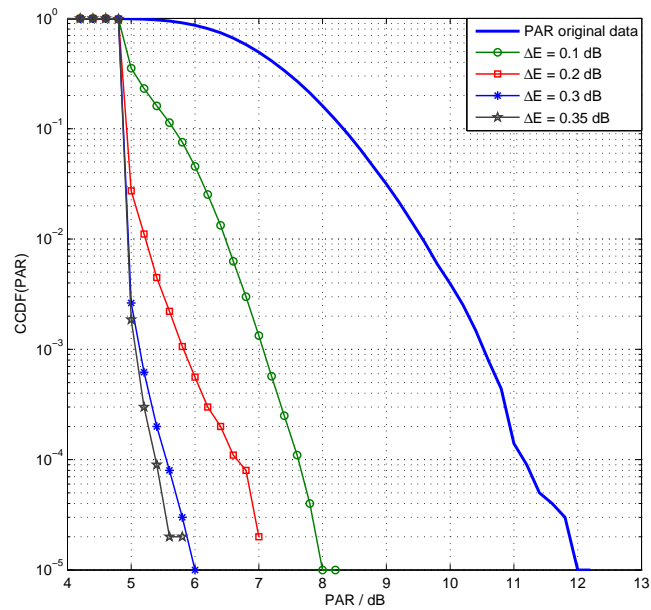


**Figure 4.13:** CCDF(PAR) of the weighted LS algorithm with a weighting factor  $\gamma = 4.0$  and PAR target value 5.0 dB for different mean power constraints  $\Delta E$  and 8 iterations

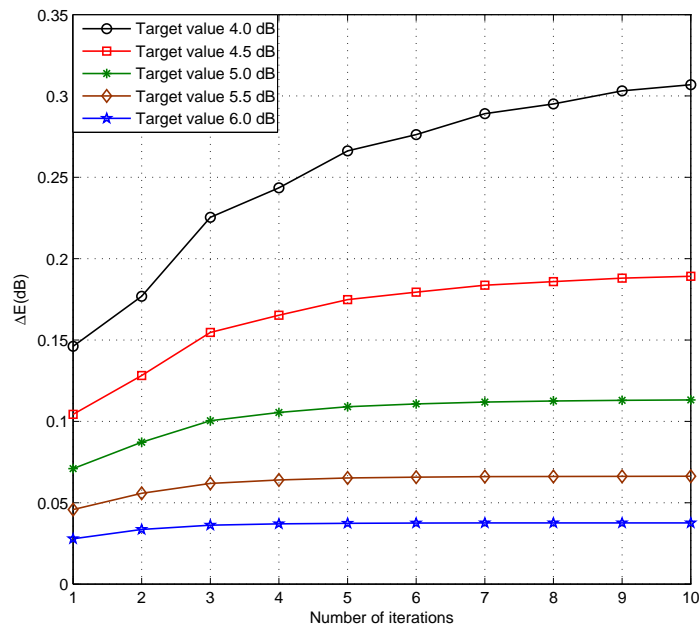


**Figure 4.14:** Mean power increase  $\Delta E$  in dB of the weighted LS algorithm depending on the number of iterations for different PAR target values and  $\gamma = 4.0$

### 1. PAR reduction capability of LS algorithm vs. TR algorithm

The TR algorithm completely operates in time domain and is the least complex algorithm. In our LS algorithm, many IFFTs are required to reach the target value,

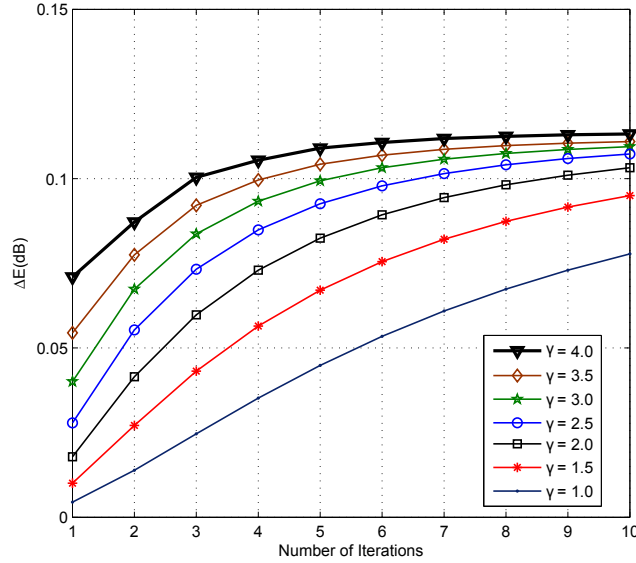


**Figure 4.15:** Mean power increase  $\Delta E$  in dB of the LS algorithm per iteration for a PAR target values of 5 dB with different weighting factors

thus, increasing the complexity. In order to provide a fair comparison of the TR algorithm to the LS algorithm, we consider a higher number of iterations for the TR algorithm as compared to the LS algorithm such that both algorithms have a comparable complexity.

Figure 4.16 shows the performance curves of the TR algorithm vs. the LS algorithm for a PAR target value of 5.0 dB. For the TR algorithm, we have considered a point-to-point,  $4 \times 4$  MIMO-OFDM system with 10 % reserved tones. Figure 4.16 shows that for the TR algorithm the gain is 1.8 dB with 5 iterations and 4.4 dB with as many as 45 iterations as compared to 4 dB and 6.4 dB with 1 and 5 iterations, respectively, using the weighted LS algorithm. The LS algorithm with 5 iterations outperforms TR with 45 iterations by 2 dB as shown in Fig. 4.16.

## 2. Capacity analysis of the LS algorithm vs. TR

In the TR algorithm, no data is transmitted on  $\theta$  reserved tones, thus, using Eq. (4.27), the channel capacity of a MIMO-OFDM system using TR is given by

$$C_T = \sum_{\substack{N-\theta \\ \text{carriers}}}^M \sum_{i=1}^M \log_2(1 + \alpha_i(n)\sigma_i^2(n)). \quad (4.33)$$

With the power allocation  $\Phi_i(n)$  to the  $i$ th channel at the  $n$ th subcarrier, the channel capacity results in

$$C_T = \max_{\Phi_i: \sum_i \Phi_i \leq \Phi} \sum_{\substack{N-\theta \\ \text{carriers}}}^M \sum_{i=1}^M \log_2 \left( 1 + \frac{\Phi_i(n)\sigma_i^2(n)}{\zeta^2} \right). \quad (4.34)$$

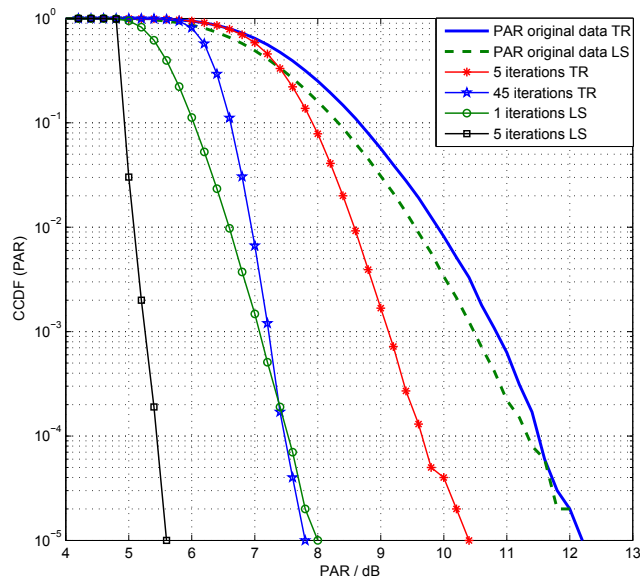


**Figure 4.16:** CCDF(PAR) of the LS algorithm and the TR algorithm with different numbers of iterations

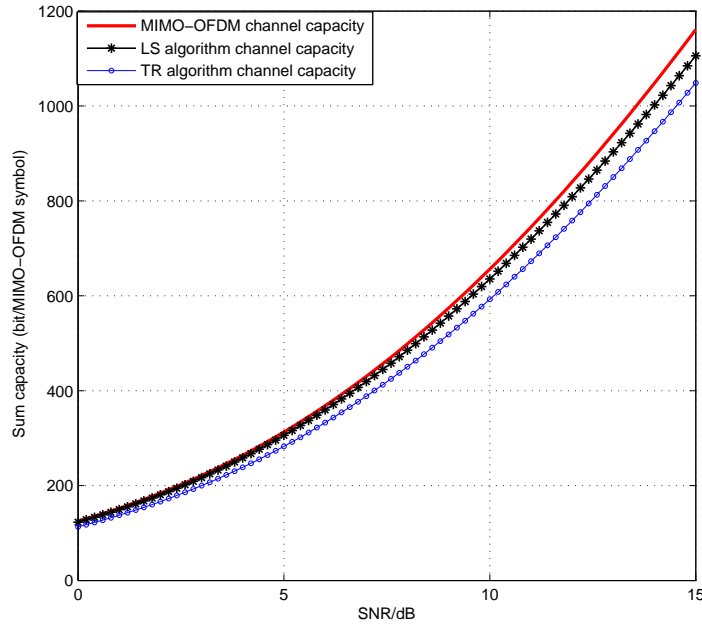
For our LS algorithm, we use equations (4.28) and (4.30) to plot the capacity curves. Figures 4.17 and 4.18 show the capacity plots of MIMO-OFDM systems using the TR. The PAR reduction capability of the TR algorithm with 10 % reserved tones is better than with 5 % [110]. Thus, for our simulation results of the channel capacity for the TR algorithm, we considered a  $4 \times 4$  MIMO-OFDM channel with 10 % reserved tones and 128 carriers. Figure 4.17 shows the capacity curves of a MIMO-OFDM system without water-filling for the TR and LS algorithms. The figure shows that the capacity loss of the TR algorithm with 10 % reserved tones is higher than with the LS algorithm.

Figure 4.18 shows the capacity curves of a MIMO-OFDM system with water-filling. In case of water-filling, the capacity loss for the LS algorithm is almost the same as for the TR algorithm.

### 3. Comparison of LS and TR algorithms under mean power constraint $\Delta E$

The LS and TR algorithms use time domain corrective signals to limit the peak values of the transmitted signal. In doing so, the mean power of the transmitted signal is increased. Thus, we compare our proposed algorithm to the TR algorithm under a mean power constraint. The relative mean transmit power increase for both algorithms is as given by Eq. (4.32).

Figure 4.19 shows the CCDF of the PAR under the mean power constraint  $\Delta E$  for the LS and TR algorithms (with 10 % reserved tones). As shown in Fig. 4.19, our LS algorithm outperforms the TR algorithm by approximately 3.6 dB at  $\Delta E = 0.3$  dB and a CCDF of  $10^{-5}$ .



**Figure 4.17:** Capacity curve of  $4 \times 4$  MIMO-OFDM system using TR (Tone Reservation) and LS (Least Squares) algorithms without water-filling, 128 carriers, 10 % reserved tones, averaged over 100,000 channel models

### Comparison to the Selected Mapping algorithm

In Selected Mapping (SLM), the original data symbols in DFT domain is multiplied with  $U$  different phasor vectors. After taking IFFTs over all such modified symbols, the one with the lowest PAR is selected for transmission. Thus, SLM requires  $U$  IFFTs to select the best symbol for transmission. Likewise, in our LS approach the algorithm switches between time and DFT domains to limit the peak values. Thus,  $i$  (where  $i$  is the total number of iterations) FFT-IFFTs pairs are required to reach the final target value. Both algorithms, thus, require some FFTs for PAR reduction. We compare our algorithm to the SLM algorithm based on the same complexity, considering the total number of FFT-IFFTs.

For comparison, we have considered a  $4 \times 4$  point-to-point MIMO-OFDM system using ordinary SLM (oSLSM), which is a direct extension of SISO SLM to MIMO. The CCDF for oSLSM [33] is given as

$$Pr\{PAR_{oSLSM} > \tau\} = 1 - (1 - (1 - (1 - e^{-\tau})^N)^U)^M, \quad (4.35)$$

assuming a complex Gaussian again.  $U$  is the total number of frames,  $N$  is the number of sub-carriers and  $\tau$  is the PAR target value (threshold value).

Figure 4.20 shows the performance curves for oSLSM vs. our LS algorithm. It is clear from the figure that our algorithm with  $i = 5$  outperforms oSLSM with  $U = 10$  (i.e., approximately the same complexity) by almost 2.8 dB. However, this gain is obtained at the expense of a negligible increase in the mean power and a slight loss in channel capacity.

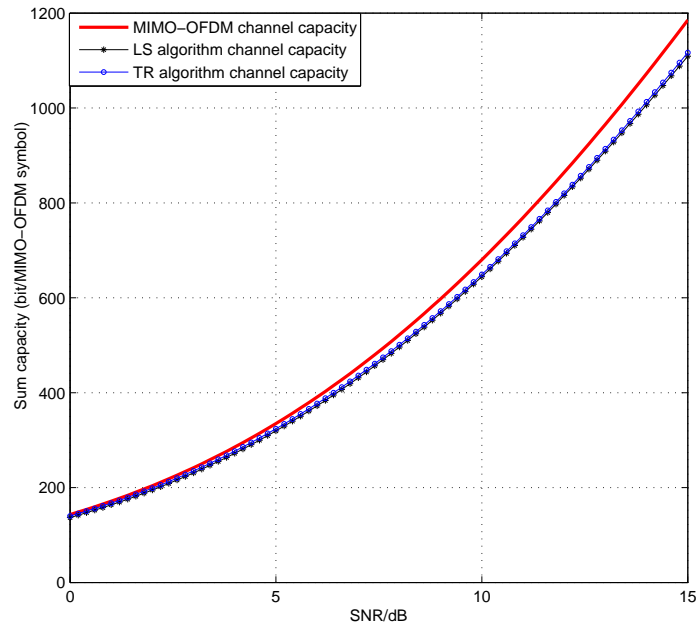


**Figure 4.18:** Capacity curve of  $4 \times 4$  MIMO-OFDM system using TR (Tone Reservation) and LS (Least Squares) algorithms with water-filling, 128 carriers, 10 % reserved tones, averaged over 100,000 channel models

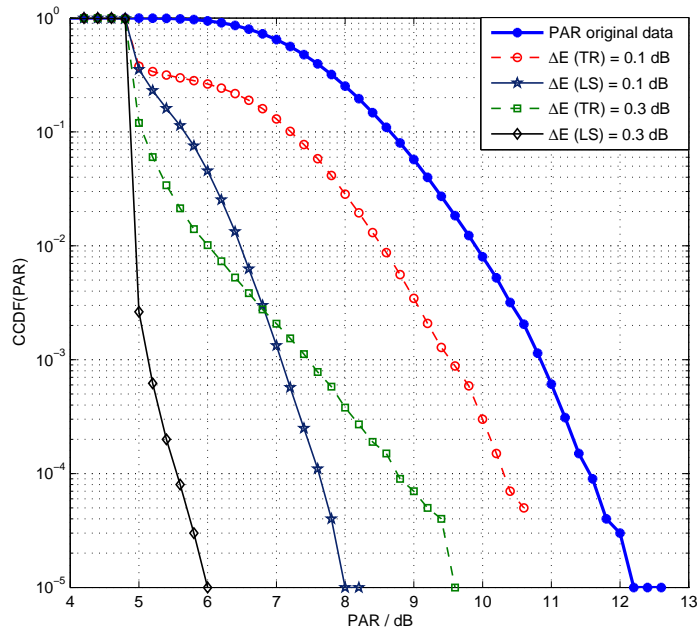


**Figure 4.19:** CCDF(PAR) of the LS algorithm vs. the TR algorithm under a mean power constraint

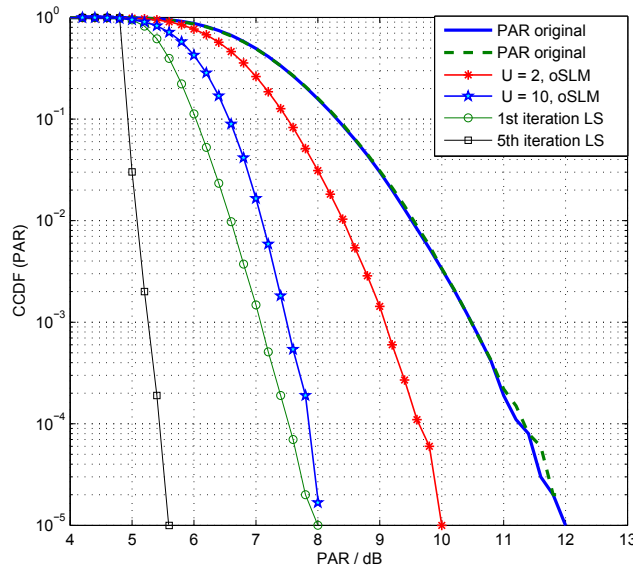


Figure 4.20: CCDF(PAR) of the LS algorithm vs. SLM

### Extension to large-scale MIMO-OFDM systems

With the advent of new applications, the demand for high data rates is increasing steadily. New concepts and new technologies have been introduced to meet the public demands. Massive or large-scale Multiple-Input Multiple-Output (MIMO) is a concept for future wireless communication systems, first proposed in [113] for multiuser MIMO (MU-MIMO) systems. The transmitter at the base station (BS) is equipped with a large number of antennas serving single antenna terminal units (TU). However, we adopt the term large-scale MIMO and extend it to a point-to-point MIMO system, where the transmitter and the receiver are supposed to be equipped with a large number of antennas in the range of hundred (e.g. communication between two BSs). We thus extend our algorithm to large-scale MIMO-OFDM systems (we have considered  $40 \times 40$  MIMO-OFDM system for our simulation) to check and evaluate the PAR reduction capability, capacity loss, and performance under mean power constraints of the proposed algorithm.

Figure 4.21 shows performance curves of a  $40 \times 40$  MIMO-OFDM system using our LS algorithm for a target PAR value of 6.5 dB. As shown in the figure, a gain of approximately 3.2 dB is obtained with the first iteration and as much as 5 dB gain is obtained at  $10^{-5}$  with as few as 8 iterations.

### Capacity analysis of large-scale MIMO systems

Figures 4.22 and 4.23 show the capacity curves for a  $40 \times 40$  MIMO-OFDM system with and without water filling respectively. For a  $40 \times 40$  MIMO-OFDM system, at low SNR values, the capacity curve of the LS-algorithm overlaps the capacity curve of the system, with a negligible loss at higher SNR values. Figure 4.22 and 4.23 also shows that the capacity loss for a  $40 \times 40$  MIMO-OFDM system using our LS algorithm is even lower than a system using TR with only 2 % reserved tones.

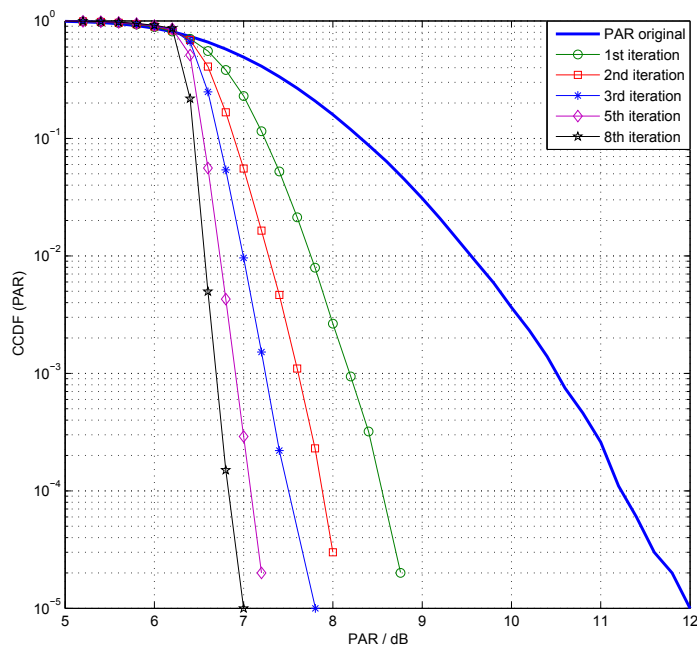


**Figure 4.21:** CCDF(PAR) of the LS algorithm for a  $40 \times 40$  MIMO-OFDM system, PAR target value = 6.5 dB,  $\gamma = 30$

### Performance under mean power constraint of large-scale MIMO systems

Figure 4.24 shows the mean power increase  $\Delta E$  per iteration for different PAR target values in dB.  $\Delta E$  is higher for lower target values as more peaks are approximated, however, the increase is still marginal in the range of one to two tenths of a decibel for 10 iterations.

Figure 4.25 shows the CCDF of the proposed algorithm, limiting  $\Delta E$  to different values. A gain of approximately 3.2 dB and 5.2 dB is obtained for  $\Delta E = 0.1$  dB and 0.5 dB, respectively.

### Capacity analysis from a random matrix theory perspective

We assumed that the last singular value is very weak and not suitable for data transmission. We make use of random matrix theory to analyze the last singular value and the capacity associated with it.

Let us consider a very large scale MIMO-OFDM system with  $M_t$  transmit and  $M_r$  receive antennas. For simplicity, let us again assume  $M_t = M_r = M$ . The channel matrix from the  $j$ th transmit to the  $i$ th receive antenna is then defined as  $\mathbf{H} = [h_{i,j}]$ . The channel matrix can be diagonalized using the SVD as  $\mathbf{H} = \mathbf{U}\mathbf{\Lambda}\mathbf{V}^H$ , where  $\mathbf{\Lambda}$  is a diagonal matrix with the of the singular values of  $\mathbf{H}$ , sorted out in a descending order. Now the question arises how small the smallest singular value  $\sigma_{min}$  of the  $\mathbf{H}$  is when the dimensionality of the system grows, i.e.,  $M \rightarrow \infty$ ?

In order to answer this question, we make use of random matrix theory for  $M \times M$  Gaussian matrices (since  $\mathbf{H}_{M \times M}$  is considered to be a Gaussian matrix). For Gaussian matrices

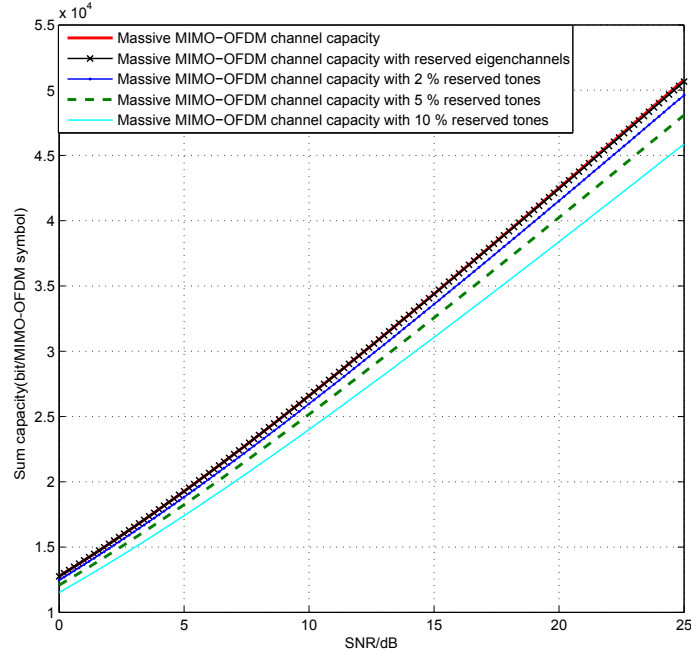


**Figure 4.22:** Capacity curves for a  $40 \times 40$  MIMO-OFDM channel with and without reserved eigenchannels / reserved tones, 128 carriers, averaged over 100,000 channel models

of very large dimension, the Complimentary Cumulative Distribution Function (CCDF) of  $M$  times the smallest singular value,  $\sigma_{min}$ , according to [117] and [119], is given as

$$\lim_{M \rightarrow \infty} P(M\sigma_{min} \geq x) = e^{-x-x^2/2}, \quad x \geq 0. \quad (4.36)$$

In terms of the Cumulative Distribution Function (CDF), Eq. (4.36) can be expressed as

$$\lim_{M \rightarrow \infty} P(M\sigma_{min} < x) = 1 - e^{-x-x^2/2}. \quad (4.37)$$

Substituting  $x/M = x'$ , to move the factor of  $M$  from the left side of the argument to the right side, leading to

$$\lim_{M \rightarrow \infty} P(\sigma_{min} < x') = 1 - e^{-x'M-(x'M)^2/2}. \quad (4.38)$$

From the CDF, the probability density function is then obtained by differentiating (4.38) with respect to  $x$  (and omitting  $'$ ), i.e.,

$$\begin{aligned} f(\sigma_{min}) &= \lim_{M \rightarrow \infty} \frac{d}{dx} \left\{ 1 - e^{-xM-(xM)^2/2} \right\} \\ &= \lim_{M \rightarrow \infty} e^{-xM-x^2M^2/2} \cdot (M + 2xM^2/2). \end{aligned}$$

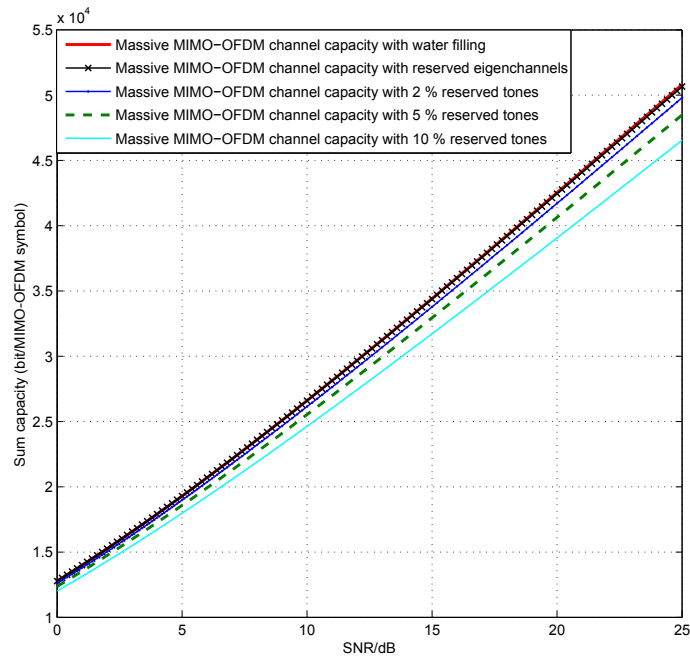


**Figure 4.23:** Capacity curves for a  $40 \times 40$  MIMO-OFDM channel with and without reserved eigenchannels / reserved tones using water filling, 128 carriers, averaged over 100,000 channel models

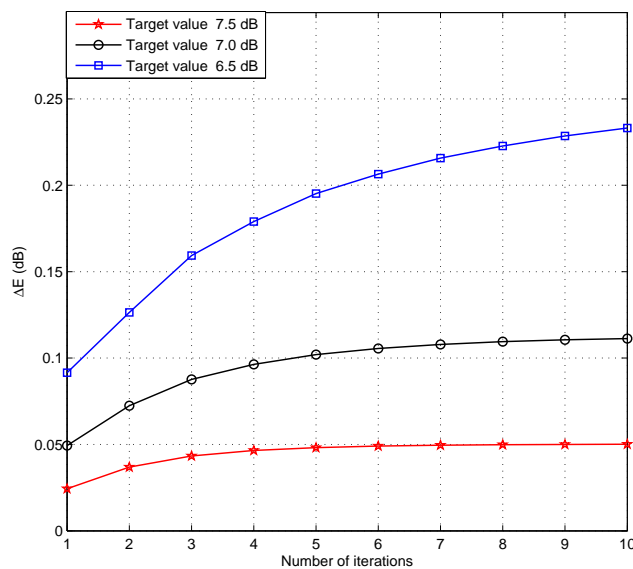


**Figure 4.24:** Mean power increase  $\Delta E$ , in dB, per iteration for different target values, weighting factor  $\gamma = 30$

Using l'Hospital's rule with respect to  $M$ , this leads to

$$f(\sigma_{min}) = \lim_{M \rightarrow \infty} [-x(1 + xM) \cdot e^{-xM - x^2 M^2 / 2}] \cdot [1 + 2xM]. \quad (4.39)$$

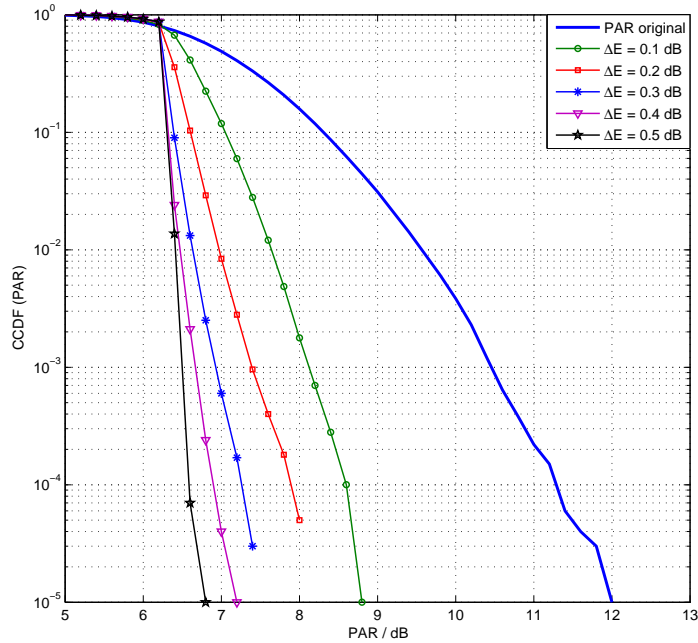


**Figure 4.25:** CCDF(PAR) of the LS algorithm of a  $40 \times 40$  MIMO-OFDM system, for a PAR target value of 6.5 dB with different mean power constraints  $\Delta E$ , weighting factor  $\gamma = 30$

Which goes to zero for  $M \rightarrow \infty$  and  $x \neq 0$ . Requiring the integral over the density  $f(\sigma_{min})$  to be one,  $f(\sigma_{min})$  tends to a Dirac impulse shape for  $M \rightarrow \infty$ . Thus, according to Eq. (4.27), the capacity associated with the reserved dimension goes to zero for higher dimensional MIMO-OFDM systems.

Figure 4.26 shows the capacity curves associated with the reserved dimension for different MIMO-OFDM systems, using Eq. (4.27) with  $\sigma_{min}$ . It is clear from the figure that as the dimensionality of MIMO-OFDM system increases, the capacity loss due to the reserved eigenchannels goes to zero, as Eq. (4.39) suggests.

The capacity loss due to reserving the weakest eigenchannel can be seen in Fig. 4.27, obtained at an SNR of 15 dB. The capacity loss due to the reserved dimension, for a  $40 \times 40$  MIMO-OFDM system, is only 7 bits and as low as 4 bits for  $80 \times 80$  MIMO-OFDM systems.

### Some considerations regarding the convergence of the least-squares PAR reduction algorithm

Let us consider a 2-dimensional Gaussian-distributed time-domain signal. The amplitude is Rayleigh distributed according to

$$p_r(a) = \frac{a}{\sigma_a^2} e^{-\frac{a^2}{2\sigma_a^2}},$$

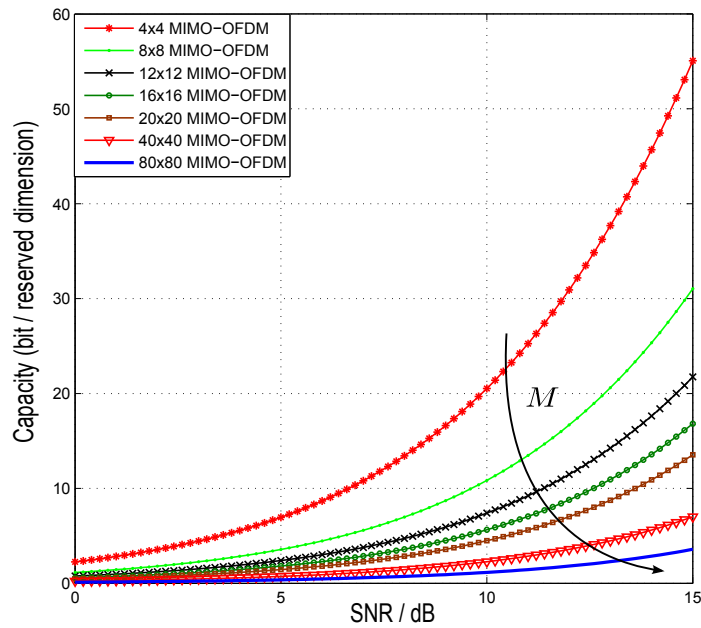


**Figure 4.26:** Capacity curves of the reserved dimension for different MIMO-OFDM systems

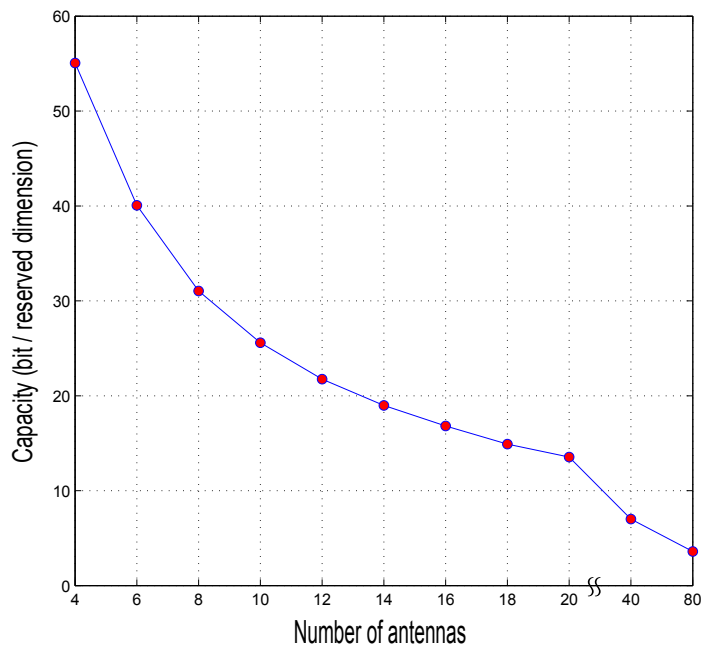


**Figure 4.27:** Capacity associated with the reserved dimension at SNR = 15 dB

where  $\sigma_a^2$  is the variance of the 1D Gaussian. Hence, the average power is  $2\sigma_a^2$ . In the LS algorithm, we approximate the peak values exceeding a given threshold value and model them by the last spatial dimension. This model function is then subtracted

from the transmitted signal in time-domain for PAR reduction, resulting in a modification in the mean power of the signal. Let  $\tau$  be the threshold value which separates the outer and inner regions as shown in Fig. 4.28. The outer region (tail of the distribution) above the threshold appears with a probability  $P_o$  given by (see App. A)

$$P_o = e^{-\frac{\tau^2}{2}}. \quad (4.40)$$

When considering the tail of the distribution (exceeding the threshold  $\tau$ ), this leads to an average tail power  $P_{\text{tail}}$ , i.e.,

$$P_{\text{tail}} = 2e^{-\frac{\tau^2}{2}} - \tau\sqrt{2\pi} \operatorname{erfc}\left(\frac{\tau}{\sqrt{2}}\right). \quad (4.41)$$

We look into the change of the average power per iteration, which gives an indication of the possible change in the least-squares sense, hence also limits of possible peak regrowth in the algorithm.

Without weighting, the effective correction amplitude is too small by a factor of  $1/M$ , hence, in a quadratic sense, this means  $1/M^2$  and hence the modification of the average power per iteration is given by

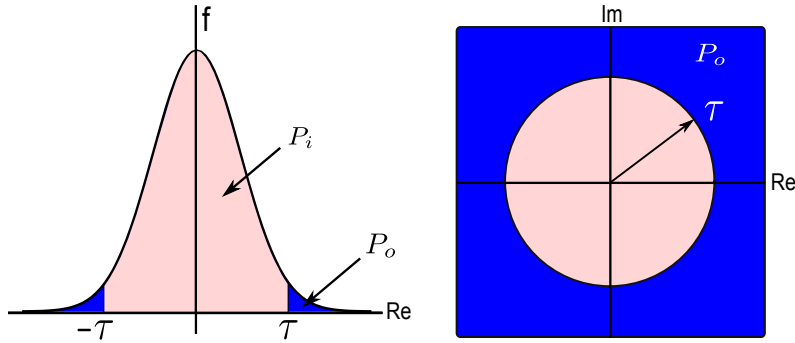


**Figure 4.28:** Probability of tail, the threshold value  $E$

$$\sigma_a^2(t+1) = \sigma_a^2(t) + \frac{1}{2} \cdot \frac{1}{M^2} \cdot P_o(t) \cdot P_{\text{tail}}(t). \quad (4.42)$$

Inserting the values for  $P_o(t)$  and  $P_{\text{tail}}(t)$ , (4.42) is rephrased as

$$\sigma_a^2(t+1) = \sigma_a^2(t) + \frac{1}{2} \cdot \frac{1}{M^2} \cdot e^{-\frac{\tau^2}{2}} \cdot \left(2e^{-\frac{\tau^2}{2}} - \tau\sqrt{2\pi} \operatorname{erfc}\left(\frac{\tau}{\sqrt{2}}\right)\right). \quad (4.43)$$

The factor  $1/2$  comes from the fact that  $\sigma_a^2$  relates to a single dimension. Only when the signal is in the outer region, the influence of the algorithm is to be considered. Then (under this condition), a power change relates to  $P_{\text{tail}}(t)$ .

An amplitude weighting by  $M$  means another factor of  $M^2$  regarding the average power, making the  $M$ -related factor disappear, hence,

$$\sigma_a^2(t+1) = \sigma_a^2(t) + \frac{1}{2} \cdot e^{-\frac{\tau^2}{2}} \cdot \left(2e^{-\frac{\tau^2}{2}} - \tau\sqrt{2\pi} \operatorname{erfc}\left(\frac{\tau}{\sqrt{2}}\right)\right). \quad (4.44)$$

Table 4.1 shows a comparison of  $\Delta E$  obtained by simulation and calculated using (4.43)

**Table 4.1:** Theoretical vs. simulated mean power increase  $\Delta E$  (in dB) for weighted and non weighted LS algorithms at the first iteration.

weighting	$\tau =$	4.0 dB	4.5 dB	5.0 dB	5.5 dB	6.0 dB
$\gamma = 1$	Theor.	0.0093	0.0064	0.0042	0.0027	0.0016
	Sim.	0.0093	0.0066	0.0045	0.0029	0.0018
$\gamma = M$	Theor.	0.1468	0.1012	0.0670	0.0424	0.0255
	Sim.	0.1461	0.1043	0.0710	0.0458	0.0278

and (4.44), for a  $4 \times 4$  MIMO-OFDM system. It is clear from the table that the calculated values match the simulated values for the first iteration.

If the approximation and the subtraction of the model function were perfect, there would have been no left-over peaks, however, the subtraction and approximation is not perfect and there are still some peaks above the threshold value. Thus, we iterate the algorithm to deal with the left-over peaks. However, after first iteration, the distribution is no longer Gaussian and we cannot still apply equations (4.43) and (4.44) to later iterations. Thus, we base our assumption on the simulated results that the LS algorithm converges to the target value.

First, we consider the relative mean power increase  $\Delta E$  of the transmit signal per iteration due to LS algorithm. In order to check for a possible peak regrowth, we consider the relative mean power increase per iteration as shown in the Fig. 4.14 obtained for a  $4 \times 4$  MIMO-OFDM system with different PAR target values and a weighting factor  $\gamma = 4$ . It is clear from the figure that for a given target value  $\tau$ , the relative mean power  $\Delta E$  decreases monotonically with the number of iterations, i.e.,

$$\Delta E^{i+1} \leq \Delta E^i.$$

A monotonic decrease in  $\Delta E$  shows that the algorithm reduces the peak values closer to the threshold in each iteration.

Table 4.2 shows the added energy  $\Delta E$  per iteration for the  $4 \times 4$  MIMO-OFDM system

**Table 4.2:** Mean power increase  $\Delta E$  (in dB) per iteration.

No. Iter.	1	2	3	4	5
$\Delta E$	0.0710	0.0163	0.0132	0.0051	0.0036
No. Iter.	6	7	8	9	10
$\Delta E$	0.0017	0.0012	0.0006	0.0004	0.0002

with a PAR target of 5.0 dB and a weighting factor  $\gamma = 4$ .

Secondly, we consider the performance curves (CCDF (PAR)) of the LS algorithm. In

order to check for the convergence of the LS algorithm, we set a very low PAR target value with a high number of iterations. Let us again consider a  $4 \times 4$  MIMO-OFDM system with a PAR target value of 4.0 dB. Figure 4.29 shows performance curves for a  $4 \times 4$  MIMO-OFDM system with a threshold value of 4.0 dB weighted with  $\gamma = 4$ . It is clear from that figure that even for this low target values, there is still no peak regrowth with as many as 25 iterations and the peaks being reduced to as close as 0.4 dB off the target value, which indicates that the proposed algorithm converges to the target value. It is also necessary to point out (the same trends has also been found by the authors in [120] and [122] for their algorithms) that the above statements do, of course, not mean that the error signal completely decreases to zero with a high number of iterations. The error signal remains constant after some iterations and a 100 % limitation to  $\tau$  is not guaranteed. However, the simulation results show that for reasonable threshold values  $\tau$ , the relative mean power increase is minor, which indicates that the chance of adding more peaks is also small, which in turn means that the designed least-squares algorithm is indeed effectively reducing peaks.

This is not a formal proof of the convergence, however, with an only minor change in the average power, essentially, the peaks are treated well, without compromising the rest of the function too much in a least-squares sense.

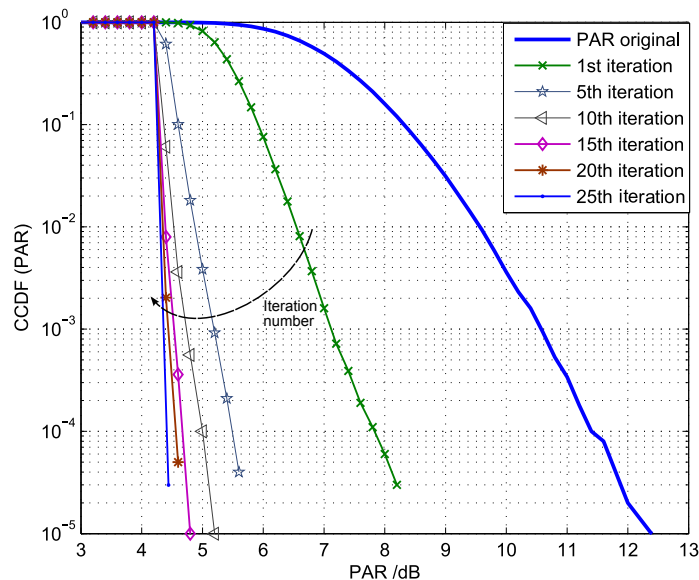


Figure 4.29: CCDF curves the LS-algorithm at a high number of iterations

## 4.2 Extension of the LS-algorithm to multi-user broadcast (BC) scenarios

In the previous section, we applied least squares approximation technique for the PAR reduction of P2P MIMO-OFDM systems, where we tried to approximate the peak excursions on the reserved spatial dimension. The idea is straight forward and can be extended to multi-user broadcast scenarios as well. However, for MU-MIMO systems, we will consider the channel associated with an inactive user for approximating the peak excursion.

Let us consider a multi-user broadcast system with a central base station equipped with  $M_t$  transmit antennas communicating with  $U$  users. For simplicity, let us assume that each user is equipped with a single receive antenna  $U_r = 1$ , such that the total number of receive antennas  $M_r = \sum U_r = U$ . For a medium to large scale multi-user broadcast system, where the base station can support a few tenths to hundreds of users, there is a high probability that one user may be inactive. This probability even increases as the system's dimensionality grows. Herein, we will thus consider that for MU BC systems, one user is inactive and not communicating with the central base station. The single inactive user, like in the case of P2P MIMO systems, will offer redundancy and the available spatial channel can thus be used for the PAR reduction of the peaks on the remaining dimensions.

### 4.2.1 System model and precoding

For a downlink multi-user scenario, we consider a central base station equipped with  $M_t$  transmit antennas communicating with  $U$  user such that  $M_t = M_r = U$ . Again, we consider perfect channel state information (perfect CSI) at the transmitter with Tomlinson-Harashima precoding for the downlink scenario. For TH precoding, using QR decomposition, the channel matrix  $\mathbf{H}$  can be rephrased as

$$\begin{aligned}\mathbf{H}^H &= \mathbf{Q}\mathbf{R} \\ \mathbf{H} &= \mathbf{R}^H \mathbf{Q}^H ,\end{aligned}\tag{4.45}$$

where  $\{\cdot\}^H$  stands for Hermitian or complex conjugate. Let  $\mathbf{S}(n)$  be the input data vector at the  $n$ th frequency bin with the inactive user set to zero, i.e.,

$$\mathbf{S}(n) = [X_{1,n}, X_{2,n}, \dots, X_{U-1,n}, 0] ,\tag{4.46}$$

where  $X_{\mu,n}$  is the input data symbol for the  $\mu$ th user at the  $n$ th carrier. Moreover, let  $\mathbf{R}(n)$  represent the vector for the inactive user, which will be used to approximate the peak excursion on the remaining dimensions, and is defined as

$$\mathbf{R}(n) = [0, 0, \dots, 0, R_n] .\tag{4.47}$$

$\underbrace{\hspace{10em}}_{U-1}$

For the downlink multi-user broadcast scenario, we consider transmitter-sided precoding with  $\mathbf{Q}$ . At the  $n$ th carrier,  $\mathbf{S}(n)$  and  $\mathbf{R}(n)$  are hence preprocessed as

$$\tilde{\mathbf{S}}(n) = \mathbf{Q}(n)\mathbf{S}(n) ,\tag{4.48}$$

and similarly

$$\tilde{\mathbf{R}}(n) = \mathbf{Q}(n)\mathbf{R}(n) .\tag{4.49}$$

The two are then transformed into time domain using a block diagonal IDFT modulator  $\mathbf{F}^{-1}$  and are combined as

$$\tilde{\mathbf{x}} = \tilde{\mathbf{s}} - \tilde{\mathbf{r}} = \mathbf{F}^{-1}(\mathbf{Q}\mathbf{S} - \mathbf{Q}\mathbf{R}) .\tag{4.50}$$

Now, the goal is to approximate the peak excursions. We will follow the procedure as had been presented for the P2P MIMO scenario. Let  $\mathbf{e}$  represents the peak excursions in time domain and let  $\mathbf{E}$  be the DFT counterpart of  $\mathbf{e}$ , i.e.,  $\mathbf{E} = \text{DFT}\{\mathbf{e}\}$ . In the Least-Squares sense,  $\mathbf{R}$  will approximate  $\mathbf{E}$  as

$$\min_{\mathbf{R}_M} \|\mathbf{Q}\mathbf{R} - \mathbf{E}\|_2^2, \quad (4.51)$$

which can be solved for  $\mathbf{R}$  in the same manner as shown in Section 4.1.3, and is given as

$$\mathbf{R}_{:M} = (\mathbf{Q}_{:M}^H \mathbf{Q}_{:M})^{-1} \mathbf{Q}_{:M}^H \mathbf{E}. \quad (4.52)$$

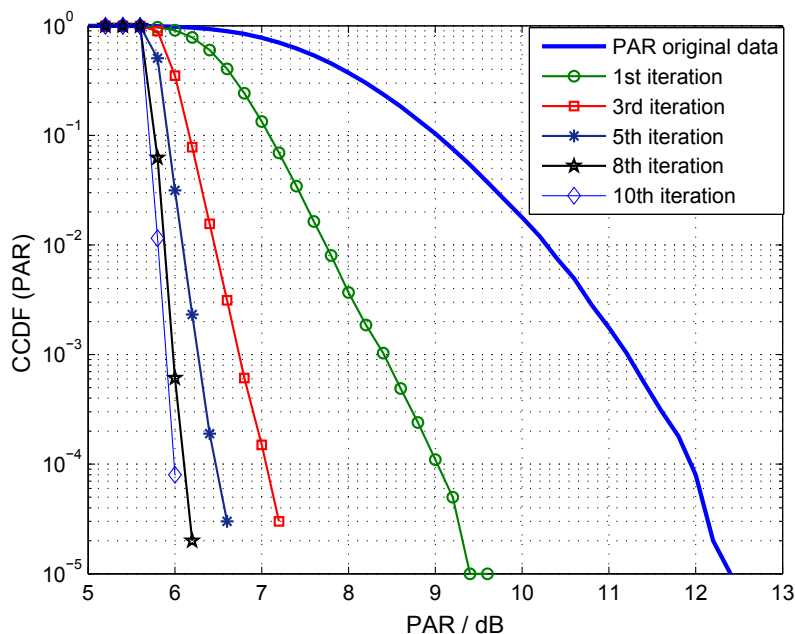
where  $\mathbf{Q}_{:M}$  is a block-diagonal matrix with the  $M$ th column of the  $\mathbf{Q}$  matrix on the diagonals. The necessary steps in the Least-Squares approximations algorithm are the same as the one presented earlier in Section 4.1.3 for the PAR reduction of P2P MIMO systems.

## 4.2.2 Results and discussion

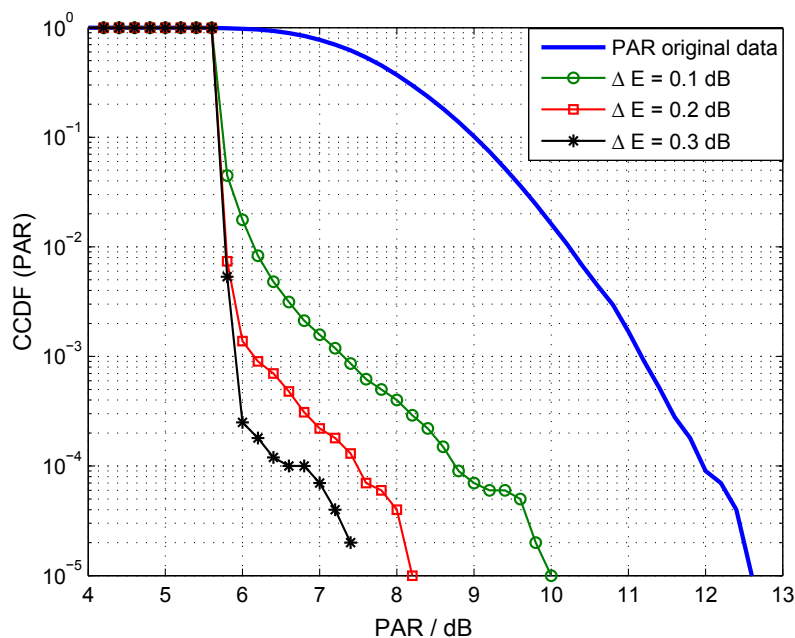
For the simulation results, we have considered a multi-user broadcast system with a central base station equipped with 10 transmit antennas, i.e.,  $M_t = 10$ . The BS is communicating with  $U = 10$  users, each equipped with a single receive antenna. The total number of receive antennas is hence  $M_r = 10$ . Moreover, we consider 128 subcarriers with 16-QAM constellations. We assume that one out the 10 users is inactive. We will use the channel of the inactive user to approximated the peak excursion on the remaining dimensions.

Figure 4.30 shows the CCDF curves for a  $10 \times 10$  multi-users BC scenario. As can be seen from the figure, a gain of approximately 3 dB is obtained with the first iteration and as much 5.8 dB with only 5 iterations. Figure 4.31 shows the CCDF (PAR) curves for a multi-user broadcast scenario, using Eq. 4.32, under different mean power constraints, with a maximum of 10 iterations. It is clear from the figure that the proposed algorithm has the least impact on the mean power. As can be seen, a gain of approximately 2.6 dB is obtained for  $\Delta E = 0.1$  dB and as much 5.0 dB for  $\Delta E = 0.3$  dB.

Figures 4.32 and 4.33 show the simulation results for a large scale multi-user BC scenario. We consider a central base station equipped with 40 transmit antennas communicating with 40 users. Again, we assume that one out of the 40 users is not active, thus, we use the respective channel for modeling the peak excursions on the remaining dimensions. The figure shows that for a PAR target value  $\tau = 7.5$  dB, a gain of approximately 4.6 dB can be obtained with as few as 8 iterations.



**Figure 4.30:** CCDF(PAR) of  $10 \times 10$  multi-user MIMO-OFDM for a PAR target value of 5.8 dB,  $\gamma = 8.5$



**Figure 4.31:** CCDF(PAR)  $10 \times 10$  multi-user MIMO-OFDM under different mean power constraints for a PAR target value of 5.8 dB,  $\gamma = 8.5$

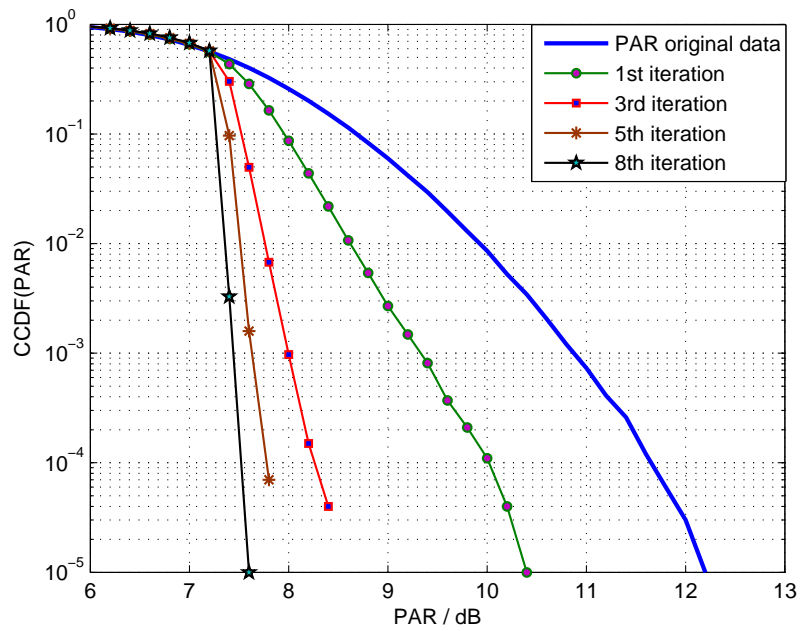


**Figure 4.32:** CCDF(PAR) of  $40 \times 40$  multi-user MIMO-OFDM for a PAR target value of 7.5 dB,  $\gamma = 25$

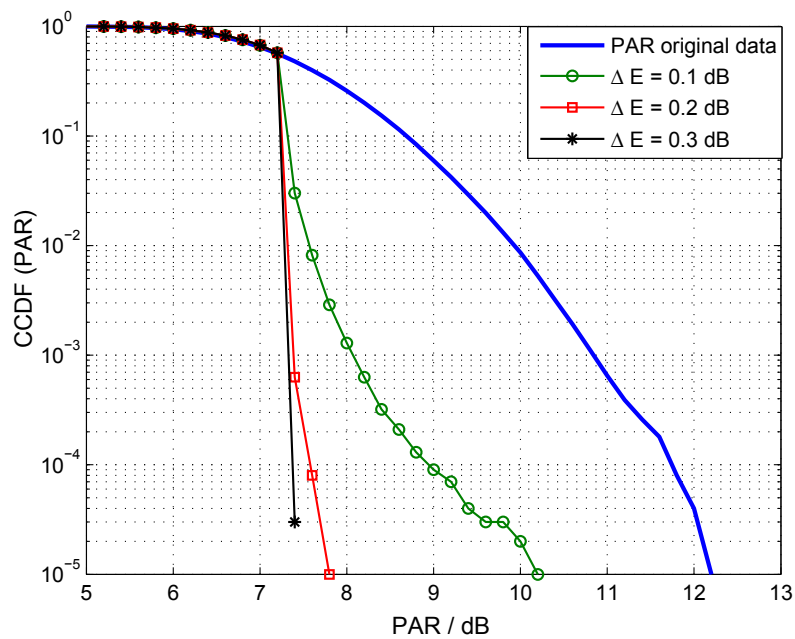


**Figure 4.33:** CCDF(PAR)  $40 \times 40$  multi-user MIMO-OFDM under different mean power constraints for a PAR target value of 7.5 dB,  $\gamma = 25$

## Chapter 5

# Optimized LDPC Code Concatenated with Trellis Shaping for PAR Reduction

In Chapters 3 and 4, we proposed PAR reduction techniques for P2P and multi-user MIMO-OFDM systems. First we extended the TR algorithm for MIMO-OFDM systems followed by our novel Least-Squares iterative algorithm. Herein, we go back and consider PAR reduction of single antenna OFDM systems. In Chapter 2, we gave a brief overview of different PAR reduction techniques most popular in literature. However, an also very promising technique amongst them is Trellis-Shaping, which results in high gains, in terms of PAR reduction, with a moderate complexity. The idea of Trellis-Shaping for PAR reduction was first proposed by Henkel and Wagner in [64]. The authors presented branch metrics for a search in the Viterbi algorithm in the time and the DFT domain. The same idea was later extended by Ochiai [69, 70], where the author devised a new branch metric based on the autocorrelation of the side-lobes in the DFT domain. Conventionally, hard decision decoding was used to extract the input bit stream from the shaping code sequence. However, to improve the system performance, the authors in [99, 100] suggested soft decision decoding using the BCJR [90] algorithm based on the compound trellis of the inverse syndrome former  $(\mathbf{H}^{-1})^T$  and the shaping code  $\mathcal{C}_s$ . To enhance the system performance further in terms of BER, the authors concatenated a regular LDPC code with Trellis Shaping for PAR reduction of a BICM-OFDM system. They used higher order  $\mathcal{M}$ -ary QAM modulation (256-QAM constellation) as modulated symbols at each tone of the OFDM system. However, as it is well known from literature, an irregular LDPC code has a better performance than a regular LDPC code. Moreover, in higher order constellations ( $\mathcal{M}$ -ary QAM), the bits constituting the QAM-symbol have different error probabilities. Thus, there is a possibility to design an LDPC code taking into account the irregularities in the bit error probabilities of the individual bits inside an  $\mathcal{M}$ -ary QAM symbol. This motivated us to design an irregular LDPC code concatenated with Trellis Shaping, based on the irregularities and the differences in the error probabilities of the individual bits inside the QAM constellation.

The rest of the chapter follows as, we start with our motivation to design an irregular LDPC code. First, in Section 5.2, we will give brief introduction to Trellis Shaping followed by the metric design for the Viterbi algorithm and the calculation of the soft output using a BCJR algorithm. Section 5.3 briefly discusses some basics of LDPC codes

followed by the optimization of an irregular LDPC code. In Section 5.4, we will describe the system model followed by the simulation results where we will compare and discuss the results obtained with both codes, i.e., with regular and irregular LDPC codes.

## 5.1 Equivalent binary channels of an $\mathcal{M}$ -ary QAM modulation

Let us consider that the trellis shaping selects a symbol from an  $\mathcal{M}$ -ary QAM constellation, with  $\mathcal{M}$  constellation points, each one carrying  $B = \log_2(\mathcal{M})$  bits. Let these bits inside a QAM symbol be labeled as  $\mathbf{b} = \{b_1, b_2, \dots, b_B\}$ . For a square  $\mathcal{M}$ -ary QAM constellation with Gray labeling (subsequently we will consider square QAM constellations with Gray mapping, else otherwise stated) the first two bits  $\{b_1, b_2\}$  are used to address one out of the four quadrants (outer QPSK) of the constellation, and are called the most significant bits (MSBs). The other bits, i.e.,  $\{b_3, b_4, \dots, b_B\}$  specify a particular point inside a quadrant of the square QAM-constellation and are known as the least significant bits (LSBs).

Moreover, as we know that inside each higher-order QAM constellation, the error probabilities for the individual bits are different, depending on the type, size, and labeling of the constellation used. Let  $P_{b_i}$  be the error probability of the  $i$ th bit. Based on the error probabilities of the individual bits, the bit vector inside the QAM symbol can thus be separated into  $N_m = B/2$  subgroups, which we will subsequently call modulation classes, i.e.,  $\mathbf{M} = \{M_1, M_2, \dots, M_{N_m}\}$ . The bits with the same error probability are thus assigned to the same modulation class. For example, the bit error probabilities of the bits which constitute the MSBs,  $\{b_1, b_2\}$ , have the same error probability, i.e.,  $P_{b_1} = P_{b_2}$ , and are hence assigned to the same modulation class,  $M_1 = \{b_1, b_2\}$ . The error probability of each modulation class  $M_i$  is then defined as  $\{P_{M_i}\}_{i=1}^{N_m}$ . Using an equivalent BPSK channel description as shown in Fig. 5.1, the individual channel variance for different modulation classes, i.e.,  $\boldsymbol{\sigma} = \{\sigma_1, \sigma_2, \dots, \sigma_{N_m}\}$ , can be computed from the bit error probabilities  $P_{b, M_i}$  [92], and is given as

$$\sigma_i^2 = \frac{1}{2\{\text{erfc}(2P_{b, M_i})\}^2}, \quad (5.1)$$

where “erfc” is the complementary error function and  $\boldsymbol{\sigma}$  is a vector for the equivalent noise of the individual channels.

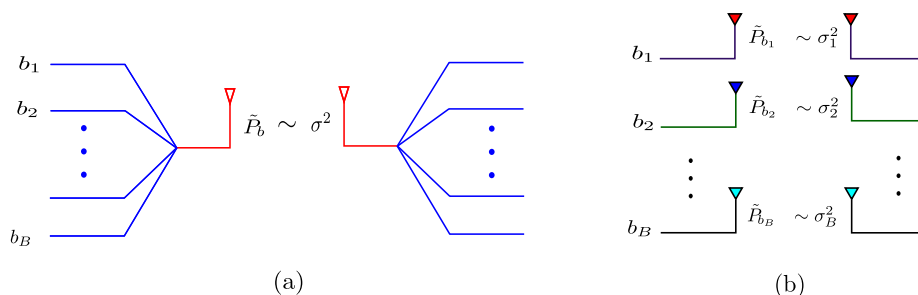


**Figure 5.1:** Binary channel assumption (a) physical channel (b) equivalent binary channels

**Example 1** Consider a square a 16-QAM constellation with Gray mapping as shown in Fig. 5.2. For a 16-QAM constellation, the total number of bits carried by a single QAM symbol is  $B = \log_2(16) = 4$ . These 4 bits can be labeled as  $[b_1, b_2, b_3, b_4]$ . In a square 16-QAM constellation with Gray mapping, the first two bits, i.e.,  $[b_1, b_2]$  are used to address one out of the four quadrants (the MSBs), while the last two bits  $[b_3, b_4]$  are used to specify a particular point in a specific quadrant (the LSBs). As shown in [93], the bit error probability of  $b_1$  and  $b_2$ , is the same, i.e.,  $P_{b_1} = P_{b_2}$ , and can be expressed as

$$P_{b_{1,2}} = 1/4 \left( \operatorname{erfc} \left( \sqrt{\frac{2\gamma}{10}} \right) + \operatorname{erfc} \left( 3\sqrt{\frac{2\gamma}{10}} \right) \right), \quad (5.2)$$

where “erfc” is the complimentary error function and  $\gamma$  is the signal-to-noise ratio with noise power spectral density  $N_0$ . Likewise for  $b_3$  and  $b_4$ ,  $P_{b_3} = P_{b_4}$  and is written as

$$P_{b_{3,4}} = 1/4 \left( 2\operatorname{erfc} \left( \sqrt{\frac{2\gamma}{10}} \right) + \operatorname{erfc} \left( 3\sqrt{\frac{2\gamma}{10}} \right) - \operatorname{erfc} \left( 5\sqrt{\frac{2\gamma}{10}} \right) \right). \quad (5.3)$$

Based on the bit error probabilities, the bits inside a 16-QAM constellation can thus be divided into two modulation classes,  $\mathbf{M} = [M_1, M_2]$ , (as we have two different error probabilities  $P_{b_{1,2}}$  and  $P_{b_{3,4}}$ ). The equivalent noise variances  $\boldsymbol{\sigma} = [\sigma_1, \sigma_2]$ , for each modulation class can be obtained using Eq. (5.1).

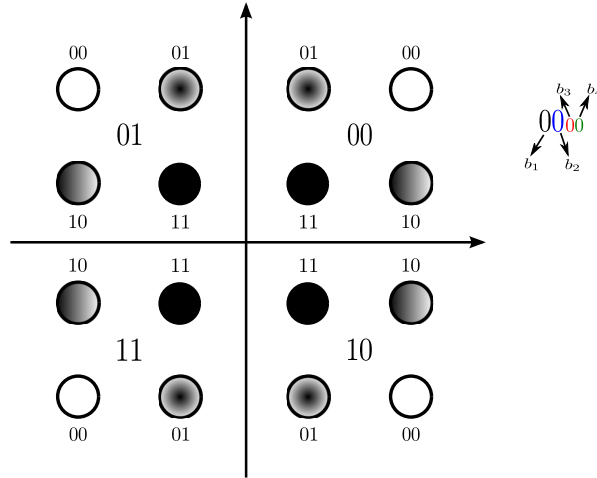


**Figure 5.2:** Square 16-QAM constellation with Gray mapping

This irregularity of the individual bits inside a QAM symbols can be exploited to optimize an LDPC code, as the individual bits have different error probabilities and thus can be protected differently inside the same QAM symbol.

## 5.2 Trellis Shaping

The basic principle of Trellis Shaping (TS) was first proposed by G. D. Forney [63]. Forney used Trellis Shaping to minimize the average power of a transmit sequence by

adding (modulo 2) a valid code sequence of the shaping code  $\mathcal{C}_s$  to the data sequence  $\mathbf{u}$  using a Viterbi algorithm, based on a branch metric (e.g. the mean power in Forney's case). However, application of the Trellis Shaping for PAR reduction of the multicarrier (OFDM) systems was first proposed by Henkel and Wagner [64], and later the idea has been extended by Ochiai [69, 70]. Forney used the mean power as a branch metric for the Viterbi algorithm. However, for PAR reduction, Henkel et al. used different metrics (e.g. the peak value) for PAR reduction. Herein, we will consider sign-bit shaping with a binary convolutional code as has been presented in [63].

A simplified block diagram of a trellis shaper is shown in Fig. 5.3. In there,  $\mathcal{C}_s$  is a binary

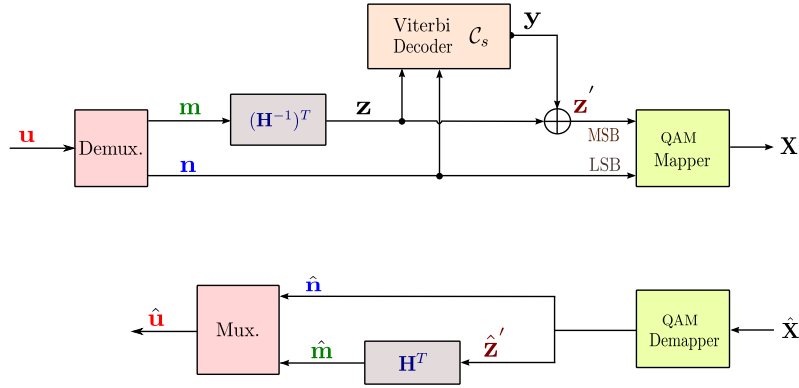


**Figure 5.3:** Block diagram of Trellis Shaping

rate- $k/n$  convolutional code (also referred to as the shaping code) with a  $k \times n$  generator matrix  $\mathbf{G}$ , where  $k$  and  $n$  stands for the number of input and output bits, respectively.  $\mathbf{H}^T$  and  $(\mathbf{H}^{-1})^T$  are the  $n \times (n - k)$  parity-check matrix (syndrome former) and its  $(n - k) \times n$  left inverse (inverse syndrome former), respectively.  $\mathbf{u}$  is the input data sequence of length  $1 \times (B - 1) \cdot N$  ( $B = \log_2(\mathcal{M})$ , where  $\mathcal{M}$  is the size of the  $\mathcal{M}$ -ary QAM constellation) prior to constellation mapping, which will be transmitted with an OFDM frame of size  $N$ . The  $1 \times (B - 1) \cdot N$  input bit sequence  $\mathbf{u}$  is first divided into  $N$  small chunks each one of size  $M = B - 1$  bits, i.e.,  $\mathbf{u} = \{\mathbf{u}_1, \mathbf{u}_2, \dots, \mathbf{u}_N\}$ , where  $\mathbf{u}_n = \{u_{1,n}, u_{2,n}, \dots, u_{B-1,n}\}$ . The input bit stream  $\mathbf{u}$  is then passed through a demultiplexer which separates  $\mathbf{u}$  into two sets of sequences  $\mathbf{m}$  and  $\mathbf{n}$ .  $\mathbf{m}$  are used to choose the MSBs (the sign bits) of the mapping constellation, i.e.,  $\mathbf{m}$  is used to select one out of the four quadrants, while  $\mathbf{n}$  is used to choose the least significant bits.  $\mathbf{m}$  is first preprocessed using the left inverse of the syndrome former  $(\mathbf{H}^{-1})^T$ , i.e.,

$$\mathbf{z} = \mathbf{m}(\mathbf{H}^{-1})^T. \quad (5.4)$$

The sequence  $\mathbf{z}$  obtained is then module-2 added to a valid code sequence  $\mathbf{y}$  in  $\mathcal{C}_s$ , where  $\mathcal{C}_s$  is the binary convolutional shaping code, i.e.,

$$\mathbf{z}' = \mathbf{z} \oplus \mathbf{y}, \quad (5.5)$$

where  $\oplus$  denotes modulo-2 addition.  $\mathbf{z}'$  is hence an element of  $\mathcal{C}_s \oplus \mathbf{z}$ . The sequence of data  $\mathbf{z}'$  represents the most significant bits of an  $\mathcal{M}$ -ary QAM constellation. Along with

the sequence of LSBs  $\mathbf{n}$ , the MSBs  $\mathbf{z}'$  determine the  $n$ th QAM constellation point as

$$X_n = \mathcal{M}(\mathbf{z}'_n; \mathbf{n}_n) = \mathcal{M}(\mathbf{z}_n \oplus \mathbf{y}_n; \mathbf{n}_n). \quad (5.6)$$

After mapping, in case of OFDM, the QAM symbols  $\mathbf{X} = X[n]$ ,  $n = 1, 2, \dots, N$  are transformed into time domain using an IFFT modulator, i.e.,  $\mathbf{x} = \text{IDFT}\{\mathbf{X}\}$ . This time-domain signal  $\mathbf{x}$  is then transmitted through a noisy channel. At the receiver, the estimated  $\hat{\mathbf{x}}$  is converted into DFT domain using an FFT demodulator, i.e.,  $\hat{\mathbf{X}} = \text{DFT}\{\hat{\mathbf{x}}\}$ . An estimate of the uncoded transmitted QAM-symbols  $\mathbf{X}$  can be obtained from  $\hat{\mathbf{X}}$  by the conventional symbol-by-symbol hard decisions detection. After hard decision decoding of the received symbols  $\hat{\mathbf{X}}$ , the main objective of the receiver is to decode the data bit sequence for the MSBs and the LSBs. In case of the LSBs, since no processing was performed at the transmitter, the estimates for the LSBs are directly mapped into the corresponding input bit estimates. In order to get an estimate of the MSBs  $\mathbf{z}'$ , we first recall some basic definitions from channel coding theory for the convolutional codes. For a convolutional code  $\mathcal{C}_s$  with a generator matrix  $\mathbf{G}$ , a valid code sequence  $\mathbf{y} \in \mathcal{C}_s$  is obtained as

$$\mathbf{y} = \mathbf{iG}, \quad (5.7)$$

where  $\mathbf{i}$  is an arbitrary input bit sequence and  $\mathbf{G}$  is the Forney generator matrix such that  $\mathbf{GH}^T = \mathbf{0}$ ,  $\mathbf{0}$  is a zero vector of size  $1 \times (n - k)$ . Moreover,  $\mathbf{y}$  is said to be a valid code sequence in  $\mathcal{C}_s$  if

$$\mathbf{yH}^T = \mathbf{0}, \quad (5.8)$$

where  $\mathbf{H}^T$  is the syndrome former for  $\mathcal{C}_s$ . In order to retrieve the input data sequence  $\mathbf{m}$ , the received sequence for the MSBs  $\hat{\mathbf{z}}'$  is processed with  $\mathbf{H}^T$ , the syndrome former of the shaping code  $\mathcal{C}_s$ , i.e.,

$$\mathbf{z}'\mathbf{H}^T = (\mathbf{z} \oplus \mathbf{y})\mathbf{H}^T = \mathbf{zH}^T \oplus \underbrace{\mathbf{yH}^T}_{=\mathbf{0}} \quad (5.9)$$

$$\mathbf{z}'\mathbf{H}^T = \mathbf{zH}^T \oplus \mathbf{0} = \mathbf{m} \underbrace{(\mathbf{H}^{-1})^T \mathbf{H}^T}_{=\mathbf{I}}$$

$$\mathbf{z}'\mathbf{H}^T = \mathbf{mI} = \mathbf{m}, \quad (5.10)$$

where  $\mathbf{I}$  is an  $(n - k) \times (n - k)$  identity matrix.

### 5.2.1 Sign-bit shaping with binary convolutional codes

Consider a convolutional shaping code  $\mathcal{C}_s$  of rate  $k/n = 1/2$ . The generator matrix  $\mathbf{G}$  for this code is  $1 \times 2$  and the syndrome former  $\mathbf{H}^T$  and its left inverse  $(\mathbf{H}^{-1})^T$  are  $2 \times 1$  and  $1 \times 2$  matrices, respectively. In the sign-bit shaping, the input bit stream  $\mathbf{m}$ , which is used to define the MSBs, is first encoded using the  $1 \times 2$  left inverse of the syndrome former  $(\mathbf{H}^{-1})^T$  according to Eq. (5.4).  $(\mathbf{H}^{-1})^T$  thus adds 1 redundant bit to each bit of the binary input sequence  $\mathbf{m}$ , resulting in a binary 2-tuple bit sequence  $\mathbf{z} = [z_n] = [z_{1,n}, z_{2,n}]$ ,  $n = 1, 2, \dots, N$ . Similarly, the binary 2-tuple valid code sequence  $\mathbf{y}$  of the shaping convolutional code  $\mathcal{C}_s$  can be defined as  $\mathbf{y} = [y_n] = (y_{1,n}, y_{2,n})$ . In the sign-bit shaping, the binary 2-tuple valid code sequence  $\mathbf{y}$  is modulo-2 added to the shaping bit sequence  $\mathbf{z}$  according to Eq. (5.5). In our PAR applications, a suitable metric needs to be chosen, which is discussed in the following section.

## 5.2.2 Metric selection for sign-bit shaping

For PAR reduction using trellis shaping, different branch metrics have been proposed for the Viterbi algorithm search by different authors [64,67,68,70]. As a first approach, Henkel and Wagner [64] proposed metrics in time as well as in DFT domain. The time-domain branch metric for searching a valid code sequence in the shaping code  $\mathcal{C}_s$ , was based on the peak power of the transmit signal, however, since the peak power is not additive, it does not fulfill the requirement to be a valid branch metric for the Viterbi algorithm (namely, the metric needs to be positive and additive). Thus, the time-domain peak power is determined at each path and the time domain vector is then updated accordingly as [64]

$$x_{k_\nu} = x_{k_{\nu-1}} + \sum_{n=(\nu-1)l+1}^{\nu l} X_n e^{j(2\pi/N)kn} \quad (5.11)$$

The results obtained with this branch metric are very promising. However, these results come with a cost, an increase in the computational complexity of the system as more IFFT/FFTs are required in case of only one IFFT/FFT. The authors also proposed an alternative branch metric in DFT domain based on the phases of the symbol and tabulation of the block transition matrix in DFT domain (for block sizes of small length). However, the DFT domain metrics were impractical for large block sizes.

In [70], Ochiai proposed a new branch metric for the Viterbi algorithm based on the minimization of the aperiodic autocorrelation of the sidelobes of an OFDM signal. Herein, else otherwise stated, we will consider the branch metric proposed by Ochiai, to search for a valid code sequence  $\mathbf{y} \in \mathcal{C}_s$  which minimizes the PAR of the transmit sequence. Subsequently, we will briefly describe essential steps in calculating the branch metric as proposed by Ochiai.

Let  $\mathbf{X} = [X_n]$ ,  $n = 1, 2, \dots, N$ , be an input data sequence, where  $X_n$  is chosen from an  $\mathcal{M}$ -ary QAM constellation. Applying the IFFT modulator, the time domain vector  $\mathbf{x} = [x_k]$ ,  $k = 1, 2, \dots, N$ , is obtained as

$$\begin{aligned} \mathbf{x} &= \text{IDFT}\{\mathbf{X}\} \\ x_k &= \frac{1}{\sqrt{N}} \sum_{n=1}^N X_n e^{j\frac{2\pi nk}{N}}, \quad k = 1, 2, \dots, N, \end{aligned} \quad (5.12)$$

where  $N$  is the frame size. The instantaneous power  $|x_k|^2$  of the time-domain OFDM signal  $\mathbf{x}$  is given as (Eq. (2.56))

$$\begin{aligned} |x_k|^2 &= x_k x_k^* = \frac{1}{\sqrt{N}} \sum_{n=1}^N X_n e^{j\frac{2\pi nk}{N}} \cdot \frac{1}{\sqrt{N}} \sum_{m=1}^N X_m e^{-j\frac{2\pi mk}{N}} \\ |x_k|^2 &= \frac{1}{N} \sum_{n=1}^N \sum_{m=1}^N X_n X_m^* e^{j\frac{2\pi k(n-m)}{N}}. \end{aligned} \quad (5.13)$$

Splitting into  $n = m$  and  $n \neq m$  and using Euler's formula, this is simplified as

$$|x_k|^2 = \underbrace{\frac{1}{N} \sum_{n=1}^N |X_n|^2}_{n=m} + \underbrace{\frac{2}{N} \sum_{n=1}^N \sum_{n \neq m} X_n X_m^* \cos \left( \frac{2\pi k}{N} (n - m) + \theta_n - \theta_m \right)}_{n \neq m} \quad (5.14)$$

$$|x_k|^2 = \underbrace{\frac{R_0}{N}}_I + \underbrace{\frac{2}{N} \sum_{n=1}^N |R_m| \cos \left( \frac{2\pi k}{N} \nu + \arg R_m \right)}_{II}. \quad (5.15)$$

The first term, i.e.,  $R_0/N$ , where  $R_0 = \sum_{n=1}^N |X_n|^2$ , is the DC component and is constant representing the average power of the transmit signal. The second term describes the signal envelope fluctuation, where  $\nu = n - m$ ,  $\arg R_m = \theta_n - \theta_m$  and  $|R_m|$  is the aperiodic autocorrelation of the QAM symbols, which can be expressed as [70],

$$|R_m| = \sum_{n=1}^{N-m} X_{n+m} X_m^*. \quad (5.16)$$

It is the second term in Eq. (5.15), which influences the PAR of an OFDM signal, hence, in order to minimize the PAR of the transmit signal, the fluctuation in the signal envelope must be minimized. A possible branch metric for the Viterbi algorithm will, thus, minimize the aperiodic autocorrelation of the sidelobes of an OFDM signal, i.e.,

$$\mathbf{y} = \arg \min_{\mathbf{y} \in \mathcal{C}_s} \sum_{m=1}^N |R_m|. \quad (5.17)$$

As we know that, for a function to work as a branch metric in the Viterbi algorithm, it must be positive and additive. In order to meet these criteria, a minimization of the squares of the absolute values of the aperiodic autocorrelation is considered as a branch metric [70]. Equation (5.17) then takes the form

$$\mathbf{y} = \arg \min_{\mathbf{y} \in \mathcal{C}_s} \sum_{m=1}^N |R_m|^2. \quad (5.18)$$

To make the branch metric (Eq. 5.18) additive, i.e., to define the  $n$ th QAM symbol by modification of the sign bit sequence  $\mathbf{z}_n$  by the binary 2-tuple code sequence  $\mathbf{y}_n$  ( $\mathbf{z}_n \oplus \mathbf{y}_n$ ), Eq. (5.18) is rephrased as

$$\mathbf{y}_n = \arg \min_{\mathbf{y}_n \in \mathcal{C}_s^n} \mu^i, \quad (5.19)$$

with  $\mu^i = \sum_{m=1}^i |R_m^i|^2$ , where  $R_m^i$  is the aperiodic autocorrelation of the input QAM symbols at length  $i$ . For sign-bit shaping with a rate-1/2 shaping code  $\mathcal{C}_s$ ,  $R_m^i$  is defined as

$$R_m^i = R_m^{i-1} + \delta_m^{i-1}, \quad i = 2, 3, \dots, N, \text{ and } m = 1, 2, \dots, i - 1, \quad (5.20)$$

where  $\delta_m^i = X_i X_{i-m}^*$ . Together with Eq. (5.18), the accumulated branch metric  $\mu^i$ , for the sign bit shaping is formulated as

$$\mu^i = \mu^{i-1} + \sum_{m=1}^{i-2} 2\mathcal{R} (R_m^{(i-1)*} \delta_m^{i-1}) + \sum_{m=1}^{i-1} |\delta_m^{i-1}|^2, \quad (5.21)$$

where the third term, i.e.,  $\sum_{m=1}^{i-1} |\delta_m^{i-1}|^2$  is a constant, does not contribute to the PAR of the transmit signal, and can be omitted in the calculation of  $\mu^i$  [70]. For PAR reduction with Trellis Shaping, we will use the metric defined by Eq. (5.21) to select a sequence of symbols with the lowest PAR.

### 5.2.3 Soft-input soft-output decoding for the shaping bits, using the BCJR algorithm

Conventionally, in order to decode the information bit sequence at the receiver, hard decision decoding on the estimates of the shaping bit sequence was performed on the channel outputs in Trellis Shaping [63, 64, 69, 70]. However, using soft decision decoding with the BCJR algorithm, the system performance can further be improved [99, 100]. We will hence consider soft decision decoding with the BCJR algorithm [90], to obtain the Log-Likelihood Ratios (LLRs) for the shaping bit sequence.

Let  $\mathbf{X} = [X_n], n = 1, 2, \dots, N$ , be the sequence of QAM-symbol selected using Trellis Shaping. The time-domain signal is obtained using an IFFT modulator, i.e.,  $\mathbf{x} = \text{IDFT}\{\mathbf{X}\}$ .  $\mathbf{x}$  is then transmitted over the channel. At the receiver, an estimate of the  $n$ th data symbol filtered by the channel, in DFT domain, can be expressed as

$$Y_n = X_n + w_n \quad (5.22)$$

where  $Y_n$  is the  $n$ th tone of the OFDM frame and  $w_n$  is the additive white Gaussian noise with single-sided power spectral density  $N_0$ .

Since no preprocessing is performed on the LSBs at the transmitter, thus, the LLRs for the LSBs are obtained directly from the channel outputs in the conventional way, i.e.,

$$\mathcal{L}_{LSBs}^n = \ln \frac{p(c_{n,i} = 0 | \mathbf{X})}{p(c_{n,i} = 1 | \mathbf{X})}, \quad (5.23)$$

where  $p(c_{n,i} = b | X_n)$  is the probability density function of the  $i$ th received bit belonging to the LSBs conditioned on the  $n$ th transmitted symbol [100] and is defined as

$$p(c_{n,i} = b | X_n) = \sum_{X \in \mathcal{X}_i^b} \mathbb{C} e^{-\left(\frac{|\hat{X}_n - X|^2}{2\sigma_M^2}\right)}, \quad (5.24)$$

where  $\mathbb{C}$  is a constant which can be omitted in the actual calculations and  $\sigma_M^2$  is the variance of the noise with power spectral density  $N_0$  of an AWGN channel.

For the MSBs, the LLRs cannot be obtained in this straight-forward manner. To obtain the soft outputs for single MSB information bits, we consider a combined trellis design based on the left inverse of the syndrome former  $(\mathbf{H}^{-1})^T$ , and the generator matrix of the shaping code  $\mathcal{C}_s$ . Based on this compound trellis, a BCJR algorithm is then used to

determine the LLRs.

Let  $N_{s_{c_s}}$  be the number of states of the shaping code  $\mathcal{C}_s$  and let  $N_{s_H}$  be the number of states of the left inverse syndrome former. Then, the total number of states of the compound trellis is  $N_{s_{ct}} = N_{s_{c_s}} \cdot N_{s_H}$ . Besides the number of states, the number of branches emanating from a state of the compound trellis equals  $2^n$  (which in our case equals  $2^2 = 4$ , See Fig. 5.9), where  $n$  is the number of output bits of the shaping code  $\mathcal{C}_s$  [100].

### BCJR algorithm

Now, to employ the BCJR algorithm for soft output calculation, let us consider  $t$  and  $\acute{t}$  representing the current and the previous states of a trellis, respectively. Let  $m_n$  be the  $n$ th bit of the input sequence which was modified to the  $n$ th binary 2-tuple MSBs  $\{\acute{z}_n^0, \acute{z}_n^1\}$ , along with LSBs, defining the  $n$ th QAM symbol. In order to get soft output out of the BCJR algorithm, we first compute the state transition probabilities  $\gamma_n(\acute{t}, t)$ , the forward recursion  $\alpha_n(t)$ , and the backward recursion  $\beta_n(\acute{t})$ . The forward recursion,  $\alpha_n(t)$ , is computed as

$$\alpha_n(t) = \sum_{i=1}^{N_{s_{ct}}} \alpha_{n-1}(\acute{t}_i) \gamma_{n-1}(\acute{t}_i, t), \quad n = 1, 2, \dots, N. \quad (5.25)$$

Similarly, the backward recursions,  $\beta_n(\acute{t})$ , is calculated using

$$\beta_n(\acute{t}) = \sum_{i=1}^{N_{s_{ct}}} \beta_{n+1}(t_i) \gamma_n(\acute{t}, t_i), \quad n = N, N-1, \dots, 1. \quad (5.26)$$

The initial conditions for the forward and backward recursions are predefined as

$$\alpha_0(t) = \begin{cases} 1, & \text{when } t = 0, \\ 0, & \text{otherwise,} \end{cases}$$

$$\beta_N(\acute{t}) = 1/N_{s_{ct}}, \quad \text{for } \acute{t} = 1, 2, \dots, N_{s_{ct}}.$$

The state transition probabilities  $\gamma_n(\acute{t}, t)$  are calculated as

$$\gamma_n(\acute{t}, t) = \prod_{j=1}^{2-1} p_{n,j}(\acute{t}, t | X_n), \quad (5.27)$$

where

$$p_{n,j}(\acute{t}, t | X_n) = \sum_{X \in \mathcal{X}_j^b} \mathbb{C}e^{-\frac{|\acute{x}_n - X_n|^2}{2\sigma_M^2}}, \quad \text{for } j = 1, 2. \quad (5.28)$$

$\gamma_n(\acute{t}, t) = 0$  if there is no branch connection between  $\acute{t}$  and  $t$ . The likelihood for the  $j$ th received bit belonging to the MSBs can then be computed as

$$p(\acute{z}_n^j = b, \mathbf{X}) = \sum_{\acute{t} \in \Gamma(b)} \alpha_n(\acute{t}) \gamma_n(\acute{t}, t) \beta_{n+1}(t), \quad (5.29)$$

where  $z_n^j$  is the  $j$ th received bit of the  $n$ th symbol which belongs to the MSBs,  $\zeta_t$  is the state transition, and  $\Gamma(b)$  is the set of state transition with value  $b$ . The LLRs for the MSBs are then calculated as

$$\mathcal{L}_{MSB}^n = \ln \frac{p(z_n^j = 0 | \mathbf{X})}{p(z_n^j = 1 | \mathbf{X})} = \ln \frac{p(z_n^j = 0, \mathbf{X})}{p(z_n^j = 1, \mathbf{X})}. \quad (5.30)$$

The LLRs obtained from the BCJR algorithms for the MSBs are fed into an LDPC decoder along with the LLRs for the LSBs to obtain the received intrinsic information for the complete bit sequence  $\mathbf{u}$ . Subsequently, we will give a brief introduction to some basics of LDPC codes followed by the optimization of the variable-node degree distribution and the code construction.

### 5.3 Irregular LDPC codes

In [99, 100], the authors used a regular LDPC code concatenated with Trellis Shaping for PAR reduction. However, we know that irregular LDPC codes usually have a better performance than regular LDPC codes. This motivated us to design an irregular LDPC code and concatenate it with Trellis Shaping for a better performance of the system as compared to the regular LDPC code solutions, in terms of bit error ratios (BER). Henceforth, we will consider an irregular LDPC code concatenated with Trellis Shaping as shown in Fig. 5.4. The input bit stream  $\mathbf{u}$  is first encoded using an irregular LDPC code. The encoded bits are then assigned to different modulation classes based on the error probabilities of the individual bits inside the QAM symbol. Now, the goal is to design an optimized irregular LDPC code. We thus exploit the irregularities inside the QAM symbol and design an irregular LDPC code based on the error probabilities of the individual bits. Herein, we first start with basics of LDPC codes followed by the optimization of the variable-node degree distribution for constructing an irregular LDPC code.

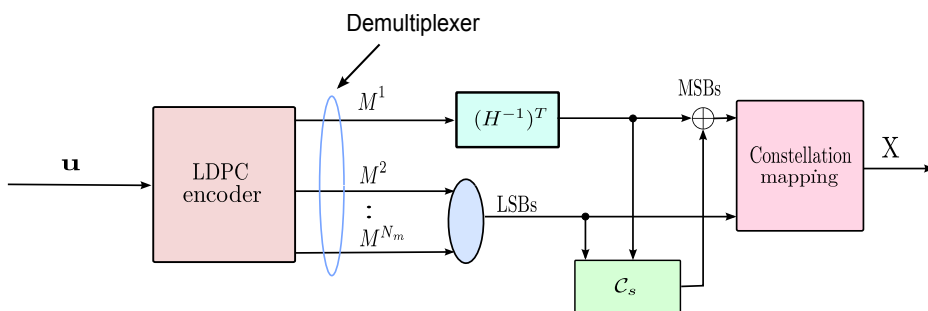


**Figure 5.4:** Block diagram of LDPC code concatenated with Trellis Shaping

#### General Description

Low-Density Parity-Check (LDPC) codes are linear block codes, first invented by Gallager in 1962 [88]. LDPC codes are characterized by a parity-check matrix  $\mathbf{H}_{n-k \times n}$ , where  $n$  is the codeword length and  $k$  is the length of the input bit vector. As the name suggests,

the parity check matrix  $\mathbf{H}$  has a very low density, i.e.,  $\mathbf{H}$  is a sparse matrix with only a few non-zero entries. Let  $\omega_r$  be the row weight, the number of ones in each row. Similarly, let  $\omega_c$  be the column weight representing the number of non-zero entries in each column. For the matrix to be called “*low-density*” the two conditions, i.e.,  $\omega_r \ll k$  and  $\omega_c \ll n$  must be satisfied. The density of the code  $\xi_{ldpc}$  is then defined as

$$\xi_{ldpc} = \omega_r/n = \omega_c/k.$$

Graphically, like all linear block codes, the parity check matrix  $\mathbf{H}$  of an LDPC code can be represented by a bipartite graph known as Tanner graph (after Tanner, [89]). A Tanner graph consists of two types of vertices or nodes,  $\mathbb{V}$  and  $\mathbb{C}$ .  $\mathbb{V} = \{V_i\}$  represents the code bits and are called the code-bit vertices or the variable nodes. The second set, i.e.,  $\mathbb{C} = \{C_j\}$  represents the parity-check sum and are called the parity-check vertices or the check nodes. A variable node  $V_i$  is connected to a check node  $C_j$  through an edge  $e_t$ . A code bit vertex  $V_i$  is said to be checked by a parity-check vertex  $C_j$ , if and only if the  $H_{i,j}$  element of the parity check matrix is a non-zero element, i.e., 1 in the binary case. The degree of a node is defined by the total number of edges connected to it. For an LDPC code, a bipartite graph is said to be regular if all variable nodes have the same degree and all check nodes have another common degree. In other words, an LDPC code is said to be regular if all rows of the parity check matrix have the same weight, i.e.,  $\omega_{r_1} = \omega_{r_2} = \dots = \omega_{r_k}$ , where  $k$  is the total number of rows, and all columns are also of the same weight. A regular LDPC code with a parity check matrix  $\mathbf{H}$  is thus completely specified by the ordered pair  $(d_v, d_c)$ , where  $d_v$  is the variable-node degree and  $d_c$  is the check-node degree.

**Example 2** Consider a rate-1/2 code with an (8,4) parity-check matrix, given as

$$\begin{pmatrix} 0 & 1 & 0 & 1 & 1 & 0 & 0 & 1 \\ 1 & 1 & 1 & 0 & 0 & 1 & 0 & 0 \\ 0 & 0 & 1 & 0 & 0 & 1 & 1 & 1 \\ 1 & 0 & 0 & 1 & 1 & 0 & 1 & 0 \end{pmatrix}, \quad (5.31)$$

with  $\omega_r = 4$  and  $\omega_c = 2$ . The Tanner graph for this matrix is shown in Fig. 5.5. In there, the circles represent the variable nodes which correspond to the columns of the parity-check matrix and the squares are the check nodes which correspond to the rows of the parity-check matrix. A variable node  $V_i$  is connected to the check node  $C_j$  through an edge  $e_t$ , which represents the non-zero element of  $\mathbf{H}$ , i.e.,  $H_{i,j} = 1$ . Moreover, in Fig. 5.5, each check node is connected to four variable nodes, i.e., the total number of edges at each check node is 4, thus, the check-node degree is  $d_c = 4$ . Likewise, each variable node is connected to two check nodes, thus,  $d_v = 2$ .

In contrast to regular LDPC codes, if the degree of the check nodes/variable nodes varies, then, this type of codes are known as irregular LDPC codes. The code cannot be specified by an ordered pair as in the case of regular LDPC code. The degree distribution of an irregular LDPC code is therefore represented by a polynomial. The variable-node and check-node degree distributions of an irregular LDPC code, written as polynomials, can

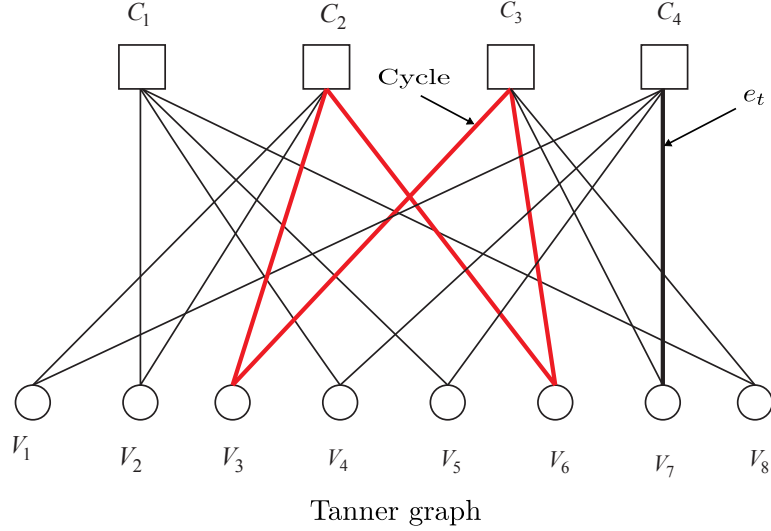


**Figure 5.5:** Tanner graph of an LDPC code

be expressed as

$$\lambda(x) = \sum_{i=2}^{d_{vmax}} \lambda_i x^{i-1} \quad \text{and} \quad \rho(x) = \sum_{i=2}^{d_{cmax}} \rho_i x^{i-1}, \quad (5.32)$$

where  $\lambda_i$  and  $\rho_i$  are the fractions of edges connected to variable and check nodes of degree  $i$ , respectively. Based on the polynomial representation, the rate of an irregular LDPC code is then defined as

$$R = 1 - \frac{\sum_{j=2}^{d_{cmax}} \rho_j / j}{\sum_{i=2}^{d_{vmax}} \lambda_i / i}. \quad (5.33)$$

### 5.3.1 Notations

Consider a UEP LDPC code with a codeword length  $N$ . In order to optimize the variable degree distribution for the LDPC code, we will make use of the irregularities, i.e., the different bit error probabilities, of the individual bits inside a QAM symbol. Let  $N_m$  be the total number of modulation classes based on the constellation used, i.e.,  $\{M_1, M_2, \dots, M_{N_m}\}$ . The proportion of bits in each modulation class  $\beta_i$  is given by a vector  $\boldsymbol{\beta} = \{\beta_1, \beta_2, \dots, \beta_{N_m}\}$ , where  $\beta_i$  is the proportion of bits assigned to the  $i$ th modulation class, with,  $\beta_j = N_j/N_c$ ,  $N_j$  is the total number of bits in modulation class  $j$  and  $N_c$  is the codeword length. Let  $\boldsymbol{\lambda}$  be the vector of the overall variable node degree distribution for all modulation classes. For a modulation class  $M_j$ ,  $\boldsymbol{\lambda}_{M_j}$  can be written as  $\boldsymbol{\lambda}_{M_j} = [\lambda_{M_j,2}, \lambda_{M_j,3}, \dots, \lambda_{M_j,d_{vmax}}]^T$ , where  $\lambda_{M_j,i}$  is the sub-degree distribution and represents the proportion of edges connected to a variable node of degree  $i$  belonging to the modulation class  $M_j$ . The overall variable node degree distribution for the  $N_m$  modulation classes is given as

$$\boldsymbol{\lambda} = \left[ \boldsymbol{\lambda}_{M_1}^T, \boldsymbol{\lambda}_{M_2}^T, \dots, \boldsymbol{\lambda}_{M_{N_m}}^T \right]^T, \quad (5.34)$$

where  $\{\cdot\}^T$  stands for transpose. Moreover, to construct an irregular LDPC code, we also need the check-node degree distribution. The check-node degree distribution is given by the vector  $\boldsymbol{\rho} = [\rho_2, \rho_3, \dots, \rho_{d_{c_{max}}}]^T$ . With  $E$  as the total number of edges,  $N_j$  and  $N_c$  in terms of  $\lambda_{M_j}$  can be obtained as

$$\sum_{i=2}^{d_{v_{max}}} \frac{\lambda_{M_{i,j}}}{i} = N_j/E \quad \text{and} \quad \sum_{j=1}^{N_m} \sum_{i=2}^{d_{v_{max}}} \frac{\lambda_{M_{i,j}}}{i} = N_c/E, \quad (5.35)$$

where  $N_j$  is the number of bit in modulation class  $j$  and  $N_c$  is the codeword length of the LDPC code.

### 5.3.2 Optimization of the variable-node degree distribution

In order to optimize the variable-node degree distribution for an irregular LDPC code, we will follow the approach of [37, 92, 94–96, 98], i.e., to optimize the variable node degree distribution for an irregular LDPC code, we will investigate the decoding behavior of the LDPC codes. LDPC codes are usually decoded by a message-passing algorithm known as sum-product or Belief Propagation (BP) algorithm. In BP, messages representing reliability (log-likelihood ratios (LLRs)), considered as Gaussian random variables, are exchanged along the edges between variable and check nodes in an iterative fashion. Let  $V_i$  be a variable node of degree  $i$  connected by an edge to a check node of degree  $j$ , i.e.,  $C_j$ . Let  $L_{V_i, C_j}$  be the message from a variable node of degree  $i$  to a degree  $j$  check node, then, the variable node update rule in belief propagation algorithm is written as

$$L_{V_i, C_j} = L_0 + \sum_{k \neq j} L_{C_k, V_i}, \quad (5.36)$$

where  $L_0$  is the channel output and the summation is over all the neighboring check nodes excluding  $C_j$ . Similarly, for a check node messages  $L_{C_j, V_i}$ , i.e., the message from a check node of degree  $j$  to a variable node of degree  $i$ , the check node update can be expressed as

$$L_{C_j, V_i} = 2 \tanh^{-1} \left( \prod_{k \neq i} \tanh(L_{V_k, C_j}) \right), \quad (5.37)$$

where the product is over all variable nodes excluding  $V_i$ . The messages at the variable nodes and the check nodes are updated by summation (variable-node update) and a product (check-node update), the algorithm is, thus, also known as sum-product algorithm. The messages along the edges are considered as independent random variables. With a Gaussian approximation, for the independent random variables, exploiting the Density Evolution (DE) algorithm, the evolution of these messages (LLRs) can be computed [37, 95]. Thus, at the  $l^{\text{th}}$  iteration, the mutual information from a check node to the variable node  $x_{cv}$  and from a variable node to a check node  $x_{vc}$  computed for a standard LDPC code using density evolution (DE) with Gaussian approximation can be expressed as

$$x_{cv}^{(l-1)} = 1 - \sum_{j=2}^{d_{c_{max}}} \rho_j J \left( \sqrt{(j-1)J^{-1}(1-x_{vc}^{(l-1)})} \right), \quad (5.38)$$

$$x_{vc}^{(l)} = \sum_{i=2}^{d_{vmax}} \lambda_i J \left( \frac{2}{\sigma^2} + (i-1)J^{-1}(x_{cv}^{(l-1)}) \right), \quad (5.39)$$

where  $J(\cdot)$  computes the mutual information, i.e.,  $x = J(m)$  given as

$$J(m) = 1 - \frac{1}{\sqrt{4\pi m}} \int_{\mathbb{R}} \log_2(1 + e^{-z}) \cdot e^{-\frac{(z-m)^2}{4m}} dz, \quad (5.40)$$

where  $z \sim N(m, 2m)$  is a consistent Gaussian random variable. In our analysis, the check-node degree distribution is not subdivided, however, the variable node degree distribution is split into sub-groups based on the modulation classes  $N_m$ . Thus, the update rule for the messages from the check node to the variable node ( $x_{cv}$ ) is not affected. However, we adapt and modify Eq. (5.39) as

$$x_{vc}^{(l)} = \sum_{j=1}^{N_m} \sum_{i=2}^{d_{vmax}} \lambda_{M_{j,i}} J \left( \frac{2}{\sigma_j^2} + (i-1)J^{-1}(x_{cv}^{(l-1)}) \right). \quad (5.41)$$

With equations (5.38) and (5.41), the density evolution for the mutual information of the LDPC code, with  $N_m$  sub-class variable-node degrees is summarized as

$$x_{vc}^{(l)} = F(\boldsymbol{\lambda}, \boldsymbol{\rho}, \boldsymbol{\sigma}^2, x_{vc}^{(l-1)}). \quad (5.42)$$

We need to ensure the convergence, i.e., the mutual information must increase per iteration, meaning

$$F(\boldsymbol{\lambda}, \boldsymbol{\rho}, \boldsymbol{\sigma}^2, x_{vc}^{(l-1)}) > x_{vc}^{(l-1)}. \quad (5.43)$$

Another important constraint to be fulfilled by the ensemble LDPC code is the stability constraint which ensures convergence of the mutual information close to one. The stability condition gives an upper limit for degree-2 variable nodes [95],

$$\frac{1}{\mathcal{X}'(0)\rho'(1)} > e^{-r} = \int_{\mathbb{R}} P_0(x) e^{-\frac{x}{2}} dx = e^{-\frac{1}{2\sigma^2}}, \quad (5.44)$$

with  $P_0(x)$  being the message density for the received values and  $\mathcal{X}'(x)$  and  $\rho'(x)$  being the derivatives of the degree polynomials. The bits in our schemes experience different channel noise with different equivalent noise variances  $\sigma_j^2$ , thus, we exploit the average density, given by utilizing the modulation class proportions  $\beta$ ,

$$e^{-r} = \int_{\mathbb{R}} \sum_{j=1}^{N_m} \beta_j \cdot P_{0,j}(x) e^{-\frac{x}{2}} dx = \sum_{j=1}^{N_m} \beta_j \cdot e^{-\frac{1}{2\sigma_j^2}}. \quad (5.45)$$

We optimized the degree distribution for different modulation classes, given a fixed check-node degree distribution. Splitting the variable-node degree distribution into subclasses results in a sum constraint. For the algorithm to converge, the sum constraint is formulated as [37]

$$\sum_{j=1}^{N_m} \sum_{i=2}^{d_{vmax}} \lambda_{M_{j,i}} = 1. \quad (5.46)$$

### 5.3.3 Optimization algorithm

With all the constraints and characterization for the density evolution algorithm, we optimized the variable-node degree distribution with a maximum degree  $d_{v_{max}}$ . Our strategy was to optimize the variable-node degree distribution which maximizes the code rate. Herein, we modify the optimization algorithm proposed in [37, 92, 98]. Table 5.1 shows the important steps of the optimization algorithm. The linear programming routine requires the check-node degree distribution  $\boldsymbol{\rho}$ , the maximum variable node degree  $d_{v_{max}}$ , proportion of the bits in various modulation classes  $\boldsymbol{\beta}$ , the required code rate  $R$  and  $\boldsymbol{\sigma}^2$  derived from the signal-to-noise ratio  $E_s/N_0$ .

**Table 5.1:** Optimization algorithm for irregular LDPC codes.

<p style="text-align: center;"><u>Optimize</u></p> $\max_{\lambda} \sum_{j=1}^{N_m} \sum_{i=2}^{d_{v_{max}}} \frac{\lambda_{M_{j,i}}}{i} \tag{5.47}$
<p>subject to</p>
<p>[1] Proportion distribution constraints</p> $\sum_{j=1}^{N_m} \sum_{i=2}^{d_{v_{max}}} \lambda_{M_{j,i}} = 1 \tag{5.48}$
<p>[2] Convergence constraint, according to (5.43)</p> $F(\boldsymbol{\lambda}, \boldsymbol{\rho}, \boldsymbol{\sigma}^2, x) > x \tag{5.49}$
<p>[3] Stability condition, according to (5.44) and (5.45)</p> $\sum_{j=1}^{N_m} \lambda_{M_{j,2}} < \left[ \sum_{j=1}^{N_m} \beta_j e^{-1/2\sigma_j^2} \cdot \sum_{m=2}^{d_{c_{max}}} \rho_m (m-1) \right]^{-1} \tag{5.50}$

### 5.3.4 Code construction

After obtaining an optimized variable-node degree distribution, the parity-check matrix  $\mathbf{H}$  is constructed using the Progressive-Edge-Growth (PEG) algorithm [10, 37]. PEG is a sophisticated algorithm which tries to maximize the length of the local girth. The graph is constructed with one edge at a time and each edge is placed in such a manner that it has the lowest impact on the local girth. The algorithm is initialized with the variable-node profile, which shows the degrees of the  $n$  variable nodes. The algorithm starts with the lowest degree variable node and progresses to the higher degree nodes, processing one variable node at a time (for all the edges connected to it). The edge selection criteria is to maximize the length of the local girth, thus, the variable node is connected to a check node which has not yet been reached. If all the check nodes have been connected with the current variable node, then the one with the maximum cycle is selected. If there is more than one option, the check node with the lowest degree is chosen. For a deep understanding, interested readers are referred to [10] and the references therein.

## 5.4 System model, results, and discussion

For the simulation results, we have considered a single-input single-output (SISO) OFDM system concatenated with LDPC code as shown in Fig. 5.6. As discussed earlier, we chose a square 256-QAM constellation with Gray mapping (Type-I in [70]). In order to have a high spectral efficiency we use a rate-6/7 LDPC codes (both regular and irregular codes) concatenated with Trellis Shaping. The length of each code is chosen such that it matches the size of one OFDM frame. We have considered an OFDM frame comprised of 128 sub-carriers modulated by 256-QAM. Each QAM symbol of the 256-QAM constellation carries  $B = \log_2(256) = 8$  bits. The total number of bits thus required to match one OFDM frame =  $128 \times 8 = 1024$ . Moreover, the LDPC code is concatenated with Trellis Shaping which adds 1 bit redundancy per QAM symbol, which in our case equals 128 bits. In order to match the size of one OFDM frame to the length of the LDPC code is, thus, chosen as 896 ( $896 + 128 = 1024$ ). The overall code rate of the system with trellis shaping then equals  $3/4$ . In order to decode the LDPC codeword, we use belief propagation with the maximum number of iterations set to 50 for both regular and irregular LDPC codes. We will also compare our results to a system without Trellis Shaping. The codeword length and the code rate for such codes are chosen to be 1024 and  $3/4$ , respectively.

As shown in the Fig. 5.6, the input bit stream  $\mathbf{u}$  is first encoded with an optimized

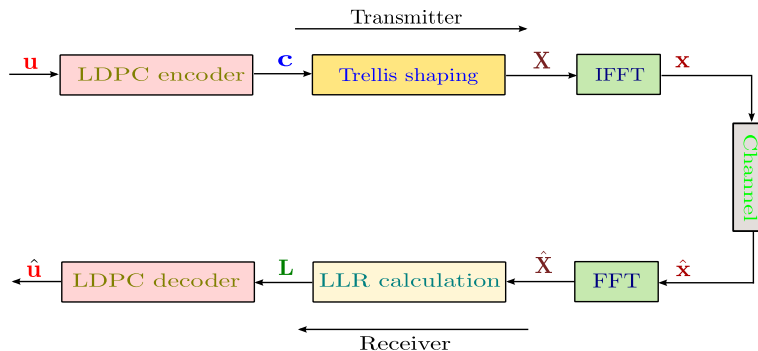


**Figure 5.6:** Irregular LDPC code concatenated with Trellis Shaping

irregular LDPC code. In order to optimize the LDPC code, we exploit the bit error probabilities of the individual bits inside the  $M$ -ary QAM symbol. For the 256-QAM constellation with Gray mapping,  $B = 8$  bits are used to represent a single symbol, labeled as  $B = \{b_1, b_2, \dots, b_8\}$ . The exact bit error probabilities for the individual bits  $\{P_{b_1}, P_{b_2}, \dots, P_{b_8}\}$  computed as in [93], are given in App. B.<sup>1</sup> As shown in [93],  $P_{b_1} = P_{b_2} = P_{b_{1,2}}, \dots, P_{b_7} = P_{b_8} = P_{b_{7,8}}$ , which in more compact form can be written as  $\mathbf{P}_b = \{P_{b_{1,2}}, P_{b_{3,4}}, \dots, P_{b_{7,8}}\}$ . For 256-QAM, we have four different error probabilities for the individual bits, thus, based on these error probabilities, we have four modulation classes,  $\mathbf{M} = \{M_1, M_2, M_3, M_4\}$ . The error probability of each modulation class is then given as the error probability of the bits constituting that class, i.e.,  $\mathbf{P}_b = \{P_{b,M_1}, P_{b,M_2}, P_{b,M_3}, P_{b,M_4}\}$ . From the bit-error probabilities of the individual bits, we will compute the individual noise variances for the different modulation classes, i.e.,  $\boldsymbol{\sigma} = \{\sigma_1, \sigma_2, \sigma_3, \sigma_4\}$ .

<sup>1</sup>The authors in [93] gives the expression for a noise with  $N_0/2$  power spectral density, however, we have modified the expressions for a noise with  $N_0$  power spectral density, i.e., we use a two-sided definition.

For the least significant bits  $\{b_3, b_4, \dots, b_8\}$ , with bit error probabilities  $\{P_{b_{3,4}}, P_{b_{5,6}}, P_{b_{7,8}}\} = \{P_{b,M_2}, P_{b,M_3}, P_{b,M_4}\}$ , no preprocessing is performed and they are mapped directly into the 256-QAM subconstellation. The noise variance of the individual modulation classes which consist of these bits are directly obtained from the error probabilities of the individual modulation classes using Eq. (5.1), i.e.,

$$\sigma_i^2 = \frac{1}{2\{\text{erfc}(2P_{b,M_i})\}^2}, \quad i = 2, 3, 4, \quad (5.51)$$

where “erfc” is the complementary error function and  $P_{b,M_i}$  is the error probability of the bits belonging to the  $i$ th modulation class.

However, in Trellis Shaping, the first two bits,  $b_1, b_2$ , are defined by the shaper. For sign-bit shaping with rate-1/2 inverse syndrome former  $(\mathbf{H}^{-1})^T$ , we must take the bit-error probability of the inverse syndrome former into consideration as well. Subsequently we show calculation of the bit error probability for the MSBs, i.e., the first modulation class  $M_1$  in the next section.

### 5.4.1 Bit error probability for the MSBs

For trellis shaping, we considered the (5, 7) convolutional code as the shaping code  $\mathcal{C}_s$ , with a generator matrix  $\mathbf{G}$ , defined as  $(1 + D^2, 1 + D + D^2)$ . The syndrome former, i.e., the parity check matrix  $\mathbf{H}$  for the shaping code is chosen as  $(1 + D + D^2, 1 + D^2)$ . The left inverse of the syndrome former  $(\mathbf{H}^{-1})^T$  is not unique, thus, we choose  $(2, 3)$ , i.e.,  $(D, 1 + D)$  as the left inverse syndrome former of the shaping code  $\mathcal{C}_s$  as shown in Fig. (5.7) [63]. In Trellis Shaping, the input bit stream used to determine the MSBs are first encoded by  $(\mathbf{H}^{-1})^T$ . We approximate the bit-error probability using the Union Bound. Based on the weight distribution of the code, the bit-error probability of the input bits encoded by the  $(\mathbf{H}^{-1})^T$  can be calculated by exploiting the Union bound defined as

$$P(b) \leq \sum_{d=d_{free}}^{\infty} A_d P_d, \quad (5.52)$$

where,  $d_{free}$  is the free distance or the minimum Hamming distance of the code,  $A_d$  is the weight distribution of the code and  $P_d$  is the probability to choose a wrong path at distance  $d$ .

The transfer function of a code is calculated from the state diagram of the code. Let

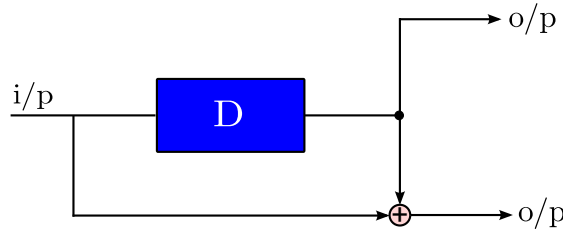


**Figure 5.7:** Inverse syndrome former  $(\mathbf{H}^{-1})^T$

us consider the state diagram of the (2,3) inverse syndrome former  $(\mathbf{H}^{-1})^T$  as shown in

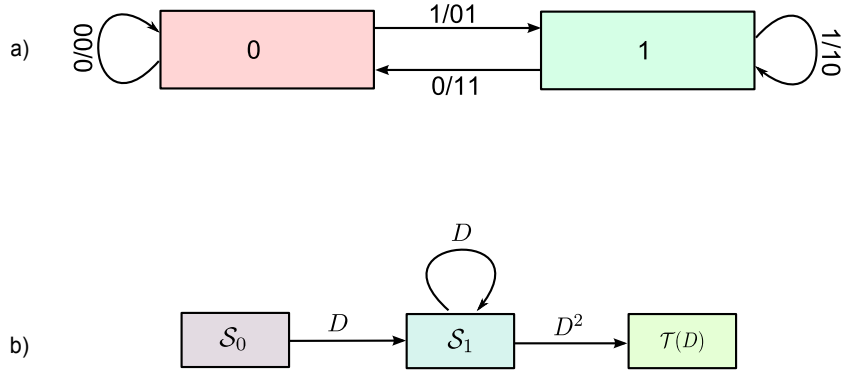


**Figure 5.8:** State diagram of  $(2, 3)$  for the inverse syndrome former  $(H^{-1})^T$ , (a) original, (b) dissected at  $\mathcal{S}_0$  for determining  $\mathcal{T}(D)$

Fig. 5.8(a). In order to find  $\mathcal{T}(D)$  from the state diagram, state 0 ( $\mathcal{S}_0$ ) is split into an initial state and a final state as shown in Fig. 5.8 (b). Now, each connecting branch in the modified state diagram is labeled by a branch “gain”,  $D^d$ , where  $d$  is the weight of the output encoded bits. The transfer function is then calculated from the transition equations of the modified state diagram, expressed as

$$\mathcal{S}_1 = D + D\mathcal{S}_1, \quad (5.53)$$

which, for  $\mathcal{S}_1$  can be solved as

$$\mathcal{S}_1 = \frac{D}{1 - D}. \quad (5.54)$$

Likewise, the transition equation for the final state can be written as

$$\mathcal{T}(D) = D^2\mathcal{S}_1. \quad (5.55)$$

Inserting  $\mathcal{S}_1$  from Eq. (5.54) into Eq. (5.55), we obtain

$$\mathcal{T}(D) = \frac{D^3}{1 - D}, \quad (5.56)$$

which can be extended using power series as

$$\mathcal{T}(D) = D^3 + D^4 + D^5 + \dots + D^{l+3} + \dots$$

In a more compact form, this can be expressed as

$$\mathcal{T}(D) = \sum_{d=3}^{\infty} A_d D^d. \quad (5.57)$$

From the union bound, the event error probability of the input bit sequence is given by the summation of the error probabilities of all the paths at distance  $d$ , i.e.,

$$P(E) < \sum_d^{\infty} A_d P_d, \quad (5.58)$$

For an AWGN channel, with single sided noise power spectral density  $N_0$ , the probability to choose a wrong path at a distance  $d$  is expressed as [12]

$$P_d = \frac{1}{2} \operatorname{erfc} \left( \sqrt{\frac{E_s}{N_0} d} \right), \quad (5.59)$$

where “erfc” is the complementary error function and  $E_s/N_0$  is the signal-to-noise ratio for an AWGN channel. Inserting the value of  $P_d$  in Eq. (5.58), the event error probability for an AWGN channel is obtained as

$$P(E) \leq \frac{1}{2} \sum_{d=d_{free}}^{\infty} A_d \operatorname{erfc} \left( \sqrt{\frac{E_s}{N_0} d} \right). \quad (5.60)$$

From the Chernoff bound, we know that  $\operatorname{erfc} \left( \sqrt{\frac{E_s}{N_0} d} \right) \approx \left( e^{-\frac{E_s}{N_0} d} \right)^d$ . Equation (5.60), thus, takes the form

$$P(E) \leq \frac{1}{2} \sum_{d=d_{free}}^{\infty} A_d \left( e^{-\frac{E_s}{N_0} d} \right)^d. \quad (5.61)$$

In order to find the bit-error probability  $P(b)$  from the event error probability  $P(E)$ , we divide  $P(E)$  by the total number of input bits to the encoder, i.e.,  $k$ . Moreover, as we know that  $E_s/N_0 = RE_b/N_0$ , where  $E_b/N_0$  is the signal-to-noise ratio per information bit and  $R$  is the code rate. Exploiting the transfer function  $\mathcal{T}(D)$ , Eq. (5.61) for the bit-error probability can be modified as

$$P(b) < \frac{1}{k} \frac{\partial \mathcal{T}(D, I)}{\partial I} \Big|_{[D=e^{-\frac{E_s}{N_0}}, I=1]} \leq \frac{1}{k} \frac{1}{2} \sum_{d=d_{free}}^{\infty} B_d \left( e^{-\frac{E_s}{N_0} d} \right)^d, \quad (5.62)$$

where  $I$  represents the number of input ones to the encoder and  $B_d$  is the total number of erroneous bits at distance  $d$ . At low error probabilities, the first term at the free distance  $d_{free}$  of the code contributes the most. Thus, Eq. (5.62) can be approximated as

$$P(b) \approx \frac{1}{k} \frac{1}{2} B_{d_{free}} \left( e^{-\frac{E_s}{N_0} d_{free}} \right)^{d_{free}}. \quad (5.63)$$

For the sign-bit shaping, the inverse syndrome former  $(\mathbf{H}^{-1})^T$  is a rate-1/2 code with  $k = 1$ . Moreover, from the transfer function  $\mathcal{T}(D)$ ,  $B_{d_{free}} = 1$ , and  $d_{free} = 3$  for the inverse syndrome former  $(\mathbf{H}^{-1})^T$ . However, the variance  $\sigma_{P_1}$  for the bits encoded by  $(\mathbf{H}^{-1})^T$  is calculated from  $P_1$ , the bit-error probability of the most significant bits of the 256-QAM symbol (as given in App. B). Using Eq. (5.1),  $\sigma_{P_1}$  can be written as

$$\sigma_{P_1}^2 = \frac{1}{2 \{ \operatorname{erfc}(2P_1) \}^2}. \quad (5.64)$$

With these values, the bit-error probability  $P_{b_{sf}}$  for the input bit sequence encoded by the inverse syndrome former is formulated as

$$P_{b_{sf}} \approx \frac{1}{2} \left( e^{-\frac{S}{N}} \right)^3, \quad (5.65)$$

**Table 5.2:** Variable-node degree distributions for irregular LDPC with/without concatenated with Trellis shaping, for a 256-QAM constellation with Gray mapping,  $N_m = 4$  modulation classes.

	$M_1$	$M_2$	$M_3$	$M_4$
with TS	$\lambda_3 = 0.08583$	$\lambda_3 = 0.0243$ $\lambda_6 = 0.29473$	$\lambda_2 = 0.05175$ $\lambda_6 = 0.10605$ $\lambda_7 = 0.09568$	$\lambda_2 = 0.08975$ $\lambda_7 = 0.03603$ $\lambda_{30} = 0.21588$
Without TS	$\lambda_6 = 0.03682$ $\lambda_7 = 0.02237$ $\lambda_{30} = 0.58173$	$\lambda_{12} = 0.17234$	$\lambda_2 = 0.04595$ $\lambda_6 = 0.03446$	$\lambda_2 = 0.04207$ $\lambda_6 = 0.04159$ $\lambda_{30} = 0.02266$

where  $S/N = E_s/N_0$  with  $N = \sigma_1^2$ . Using Eq. (5.1), the noise variance  $\sigma_1^2$  for the bits in modulation class  $M_1$ , can then be calculated as

$$\sigma_1^2 = \frac{1}{2\{\operatorname{erfc}(2P_{b_{sf}})\}^2}. \quad (5.66)$$

The variance vector  $\boldsymbol{\sigma}$  for all individual modulation classes is then given as

$$\boldsymbol{\sigma} = [\sigma_1, \sigma_2, \sigma_3, \sigma_4]. \quad (5.67)$$

$\sigma_i$  is the variance of the  $i$ th modulation class of the 256-QAM constellation.

Based on  $\boldsymbol{\sigma}$ , we optimize the variable-node degree distribution  $\boldsymbol{\lambda}$  for a given check-node degree distribution  $\boldsymbol{\rho}$ . The check-node degree distribution  $\rho(x)$  considered herein is  $\rho(x) = 0.8266 x^{34} + 0.1345 x^{35} + 0.0087 x^{70} + 0.0302 x^{71}$  [95]. Other parameters required for the optimization of the degree distribution are,  $R = 6/7$ ,  $d_{v_{max}} = 30$  and the proportion of bits in each modulation class  $\boldsymbol{\beta} = [128/896, 256/896, 256/896, 256/896]$ . Table 5.2 shows the optimized variable-node degree distribution using the procedure as explained in Section 5.3.2 and the Linear Program in Section 5.3.3 with the given parameters. Table 5.2 also shows the variable-node degree distribution for an irregular LDPC code without trellis shaping, with parameters,  $R = 3/4$ ,  $N_c = 1024$ ,  $d_{v_{max}} = 30$ , and  $\boldsymbol{\beta} = [0.25, 0.25, 0.25, 0.25]$ .

After obtaining the optimized variable node degree distribution, we next construct the  $\mathbf{H}$  matrix using the PEG algorithm. For a 256-QAM constellation, we have four modulation classes, the variable-node degree distribution is thus divided into four sub-degree distributions. In order to ensure that each bit node is protected with the proper noise level, the bit nodes are flagged from 1 - 4, depending on the modulation class they belong to, using the information from the  $\mathbf{H}$  matrix. We have considered the equivalent binary channels, i.e., transmitted the encoded data over the binary channels with noise variances  $\boldsymbol{\sigma}$ .

At the receiver, for the LDPC decoder, the log-likelihood ratios (LLRs) for the LSBs (modulation classes  $M_2, M_3, M_4$ ) are obtained directly from the channel output. However, for the MSBs, the output bit sequence was selected on the combined output of the (2,3) inverse syndrome former  $(H^{-1})^T$  and the (5,7) shaping code  $\mathcal{C}_s$  as shown in Fig. 5.9. To decode the sequence selected by a trellis shaper, we use the BCJR algorithm based on the

compound trellis diagram of the inverse syndrome former and the convolutional shaping code as shown in Fig. 5.10. The number of states of the (2,3)  $(H^{-1})^T$ ,  $N_{s_H} = 2$ , and that of the (5,7)  $\mathcal{C}_s$ ,  $N_{s_{C_s}} = 4$ . Thus, the total number of states of the compound trellis  $N_{s_{ct}} = N_{s_H} \cdot N_{s_{C_s}} = 8$ . Moreover, each state extends 4 branches to the following states. The soft output, i.e., the LLRs obtained from the BCJR algorithm along with the LLRs for the LSBs are then used as inputs to the LDPC decoder.

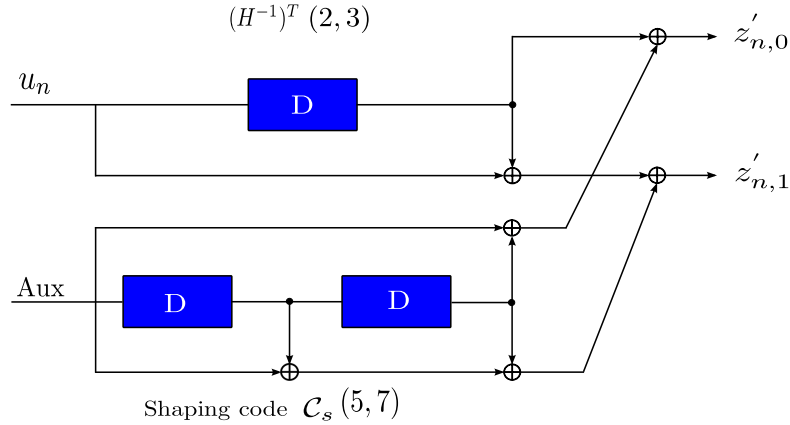


**Figure 5.9:** Trellis shaping with the (2, 3) inverse syndrome former  $(H^{-1})^T$  and the (5, 7) shaping code  $\mathcal{C}_s$

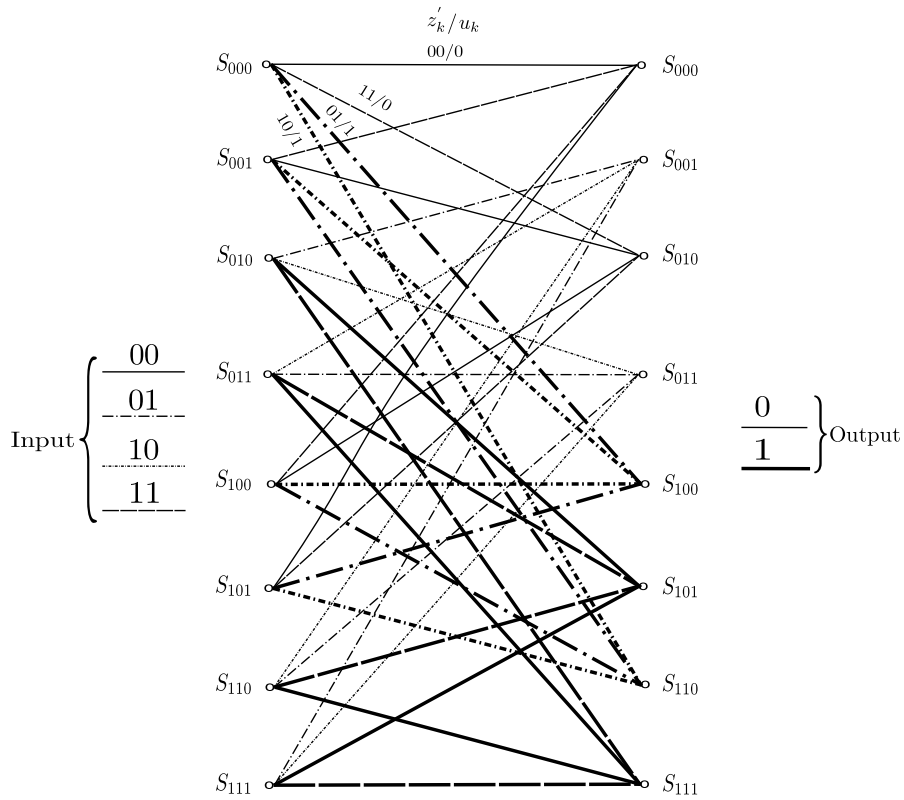


**Figure 5.10:** Compound trellis diagram for the Trellis Shaper of Fig. 5.9

### Performance at the transmitter, PAR reduction

Figure. 5.11 shows the CCDF of the PAR for an OFDM system with and without Trellis Shaping. A gain of approximately 4.1 dB at  $10^{-5}$  can be obtained using Trellis Shaping.

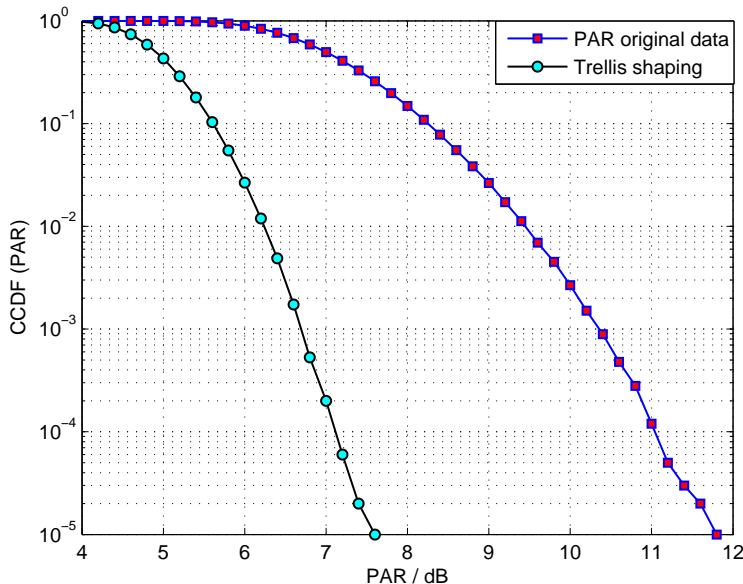


**Figure 5.11:** CCDF(PAR) of Trellis Shaping for OFDM system,  $N = 128$

### FER of irregular vs. regular LDPC codes

As we stated earlier, irregular LDPC codes usually have better performances than regular ones for long codes. Herein, we provide a comparison of the irregular and the regular LDPC code, with and without Trellis Shaping. In order to compare our result, we consider a (3,21) regular LDPC code with the same code rate as irregular LDPC codes. The  $\mathbf{H}$  matrix for the regular LDPC code is constructed using a random method.

Figure 5.12 shows the performance curves for irregular and regular LDPC codes. In case of Trellis Shaping, the system performance can be improved by 0.6 dB when using irregular LDPC codes as compared to regular LDPC codes. The figure also shows the FER curves for a system using LDPC codes concatenated with OFDM without Trellis Shaping. Even for the systems without Trellis Shaping the irregular LDPC codes outperforms the regular codes. However, the frame-error ratio gap between the LDPC code concatenated with Trellis Shaping and without Trellis Shaping is primarily due to the different code rates used, i.e., 6/7 in case of Trellis Shaping and 3/4 without Trellis Shaping.

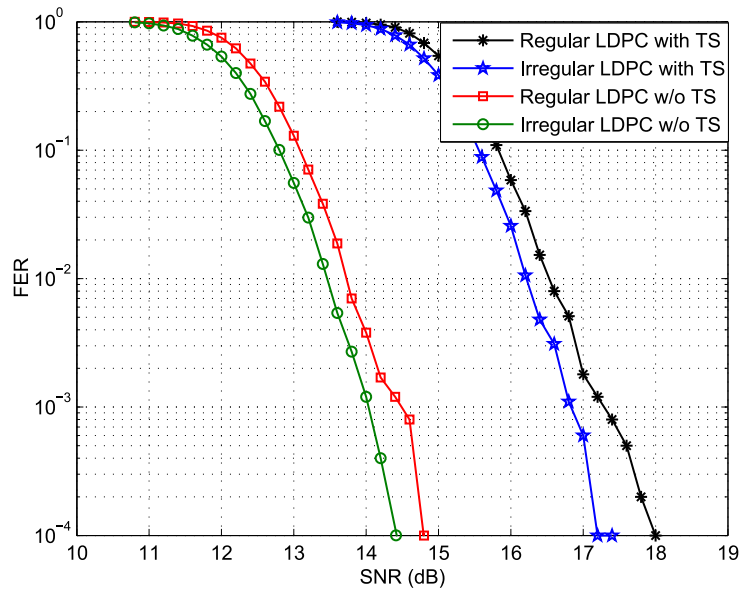


**Figure 5.12:** FER curves for irregular vs. regular LDPC codes with and without Trellis Shaping

# Chapter 6

## Summary

Herein, we proposed PAR reduction algorithms to limit the peak excursions in point-to-point and multi-user MIMO-OFDM systems. We also investigated Trellis Shaping and improved the system performance in terms of BER by concatenating an optimized irregular LDPC code with Trellis Shaping for PAR of single antenna systems.

In the first part, we presented the OFDM system and different MIMO scenarios. We addressed the PAR problem statement along with consequences of high PAR caused by an OFDM system. A mathematical as well as a statistical analysis of the PAR was provided for an in-depth understanding of the PAR problem statement. From the brief overviews of the different approaches made so far, to limit the peak excursions, Tone Reservation (TR) is the least complex approach with higher gains. Besides TR, Trellis Shaping is also a promising technique with very promising results.

Since Tone Reservation is the least complex algorithm for single antenna systems, with this motivation, we first extended TR algorithm for PAR reduction of multi-antenna MIMO-OFDM system. For a P2P MIMO-OFDM system, the weakest eigenchannel(s) were reserved to generate a spiky function for PAR reduction. Based on the last column of the preprocessing matrix, two approaches were proposed to obtain an optimum spiky function. We showed that using the complex conjugate of the respective component of the last column of the preprocessing matrix results in an almost optimum spiky function. For a multi-user broadcast scenario, TR is the best choice for PAR reduction. For the broadcast scenario, the spiky function is generated on a small number of tones reserved on all spatial dimensions. Therefore, no implication needs to be considered at the transmitter as well as the receiver ends which makes TR the most suitable candidate. We justified the effectiveness of the proposed algorithm by extensive simulation results both with and without mean power constraint.

We also proposed an alternative Least-Squares iterative algorithm for the PAR reduction of multi-antenna systems. We showed that the weakest eigenchannels can also be used to approximate and model the peak excursions in a Least-Squares sense. However, besides the peak excursions, the algorithm approximates zeros in the remaining dimensions as well, a drawback of using an  $l_2$  norm instead of an  $l_\infty$  norm, which reduces the result by a factor equal to  $M$ . We then showed that by weighting the modeled function, the algorithm converges faster to the target values and leads to optimum performance. Simulation results shows that higher gains in the range of 6-7 dB can be obtained with the proposed algorithm. However, the gain obtained, of course, depends on the complexity (number of iterations), target value, and the weighting factor, with cost paid in the form

of capacity loss and mean power increase. In order to investigate the capacity loss associated with the weakest eigenchannel, we made use of the random matrix theory. We showed that the capacity loss associated with the weakest eigenchannels is very small, which for low-dimensional MIMO is approximately the same as the capacity associated with 10 % reserved tones in case of TR algorithm and goes to zero for high dimensional Massive MIMO systems. We also computed the increase in the mean power of the transmit signal due to the proposed algorithm. It has been found that the increase is very low, only a few tenths of a dB. We next extended our Least-Squares algorithm to multi-user broadcast scenarios. We considered medium to massive multi-user MIMO, with one inactive user. We showed that the channel associated with the inactive user can be used in the similar fashion to approximate the peak excursion for the BC channel. We compared our LS algorithm to TR and SLM algorithms and found that our algorithm outperform these algorithm in terms of their PAR reduction capability. Moreover, the capacity loss and increase in the mean transmit power is very low in comparison to the TR algorithm. Form the simulation results we can conclude that our LS algorithm is the best choice as an alternative to the existing TR and SLM algorithms for MIMO-OFDM.

Trellis shaping is a promising technique for PAR reduction, however, with some open problem in the optimum link to error correcting codes. In the last part, we thus concatenated an optimized irregular LDPC code with Trellis Shaping for PAR reduction in single antenna OFDM. For the irregular LDPC code, we optimized the variable-node degree distribution based on the irregularities of the individual bits inside a higher order  $\mathcal{M}$ -ary QAM constellation. For the input bit sequence encoded by the inverse syndrome former, which are used to define the MSBs along with the valid code sequence from the shaping code, the bit error probability were calculated exploiting the transfer function of the inverse syndrome former. We also presented soft decision decoding of the input bit sequence encoded by the inverse syndrom former. The soft decision decoding is carried out using a BCJR algorithm based on the compound trellis of the shaping code and the inverse syndrome former. We showed through simulation results that the system performance can be improved by concatenating an irregular LDPC code with Trellis Shaping as compared to using a regular LDPC code as in earlier works.

# Appendix A

## Convergence of the Least-Squares algorithm

The probability density function of a two-dimensional Gaussian, in Cartesian coordinates, is given as

$$P(x, y) = \frac{1}{2\pi} \int \int e^{-\frac{(x^2+y^2)}{2}} dx dy . \quad (\text{A.1})$$

Converting Cartesian coordinates into polar coordinates, substituting  $r^2 = x^2 + y^2$  and  $dx dy = r dr d\theta$ , (A.1) is rephrased as

$$P(r, \theta) = \frac{1}{2\pi} \int \int e^{-\frac{r^2}{2}} r dr d\theta . \quad (\text{A.2})$$

However, we need to integrate from some radius onward to infinity. Let  $\tau$  be the threshold value, then, the probability  $P_o$ , that any value falls outside this radius (probability that the peak value of a time domain sample is exceeding the given threshold value in Fig. 4.28), is

$$\begin{aligned} P_o &= \frac{1}{2\pi} \int_0^{2\pi} \int_{\tau}^{\infty} e^{-\frac{r^2}{2}} r dr d\theta \\ &= \frac{1}{2\pi} \int_0^{2\pi} d\theta \int_{\tau}^{\infty} e^{-\frac{r^2}{2}} r dr \\ &= -e^{-\frac{r^2}{2}} \Big|_{\tau}^{\infty} \\ P_o &= e^{-\frac{\tau^2}{2}} . \end{aligned} \quad (\text{A.3})$$

The average tail power  $P_{\text{tail}}$  of the two-dimensional Gaussian distribution is then derived as

$$\begin{aligned}
 P_{\text{tail}} &= \frac{1}{2\pi} \int_0^{2\pi} \int_{\tau}^{\infty} e^{-\frac{r^2}{2}} r (r - \tau)^2 dr d\theta \\
 &= \frac{1}{2\pi} \int_0^{2\pi} d\theta \int_{\tau}^{\infty} e^{-\frac{r^2}{2}} r (r - \tau)^2 dr \\
 &= \frac{1}{2\pi} 2\pi \int_{\tau}^{\infty} e^{-\frac{r^2}{2}} r (r - \tau)^2 dr \\
 &= \int_{\tau}^{\infty} e^{-\frac{r^2}{2}} r (r - \tau)^2 dr \\
 &= \int_{\tau}^{\infty} e^{-\frac{r^2}{2}} r (r^2 + \tau^2 - 2\tau r) dr \\
 P_{\text{tail}} &= \int_{\tau}^{\infty} e^{-\frac{r^2}{2}} (r^3 + r\tau^2 - 2\tau r^2) dr \tag{A.4}
 \end{aligned}$$

Equation (A.4) can be rephrased as

$$P_{\text{tail}} = \underbrace{\int_{\tau}^{\infty} r^3 e^{-\frac{r^2}{2}} dr}_{\text{I}} - 2\tau \underbrace{\int_{\tau}^{\infty} r^2 e^{-\frac{r^2}{2}} dr}_{\text{II}} + \tau^2 \underbrace{\int_{\tau}^{\infty} r e^{-\frac{r^2}{2}} dr}_{\text{III}} . \tag{A.5}$$

For convenience, we will solve each integral separately and then insert the individual results into Eq. (A.5) to obtain the final result. However, before going to the solution, we recall that

$$\frac{d}{dr} e^{-\frac{r^2}{2}} = -r e^{-\frac{r^2}{2}} ,$$

or conversely,

$$\int r e^{-\frac{r^2}{2}} dr = -e^{-\frac{r^2}{2}} .$$

We will use this to solve the above integrals.

### Integral I

$$\int_{\tau}^{\infty} r^3 e^{-\frac{r^2}{2}} dr$$

By partial integration, the solution follows as

$$\begin{aligned}
 \int_{\tau}^{\infty} r^3 e^{-\frac{r^2}{2}} dr &= \int_{\tau}^{\infty} r^2 r e^{-\frac{r^2}{2}} dr \\
 &= r^2 \int_{\tau}^{\infty} r e^{-\frac{r^2}{2}} dr - \int_{\tau}^{\infty} \left[ \frac{d}{dr} r^2 \int r e^{-\frac{r^2}{2}} dr \right] dr \\
 &= -r^2 e^{-\frac{r^2}{2}} \Big|_{\tau}^{\infty} + 2 \int_{\tau}^{\infty} r e^{-\frac{r^2}{2}} dr \\
 &= -r^2 e^{-\frac{r^2}{2}} \Big|_{\tau}^{\infty} - 2e^{-\frac{r^2}{2}} \Big|_{\tau}^{\infty} \\
 \int_{\tau}^{\infty} r^3 e^{-\frac{r^2}{2}} dr &= \tau^2 e^{-\frac{\tau^2}{2}} + 2e^{-\frac{\tau^2}{2}} .
 \end{aligned} \tag{A.6}$$

**Integral II**

$$\begin{aligned}
 &2\tau \int_{\tau}^{\infty} r^2 e^{-\frac{r^2}{2}} dr \\
 \int_{\tau}^{\infty} r^2 e^{-\frac{r^2}{2}} dr &= \int_{\tau}^{\infty} r r e^{-\frac{r^2}{2}} dr \\
 &= r \int_{\tau}^{\infty} r e^{-\frac{r^2}{2}} dr - \int_{\tau}^{\infty} \left[ \frac{d}{dr} r \int r e^{-\frac{r^2}{2}} dr \right] dr \\
 &= -r e^{-\frac{r^2}{2}} \Big|_{\tau}^{\infty} + \int_{\tau}^{\infty} e^{-\frac{r^2}{2}} dr \\
 &= \tau e^{-\frac{\tau^2}{2}} + \sqrt{2\pi} Q(\tau) \\
 2\tau \int_{\tau}^{\infty} r^2 e^{-\frac{r^2}{2}} dr &= 2\tau^2 e^{-\frac{\tau^2}{2}} + \tau \sqrt{8\pi} Q(\tau) .
 \end{aligned} \tag{A.7}$$

**Integral III**

$$\begin{aligned}
 &\tau^2 \int_{\tau}^{\infty} r e^{-\frac{r^2}{2}} dr \\
 \int_{\tau}^{\infty} r e^{-\frac{r^2}{2}} dr &= -e^{-\frac{r^2}{2}} \Big|_{\tau}^{\infty} \\
 &= e^{-\frac{\tau^2}{2}} \\
 \tau^2 \int_{\tau}^{\infty} r e^{-\frac{r^2}{2}} dr &= \tau^2 e^{-\frac{\tau^2}{2}} .
 \end{aligned} \tag{A.8}$$

Now inserting the results of the integrals I, II, and III into (A.5), we obtain

$$\begin{aligned}
 P_{\text{tail}} &= \tau^2 e^{-\frac{\tau^2}{2}} + 2e^{-\frac{\tau^2}{2}} + \tau^2 e^{-\frac{\tau^2}{2}} \\
 &\quad - 2\tau^2 e^{-\frac{\tau^2}{2}} - \tau \sqrt{8\pi} Q(\tau) \\
 &= 2e^{-\frac{\tau^2}{2}} - \tau \sqrt{8\pi} Q(\tau) .
 \end{aligned} \tag{A.9}$$

In case of using *erfc*, we might rephrase Eq. (A.9) as

$$P_{\text{tail}} = 2e^{-\frac{\tau^2}{2}} - \tau \sqrt{2\pi} \operatorname{erfc} \left( \frac{\tau}{\sqrt{2}} \right) . \tag{A.10}$$

## Appendix B

# Bit error probabilities of a 256-QAM symbol

As given in [93], the bit error probabilities of the individual bits inside 256-QAM constellation, with Gray mapping, are given as

$$P_{b_{1,2}} = 1/16 \left( \begin{array}{l} \operatorname{erfc} \left( \sqrt{\frac{5\gamma}{48}} \right) + \operatorname{erfc} \left( 3\sqrt{\frac{5\gamma}{48}} \right) + \operatorname{erfc} \left( 5\sqrt{\frac{5\gamma}{48}} \right) \\ + \operatorname{erfc} \left( 7\sqrt{\frac{5\gamma}{48}} \right) + \operatorname{erfc} \left( 9\sqrt{\frac{5\gamma}{48}} \right) + \operatorname{erfc} \left( 11\sqrt{\frac{5\gamma}{48}} \right) \\ + \operatorname{erfc} \left( 13\sqrt{\frac{5\gamma}{48}} \right) + \operatorname{erfc} \left( 15\sqrt{\frac{5\gamma}{48}} \right) \end{array} \right) \quad (\text{B.1})$$

$$P_{b_{3,4}} = 1/16 \left( \begin{array}{l} 2 \operatorname{erfc} \left( \sqrt{\frac{5\gamma}{48}} \right) + 2 \operatorname{erfc} \left( 3\sqrt{\frac{5\gamma}{48}} \right) + 2 \operatorname{erfc} \left( 5\sqrt{\frac{5\gamma}{48}} \right) \\ + 2 \operatorname{erfc} \left( 7\sqrt{\frac{5\gamma}{48}} \right) + \operatorname{erfc} \left( 9\sqrt{\frac{5\gamma}{48}} \right) + \operatorname{erfc} \left( 11\sqrt{\frac{5\gamma}{48}} \right) \\ + \operatorname{erfc} \left( 13\sqrt{\frac{5\gamma}{48}} \right) + \operatorname{erfc} \left( 15\sqrt{\frac{5\gamma}{48}} \right) - \operatorname{erfc} \left( 17\sqrt{\frac{5\gamma}{48}} \right) \\ - \operatorname{erfc} \left( 19\sqrt{\frac{5\gamma}{48}} \right) - \operatorname{erfc} \left( 21\sqrt{\frac{5\gamma}{48}} \right) - \operatorname{erfc} \left( 23\sqrt{\frac{5\gamma}{48}} \right) \end{array} \right) \quad (\text{B.2})$$

$$P_{b_{5,6}} = 1/16 \left( \begin{array}{l} 4 \operatorname{erfc} \left( \sqrt{\frac{5\gamma}{48}} \right) + 4 \operatorname{erfc} \left( 3\sqrt{\frac{5\gamma}{48}} \right) + 3 \operatorname{erfc} \left( 5\sqrt{\frac{5\gamma}{48}} \right) \\ + 3 \operatorname{erfc} \left( 7\sqrt{\frac{5\gamma}{48}} \right) - 3 \operatorname{erfc} \left( 9\sqrt{\frac{5\gamma}{48}} \right) - 3 \operatorname{erfc} \left( 11\sqrt{\frac{5\gamma}{48}} \right) \\ - 2 \operatorname{erfc} \left( 13\sqrt{\frac{5\gamma}{48}} \right) - 2 \operatorname{erfc} \left( 15\sqrt{\frac{5\gamma}{48}} \right) + 2 \operatorname{erfc} \left( 17\sqrt{\frac{5\gamma}{48}} \right) \\ + 2 \operatorname{erfc} \left( 19\sqrt{\frac{5\gamma}{48}} \right) + \operatorname{erfc} \left( 21\sqrt{\frac{5\gamma}{48}} \right) + \operatorname{erfc} \left( 23\sqrt{\frac{5\gamma}{48}} \right) \\ - \operatorname{erfc} \left( 25\sqrt{\frac{5\gamma}{48}} \right) - \operatorname{erfc} \left( 27\sqrt{\frac{5\gamma}{48}} \right) \end{array} \right) \quad (\text{B.3})$$

$$P_{b_{7,8}} = 1/16 \left( \begin{array}{l} 8 \operatorname{erfc} \left( \sqrt{\frac{5\gamma}{48}} \right) + 7 \operatorname{erfc} \left( 3\sqrt{\frac{5\gamma}{48}} \right) - 7 \operatorname{erfc} \left( 5\sqrt{\frac{5\gamma}{48}} \right) \\ -6 \operatorname{erfc} \left( 7\sqrt{\frac{5\gamma}{48}} \right) + 6 \operatorname{erfc} \left( 9\sqrt{\frac{5\gamma}{48}} \right) + 5 \operatorname{erfc} \left( 11\sqrt{\frac{5\gamma}{48}} \right) \\ -5 \operatorname{erfc} \left( 13\sqrt{\frac{5\gamma}{48}} \right) - 4 \operatorname{erfc} \left( 15\sqrt{\frac{5\gamma}{48}} \right) + 4 \operatorname{erfc} \left( 17\sqrt{\frac{5\gamma}{48}} \right) \\ +3 \operatorname{erfc} \left( 19\sqrt{\frac{5\gamma}{48}} \right) - 3 \operatorname{erfc} \left( 21\sqrt{\frac{5\gamma}{48}} \right) - 2 \operatorname{erfc} \left( 23\sqrt{\frac{5\gamma}{48}} \right) \\ +2 \operatorname{erfc} \left( 25\sqrt{\frac{5\gamma}{48}} \right) + \operatorname{erfc} \left( 27\sqrt{\frac{5\gamma}{48}} \right) - \operatorname{erfc} \left( 29\sqrt{\frac{5\gamma}{48}} \right) \end{array} \right) \quad (\text{B.4})$$

# Appendix C

## Own Publications

1. A. Wakeel, D. Kronmueller, W. Henkel, and H. B. Neto “Leaking Interleavers for UEP Turbo Codes,” *International Symposium on Turbo Codes*, Brest, France, August 2010.
2. W. Henkel, A. Wakeel, and M. Taseska, “Peak-to-average ratio reduction with tone reservation in multi-user and MIMO-OFDM,” *1st IEEE International Conference on Communications China (ICCC)*, Beijing, China, August 2012.
3. A. Wakeel and W. Henkel, “Effect of the threshold offset on the performance of UEP-LDPC codes,” *2nd IEEE International Conference on Communication in China (ICCC)*, Xian, China, August 2013.
4. A. Wakeel and W. Henkel, “Least-squares iterative PAR reduction for MIMO-OFDM systems,” *IEEE Global Communications Conference (Globecom 2014)*, Texas, USA, December 2014.
5. A. Wakeel and W. Henkel, “Least-squares iterative PAR reduction for point-to-point large-scale MIMO-OFDM systems,” *IEEE International Conference on Communications*, Sydney, Australia, June 2014.
6. A. Wakeel and W. Henkel, “Multi-Edge-Type LDPC code concatenated with Trellis Shaping for PAR reduction,” *IEEE International Symposium on Information Theory (ISIT 2016)*, Barcelona, Spain (Submitted).
7. A. Wakeel and W. Henkel, “Extension of Tone Reservation algorithm for PAR Reduction in MIMO-OFDM systems,” *IEEE Transactions on Communications* (Submitted).
8. A. Wakeel and W. Henkel, “Least-Squares iterative PAR reduction for MIMO-OFDM systems,” *IEEE Transactions on Communications* (In process to be Submitted).

# Bibliography

- [1] C. E. Shannon, "A mathematical theory of communication," *Bell Systems Technical Journal*, pp. 623-656, October 1948.
- [2] L. Hanzo, M. Münster, B. J. Choi, and T. Keller, *OFDM and MC-OFDMA for Broadband Multi-User Communicataions, WLANs and Broadcasting*, John Wiley and sons Ltd., 2003.
- [3] A. Goldsmith, *Wireless Communications*, Cambridge University Press, 2005.
- [4] A. F. Molisch, *Wireless Communications*, John Wiley and sons Ltd., 2005.
- [5] D. Tse and P. Visawanath, *Fundamentals of Wireless Communication*, Cambridge University Press, 2005.
- [6] T. M. Cover and J. A. Thomas, *Elements of Information Theory*, Second edition, John Wiley and sons Ltd., 2006.
- [7] R. van Nee and R. Prasad, *OFDM for Wireless Multimedia Communications*, Artech House, Boston, 2000.
- [8] A. Paulraj, R. Nabar, and D. Gore, *Introduction to Space-Time Wireless Communications*, Cambridge University Press, 2003.
- [9] S. Lin and D. J. Costello, *Error Control Coding*, Pearson Education International, 2004.
- [10] W. E. Ryan and S. Lin, *Channel Codes, Classical and Modern*, Cambridge University Press, 2009.
- [11] A. V. Oppenheim, R. W. Schaffer, and J. R. Buck, *Discrete-Time Signal Processing*, Printice Hall International, 1999.
- [12] W. Henkel, *Wireline Communication*, An online book project of the wireline communication course at Jacobs University Bremen, Germany, [http://www.trsys.faculty.jacobs-university.de/wp-content/uploads/2014/01/DSL\\_book\\_project.pdf](http://www.trsys.faculty.jacobs-university.de/wp-content/uploads/2014/01/DSL_book_project.pdf).
- [13] W. Henkel, *Channel Coding*, Jacobs University Bremen, Germany, 2009.
- [14] T. J. Lim, *Notes for ECE1250 data communications*, Edwards S. Rogers Sr. Dept. of Elect. and Comp. Engineering, University of Toronto, Canada.
- [15] J. M. Cioffi, *EE 379C advanced digital communication course notes*, Stanford University, Stanford, CA, <http://www.stanford.edu/class/ee397/reader.html>.

- [16] R. W. Chang, "Synthesis of band-limited orthogonal signals for multichannel data transmission," *Bell Systems Technical Journal*, Vol. 45, pp. 1775-1796, December 1966.
- [17] B. R. Saltzberg, "Performance of an efficient parallel data transmission system," *IEEE Transactions on Communications*, Vol. 15, No. 6, pp. 805-811, December 1967.
- [18] R. R. Mosier and R. G. Clabaugh, "Kineplex, A bandwidth-efficient binary transmission system," *AIEE Transactions*, Vol. 76, pp. 723-728, January 1958.
- [19] M. S. Zimmerman and A. L. Kirsch, "The AN/GSC-10 (KATHRYN) variable rate data modem for HF radio," *IEEE Transactions on Communication Technology*, Vol. 15, No. 2, pp. 197-204, April 1967.
- [20] G. C. Porter, "Error distribution and diversity performance of a frequency-differential PSK HF modem," *IEEE Transactions on Communication Technology*, Vol. 16, No. 4, pp. 567-575, August 1968.
- [21] S. B. Weinstein and P. M. Ebert, "Data transmission by frequency-division multiplexing using the discrete fourier transform," *IEEE Transactions on Communication Technology*, Vol. 19, No. 5, pp. 628-634, October 1971.
- [22] A. Peled and A. Ruiz, "Frequency domain data transmission using reduced computational complexity algorithms," *IEEE International Conference on Acoustic, Speech and Signal Processing*, Colorado, USA, April 1980.
- [23] B. Hirosaki, "An analysis of automatic equalizer for orthogonally multiplexed QAM Systems," *IEEE Transactions on Communications*, Vol. 28, No. 1, pp. 73-83, January 1980.
- [24] B. Hirosaki, "An orthogonally multiplexed QAM system using the discrete fourier transform," *IEEE Transactions on Communications*, Vol. 29, No. 7, pp. 982-989, July 1981.
- [25] M. Alard and R. Lassalle, "Principles of modulation and channel coding for digital broadcasting for mobile receivers," *EBU Review Technical*, pp. 168-190, August 1987.
- [26] S. B. Weinstein, "The history of orthogonal frequency-division," *IEEE Communication Magazine*, Vol. 47, pp. 26-35, November 2009.
- [27] W. Y. Zou and Y. Wu, "COFDM- An overview," *IEEE Transactions on Broadcasting*, Vol. 41, No. 1, pp. 1-8, March 1995.
- [28] M. D. Nisar, W. Utschick, H. Nottensteiner, T. Hindelang, "Channel estimation and equalization of OFDM systems with insufficient cyclic prefix," *IEEE Vehicular Technology Conference*, Dublin, Ireland, April 2007.
- [29] G. Ginis and J. M. Cioffi, "Vectored transmission for digital subscriber line systems," *IEEE Journal on Selected Areas in Communication*, Vol. 20, pp. 1085-1104, June 2002.
- [30] P. S. Chow, J. M. Cioffi, and J. A. C. Bingham "A practical discrete multitone transceiver loading algorithm for data transmission over spectrally shaped channels," *IEEE Transactions on Communications*, Vol. 43, No. 2/3/4, pp. 773-775, April 1995.

- [31] J. Tellado, *Peak-to-average power reduction for multicarrier modulation*, Ph.D. thesis, Stanford University, USA, September 1999.
- [32] S. Hussain, *Peak-to-average power ratio analysis and reduction of cognitive radio signals*, Ph.D. thesis, University of Rennes, France, October 2009.
- [33] C. Siegel, *Peak-to-average power reduction for multi-antenna OFDM via multiple signal representation*, Ph.D. thesis, Friedrich Alexander Universität Erlangen, Nürnberg, Germany, 2010.
- [34] G. Hill, *Peak power reduction in orthogonal frequency division multiplexing transmitters*, Ph.D. thesis, Victoria University of Technology, Australia, March 2011.
- [35] M. Taseska, *Peak-to-average power ratio reduction in MIMO broadcast OFDM systems using tone reservations*, B.Sc. thesis, Jacobs University Bremen, Germany. June 2010.
- [36] K. S. Hassan, *Unequal error protection adaptive modulation in multicarrier systems*, Ph.D. thesis, Jacobs University Bremen, Germany, November 2011.
- [37] N. von Deetzen, *Modern Coding Schemes for Unequal Error Protection*, Ph.D. Thesis Jacobs University Bremen, Germany, January 2009.
- [38] H. Määttänen, *MIMO OFDM*, S-72.333 Postgraduate course in radio communications.
- [39] A. D. S. Jayalath and C. Tellambura, "Reducing the out of band radiation of OFDM using an extended guard interval," *IEEE Vehicular Technology Conference*, New Jersey, USA, 2001.
- [40] T. Lee and H. Ochiai, "Characterization of power spectral density for nonlinear amplified OFDM signals based on cross-correlation coefficient," *EURASIP Journal of Wireless Communications and Networking*, 2014.
- [41] A. A. M. Saleh, "Frequency-independent and frequency-dependent nonlinear models of TWT amplifiers," *IEEE Transactions on Communications*, Vol. 29, No. 11, pp. 1715-1720, November 1991.
- [42] C. Rapp, "Effect of HPA-nonlinearity on a 4-DPSK/OFDM-signal for a digital sound broadcasting system," *In Proc. 2nd European Conference on Satellite Communications*, Liege, Belgium, October 1991.
- [43] G. Santella and F. Mazzenga, "A hybrid analytical-simulation procedure for performance evaluation in M-QAM-OFDM schemes in presence of nonlinear distortions," *IEEE Transactions on Vehicular technology*, Vol. 47, No. 1, pp. 142-151, February 1998.
- [44] S. H. Han and J. H. Lee, "An overview of peak-to-average power ratio reduction techniques for multicarrier transmission," *IEEE Transactions on Wireless communications*, Vol. 12, No. 2 pp. 56-64, April 2005.
- [45] T. Jiang and Y. Wu, "An overview: peak-to-average power ratio reduction techniques for OFDM signals," *IEEE Transactions of Broadcasting*, Vol. 45, No. 2, pp. 257-268, June 2008.

- [46] C. Schurgers and M. B. Srivastava, "A systematic approach to peak-to-average power ratio in OFDM," Electrical Engineering Department, University of California at Los Angeles (UCLA), USA.
- [47] R. Gross and D. Veeneman, "SNR and spectral properties for a clipped DMT ADSL signal," *IEEE International Conference on Communications*, Los Angeles, USA, May 1994.
- [48] R. O'Neill and L. B. Lopes, "Envelope variation and spectral splatter in clipped multicarrier signals," *IEEE International Symposium on Personal, Indoor and Mobile Radio communications*, Toronto, Canada, September 1995.
- [49] D. J. G. Mestdagh and P. M. P. Spruyt, "A method to reduce the probability of clipping in DMT-Based transceivers," *IEEE Transactions on Communications*, Vol. 44, No. 10, pp. 1234-1238, October 1996.
- [50] X. Li and L. J. Cimini, "Effects of clipping and filtering on the performance of OFDM," *IEEE Communications Letters*, Vol. 2, No. 5, pp. 131-133, May 1998.
- [51] J. Armstrong, "New OFDM peak-to-average power ratio reduction scheme," *IEEE Vehicular Technology Conference*, Rhodes, Greece, May 2001.
- [52] J. Armstrong, "Peak-to-average power ratio reduction for OFDM by repeated clipping and frequency domain filtering," *Electronics Letters*, Vol. 38, No. 5 February 2002.
- [53] L. Wang and C. Tellambura, "Clipping-noise guided sign-selection for PAR reduction in OFDM systems," *IEEE Transactions on Signal Processing*, Vol. 56, No. 11, pp. 5644-5653, November 2008.
- [54] Y. C. Wang and Z. Q. Lou, "Optimized iterative clipping and filtering for PAPR reduction of OFDM signals," *IEEE Transactions on Communications*, Vol. 59, No. 1, pp. 33-36, January 2011.
- [55] R. Nee and A. Wild, "Reducing the peak-to-average power ratio of OFDM," *IEEE Vehicular Technology Conference*, Ottawa, Canada, May 1998.
- [56] W. Henkel, "Analog codes for peak-to-average ratio reduction," *4th International OFDM Workshop*, Hamburg, Germany, September 1999.
- [57] R. W. Bäuml, R. F. H. Fischer, and J. B. Huber, "Reducing the peak-to-average power ratio of multicarrier modulation by Selected Mapping," *Electronics Letters*, Vol. 32, No. 22, October 1996.
- [58] S.H. Müller and J.B. Huber, "OFDM with reduced peak-to-average power ratio by optimum combination of Partial Transmit Sequences," *Electronics Letters*, vol. 33, No. 5, February 1997.
- [59] S.H. Müller and J.B. Huber, "A comparison of peak power reduction schemes for OFDM," *IEEE Global Telecommunications Conference*, Arizona, USA, November 1997.

- [60] J. Tellado and J.M. Cioffi, "Peak power reduction for multicarrier transmission," Information Systems Laboratory, Stanford University.
- [61] W. Henkel and V. Zrno, "PAR reduction revisited: an extension to Tellado's method," *6th International OFDM Workshop*, Hamburg, Germany, September 2001.
- [62] W. Henkel, S. Trautmann, V. Zrno, and P. Aggarwal, "Tone Reservation and trellis partial transmit sequences," *9th International OFDM-Workshop*, Dresden, Germany, September 2004.
- [63] G. D. Forney, "Trellis Shaping," *IEEE Transactions on Information Theory*, Vol. 38, pp. 281-300, March 1992.
- [64] W. Henkel and B. Wagner, "Another application for Trellis Shaping: PAR reduction for DMT (OFDM)," *IEEE Transactions on Communications*, Vol. 48, No. 9, pp. 1471-1476, September 2000.
- [65] W. Henkel and V. Azis, "Partial transmit sequences and Trellis Shaping," *5th International ITG Conference on Source and Channel Coding*, Erlangen, Germany, January 2004.
- [66] V. Azis, *Impact of clipping in multi-carrier systems and countermeasures*, MSc Thesis, Hochschule Bremen and FH Darmstadt, 2003.
- [67] T. T. Nguyen and L. Lampe, "On Trellis Shaping for PAR reduction in OFDM systems," *IEEE Transactions on Communications*, Vol. 55, No. 9, pp. 1678-1682, September 2007
- [68] S. Fei, Y. Yong, Z. Shijie, and S. Dechun, "A novel PAPR reduction with Trellis Shaping in NC-OFDM in cognitive radio," *Journal of Electronics (China)*, Vol. 26, No. 3, pp. 296-302, May 2009
- [69] H. Ochiai, "A new Trellis Shaping design for OFDM," *5th International Symposium on Wireless Personal Multimedia Communications*, Honolulu, Hawaii, October 2002.
- [70] H. Ochiai, "A novel Trellis-Shaping design with both peak and average power reduction for OFDM systems," *IEEE Transactions on Communications*, Vol. 52, No. 11 pp. 1916-1926, November 2004.
- [71] R. Yoshizawa and H. Ochiai, "Performance comparison of trellis-shaped OFDM systems over nonlinear channels," *14th International Symposium on Wireless Personal Multimedia Communications*, Brest, France, October 2011.
- [72] H. Ochiai and H. Imai, "Performance of deliberate clipping with adaptive symbol selection for strictly band-limited OFDM systems," *IEEE Journal on Selected Areas in Communications*, Vol. 18, No. 11, pp. 2270-2276, November 2000.
- [73] H. Ochiai and H. Imai, "On the distribution of the peak-to-average power ratio in OFDM signals," *IEEE Transactions on Communications*, Vol. 49, No. 2, pp. 282-288, February 2001.

- [74] Y. L. Lee, Y. H. You, W. G. Jeon, J. H. Paik, and H. K. Song, "Peak-to-average power ratio in MIMO-OFDM systems using Selective Mapping," *IEEE Communications Letters*, Vol. 7, No. 12, pp. 575-577, December 2003.
- [75] M. S. Baek, M. J. Kim, Y. H. You, and H. K. Song, "Semi-blind channel estimation and PAR reduction for MIMO-OFDM system with multiple antennas," *IEEE Transactions on Broadcasting*, Vol. 50, No. 11, pp. 414-424, December 2004.
- [76] C. Siegl and Robert F. H. Fischer, "Peak-to-average power ratio reduction in multi-user OFDM," *International Symposium on Information Theory 2007*, Nice, France, June 2007.
- [77] Robert F. H. Fischer and M. Hoch, "Directed Selected Mapping for peak-to-average power ratio reduction in MIMO OFDM," *Electronics Letters*, Vol. 42, No. 22, October 2006.
- [78] Robert F. H. Fischer and M. Hoch, "Peak-to-average power ratio reduction in MIMO OFDM," *International Conference on Communication*, Glasgow, Scotland, June 2007.
- [79] C. Siegl and Robert F. H. Fischer, "Directed Selected Mapping for peak-to average ratio reduction in single-antenna OFDM," *International OFDM Workshop*, Hamburg, Germany, August 2007.
- [80] C. Siegl and Robert F. H. Fischer, "Selected Sorting for PAR reduction in OFDM multi-user broadcast scenarios," *International ITG Workshop 2009*, Berlin, Germany, February 2009.
- [81] C. Siegl and R. F. H. Fischer, "Asymptotic performance analysis and successive Selected Mapping for PAR reduction in OFDM," *IEEE Transactions on Signal Processing*, Vol. 58, No. 6, pp. 3228-3237, June 2010.
- [82] S. Umeda, S. Suyama, H. Suzuki, and K. Fukawa, "Low complexity PAPR reduction method for multi-user MIMO-OFDM systems with block diagonalization," *15th International OFDM Workshop*, Hamburg, Germany, September 2010.
- [83] J. Gao, J. Wang, and Z. Xie, "Peak-to-average power ratio reduction for MIMO-OFDM systems with decomposed Selected Mapping," *International Journal of Information and Systems Sciences*, Vol. 3, No. 3-4, pp. 572 - 580, November 2008.
- [84] C. Siegl and R. F. H. Fischer, "Partial Transmit Sequences for peak-to-average power ratio reduction in multiantenna OFDM," *EURASIP Journal on Wireless Communications and Networking*, Vol. 2008, pp. 1-11, January 2008.
- [85] M. Tan, Z. Latinovic, and Y. Bar-Ness, "STBC MIMO-OFDM peak-to-average power ratio reduction by cross-antenna rotation and inversion," *IEEE Communications Letters*, Vol. 9, No. 7, pp. 592-594, July 2005.
- [86] T. Jiang and C. Li, "Simple alternative multisequences for PAPR reduction without side information in SFBC MIMO-OFDM Systems," *IEEE Transactions on Vehicular Technology*, Vol. 61, No. 7, pp. 3311-3315, September 2012.

- [87] B. Rihawi and Y. Louet, "PAPR reduction scheme with SOCP for MIMO-OFDM," *International Conference on Wireless Communications, Networking and Mobile Computing*, Shanghai, China, September 2007.
- [88] R. Gallager, "Low-Density Parity-Check Codes," *IEEE Transactions on Information Theory*, Vol. 8, pp. 21-28, January 1962.
- [89] M. Tanner, "A recursive approach to low complexity codes," *IEEE Transactions on Information Theory*, Vol. 27, No. 5, pp. 533-547, September 1981.
- [90] L. Bahl, J. Cocke, F. Jelineka, and J. Raviv, "Optimal decoding of linear block codes for minimizing symbol error rate," *IEEE Transactions on Information Theory*, Vol. 20, No. 2, pp. 248-287, March 1974.
- [91] N. von Deetzen and S. Sandberg, "On the UEP capabilities of several LDPC construction algorithms," *IEEE Transactions on Communications*. Vol. 58, No. 11, pp. 3041 - 3046, November 2010.
- [92] S. Sandberg and N. von Deetzen, "Design of bandwidth efficient unequal error protection LDPC codes," *IEEE Transactions on Communications*. Vol. 58, No. 3, pp. 802 - 811, March 2010.
- [93] D. Yoon, K. Cho, and J. Lee, "Bit error probability of  $M$ -ary quadrature amplitude modulation," *Vehicular Technology Conference*, Massachusetts, USA, September 2000.
- [94] T. J. Richardson and R. L. Urbanke, "The capacity of low-density parity-check codes under message-passing decoding," *IEEE Transactions on Information Theory*, Vol. 47, No. 2, pp. 599-618, February 2001.
- [95] T. J. Richardson, M. A. Shokrollahi, and R. L. Urbanke, "Design of capacity-approaching irregular low-density parity-check codes," *IEEE Transactions on Information Theory*, Vol. 47, No. 2, pp. 619-637, February 2001.
- [96] S. Y. Chung, T. J. Richardson, and R. L. Urbanke, "Analysis of sum-product decoding of low-density parity-check codes using Gaussian approximation," *IEEE Transactions on Information Theory*, Vol. 47, No. 2, pp. 657-699, February 2001.
- [97] A. Wakeel and W. Henkel, "Effect of the threshold offset on the performance of UEP-LDPC codes," *2nd IEEE International Conference on Communication in China (ICCC)*, Xian, China, August 2013.
- [98] A. Filip and W. Henkel, "Hierarchical modulation to support low-density parity-check code design?," *9th International ITG Conference on Source and Channel Coding (SCC)*, Munich, Germany, January 2013.
- [99] R. Yoshizawa and H. Ochiai, "A serial concatenation of coding and trellis shaping for OFDM systems with peak power reduction," *IEEE International Symposium on Information Theory (ISIT)*, Cambridge, USA, July 2012.
- [100] R. Yoshizawa and H. Ochiai, "A Trellis Shaping for peak and average power reduction of BICM-OFDM signals," *IEEE Transactions Wireless Communications*, Vol. 14, No. 2, pp. 1143-1154, February 2015.

- [101] S. Shepherd, J. Orriss, and S. Barton, "Asymptotic limits in peak envelop power reduction by redundant coding in orthogonal frequency division multiplex modulation," *IEEE Transactions on Communications*, Vol. 46, No. 1, pp. 5 - 10, January 1998.
- [102] B. M. Popovic, "Synthesis of power efficient multitone signals with flat amplitude spectrum," *IEEE Transactions on Communications* Vol. COM-39, pp. 1031 - 1033, July 1991.
- [103] R. Laroia, N. Farvadin, and S. A. Tretter, "On optimal shaping of multidimensional constellations," *IEEE Transactions on Information Theory*, Vol. 40, No. 4, pp. 1044-1056, July 1994.
- [104] W. Henkel and V. Azis, "The analytic treatment of the error probability due to clipping - a solved problem?," *International Symposium on Information Theory and its Applications*, Parma, Italy, October 2004.
- [105] A. Eltholth, A. Mikhail, A. Elshirbini, M. Moawad, and A. Abdelfattah, "Peak-to-average power ratio reduction in OFDM systems using Huffman coding," *International Journal of Electrical, Computer, Energetic, Electronic and Communication Engineering* Vol. 2, No. 7, pp. 1365 - 1369, September 2008.
- [106] A. Jaynlath and C. Tellambura, "Peak-to-average power ratio reduction of an OFDM signal using data permutation with embedded side information," *IEEE International Symposium on Circuits and Systems*, Sydney, Australia, May 2001.
- [107] R. Baxley and G. Tong Zhou, "Comparing Selected Mapping and Partial Transmit Sequence for PAR reduction," *IEEE Transactions on Broadcasting*, Vol. 53, No. 4, pp. 797 - 803, December 2007.
- [108] G. Wunder and H. Boche, "The impact of nonlinear devices on the symbol error rate in broadband OFDM," *56th IEEE Semiannual Vehicular Technology Conference*, Vancouver, Canada, September 2002.
- [109] B. S. Krongold and D. L. Jones, "An active-set approach for OFDM PAR reduction via Tone Reservation," *IEEE Transactions on Signal Processing*, Vol. 52, No. 2, pp. 495-509, February 2004.
- [110] W. Henkel, A. Wakeel, and M. Taseska, "Peak-to-average ratio reduction with tone reservation in multi-user and MIMO-OFDM," *1st IEEE International Conference on Communications China (ICCC)*, Beijing, China, August 2012.
- [111] A. Wakeel and W. Henkel, "Least-Squares iterative PAR reduction for MIMO-OFDM systems," *IEEE Global Communications Conference (Globecom 2014)*, Texas, USA, December 2014.
- [112] A. Wakeel and W. Henkel, "Least-Squares iterative PAR reduction for point-to-point large-scale MIMO-OFDM systems," *IEEE International Conference on Communications*, Sydney, Australia, June 2014.
- [113] T. L. Marzetta, "Non co-operative cellular wireless with unlimited number of base station antennas," *IEEE Transactions on Wireless Communications*, Vol. 9, No. 11, pp. 3590 - 3600, November 2010.

- [114] E. G. Larson, F. Tufvesson, O. Edfors, and T. L. Marzetta, "Massive MIMO for next generation wireless systems," *IEEE Communications Magazine*, Vol. 52, No. 2, pp. 186 - 195, Feb 2014.
- [115] E. Telatar, "Capacity of multi-antenna Gaussian channels," *European Transactions on Telecommunications*, Vol. 10, No. 6, pp. 585 - 596, November 1998.
- [116] D. P. Palomar and J. R. Fonollosa, "Practical algorithm for a family of waterfilling solutions," *IEEE Transactions on Signal processing*, Vol. 53, No. 2, pp. 686 - 695, February 2005.
- [117] A. Edelman, "Eigenvalues and condition numbers of random matrices," Ph.D. Thesis, Massachusetts Institute of Technology, May 1989.
- [118] J. Shen, "On the singular values of Gaussian random matrices," *Linear Algebra and its Applications*, Vol. 326, No. 1-3, pp. 1 - 14, March 2001.
- [119] S. Verdu, "Random matrix theory and its application to statistics and wireless communications," Class notes, Princeton University, February 2006.
- [120] M. Friese, "Multitone signal with low Crest factor," *IEEE Transactions on Communications*, Vol. 45, No. 10, pp. 1338 - 1344, October 1997.
- [121] A. V. D. Bos, "A new method for synthesis of low-peak-factor signals," *IEEE Transactions on Acoustics, Speech and Signal processing*, Vol. ASSP-35, No. 1, pp. 120 - 122, January 1987.
- [122] E. V. D. Ouderaa, J. Schoukens, and J. Renneboog, "Peak factor minimization using time-frequency domain swapping algorithm," *IEEE Transactions on Instrumentation and Measurement*, Vol. 37, No. 1, pp. 145 - 147, March 1988.
- [123] V. T. Tom, T. F. Quatieri, M. H. Hayes, and J. H. McClellan, "Convergence of iterative nonexpensive signal reconstruction algorithms," *IEEE Transactions on Acoustics, Speech and Signal processing*, Vol. ASSP-29, No. 5, pp. 1052 - 1058, October 1981.
- [124] A. R. S. Bahai, M. Singh, A. J. Goldsmith, and B. R. Saltzberg, "A new approach for evaluating clipping distortion in multicarrier systems," *IEEE Journal on Selected Areas in Communications*, Vol. 20, No. 5, pp. 1037 - 1047, June 2002.